10-30-2020

Parametric Investigation of the Core Geometry of an IPMSM to Reduce Vibrations

Niccolò Remus
University of Windsor

Parametric Investigation of the Core Geometry of an IPMSM to Reduce Vibrations

By

Niccolò Remus

A Thesis
Submitted to the Faculty of Graduate Studies
through the Department of Mechanical, Automotive, and Materials Engineering
in Partial Fulfillment of the Requirements for
the Degree of Master of Applied Sciences
at the University of Windsor

Windsor, Ontario, Canada

2020

Parametric Investigation of the Core Geometry of an IPMSM to Reduce Vibrations

by

Niccolò Remus

APPROVED BY:

_____

I. Xu
Department of Civil and Environmental Engineering

_____

G. Rankin
Department of Mechanical, Automotive, and Materials Engineering

_____

N. C. Kar, Co-Advisor
Department of Electrical and computer engineering

_____

C. Novak, Co-Advisor
Department of Mechanical, Automotive, and Materials Engineering

September 8, 2020

DECLARATION OF ORIGINALITY

I hereby certify that I am the sole author of this thesis and that no part of this thesis has been published or submitted for publication.

I certify that, to the best of my knowledge, my thesis does not infringe upon anyone's copyright nor violate any proprietary rights and that any ideas, techniques, quotations, or any other material from the work of other people included in my thesis, published or otherwise, are fully acknowledged in accordance with the standard referencing practices. Furthermore, to the extent that I have included copyrighted material that surpasses the bounds of fair dealing within the meaning of the Canada Copyright Act, I certify that I have obtained a written permission from the copyright owner(s) to include such material(s) in my thesis and have included copies of such copyright clearances to my appendix.

I declare that this is a true copy of my thesis, including any final revisions, as approved by my thesis committee and the Graduate Studies office, and that this thesis has not been submitted for a higher degree to any other University or Institution.

ABSTRACT

Electrification has been a significant trend in the automotive industry for the past decades, but only during recent years electric vehicles have started being manufactured on a mass scale. The need of virtual improvement practices to reduce development costs and obtain best in class performances, coupled with the relatively new mass implementation of electric motors as traction sources on vehicles, drives the pursuit of best practices to deliver improved vibration performances with the help of computer aided engineering. This thesis reviews the state of the art of electric traction motor for passenger vehicles, analyzing their sources of vibrations and evaluating different strategies to mitigate them.

The proposed solution is a parametric study based on a multiphysics model aimed at minimizing vibrations of the stator teeth, by acting on some key geometric parameters which define elements of the electric machine core. The goal is to minimize the effect of the electromagnetic forces acting on the stator teeth, over a range of rotational speeds that simulates real working condition of a passenger vehicle traction motor, which in turns allows to mitigate the vibrations of the motor and improve comfort of driver and occupants. This is achieved by reducing both the radial maximum acceleration and maximum amplitude of oscillations measured in the radial direction at the stator teeth tips.

DEDICATION

To my parents, Eugenio and Donatella

For always being supportive with the decisions I made throughout my life, despite I stubbornly and repeatedly chose a path they had no experience in walking. Thank you for always being there at my return, regardless of how far away from home I seemed to have been wanting to go.

To my siblings, Gaia and Jacopo,

For showing me that love and affection come in many forms, and that blood really is thicker than water, even if the water in question is the whole Atlantic Ocean.

To the rest of my family and my friends,

For being there for me when I needed them, and for always reminding me that I am loved and worthy of love.

ACKNOWLEDGEMENTS

I want to thank Politecnico di Torino, the University of Windsor, and Fiat Chrysler Automobiles for giving me the opportunity to take part to the Dual International Double Degree Program, which brought me to Windsor and trough which I have met many formidable professionals and individuals.

Specifically, I want to show my gratitude to my academic advisors at the University of Windsor, Drs. Colin Novak and Narayan Kar for investing in me with this project, from which I have gained knowledge and insight thanks to their counsel and the resources they have put at my disposal.

Similarly, I want to acknowledge my appreciation for my Politecnico di Torino advisors, Profs. Andrea Tonoli and Gianmario Pellegrino.

Next, I want to thank my industry mentors, Eng. Massimiliano Garganese and Dr. Mohammad Toulabi, for their continuous and extremely valuable support and advice throughout the course of this project.

Moreover, I want to express my appreciation for all the work of Mrs. Marie Mills, Dr. Jennifer Johrendt, Eng. Edoardo Rabino, and Prof. Giovanni Belingardi, without whom none of this would have been possible.

I also want to thank my CHARGE Labs partners, and specifically Drs. Mukundan and Dhulipati, for always been available and willing to help me.

Last but not least, I want to thank all the friends I have made who have helped getting through this: the exchange students, the FCA crew, DJ Mele, and particularly my fellow adventurer and favourite Italian redneck Luigi Sacchetti, who constantly supported, and endured me, for the past year.

TABLE OF CONTENTS

LIST OF TABLES

LIST OF FIGURES

LIST OF APPENDICES

LIST OF ABBREVIATIONS

AC	Alternating Current
A-WSPL	A-Weighted Sound Power Level
BEM	Boundary Element Method
BEMF	Back Electromotive Force
BEV	Battery Electric Vehicle
CAD	Computer Aided Design
CAE	Computer Aided Engineering
DC	Direct Current
DoE	Design of Experiments
EM	Electromagnetic
EMF	Electromotive Force
EV	Electric Vehicle
FCEV	Fuel Cell Electric Vehicle
FEA	Finite Element Analysis
FEM	Finite Element Method
FFT	Fast Fourier Transform
HEV	Hybrid Electric Vehicle
IM	Induction motor
IPMSM	Interior Permanent Magnets Synchronous Machine
MSM	Modal Superposition Method
NVH	Noise and Vibration Harshness
OEM	Original Equipment Manufacturer
PCFM	Periodic Carrier Frequency Modulation
PM	Permanent Magnets
PM-RSM	Permanent Magnets-assisted Reluctance Synchronous Motor
PMSM	Permanent Magnets Synchronous Machine
PWM	Pulse Width Modulation
RCFM	Random Carrier Frequency Modulation

RPWM	Random Pulse Width Modulation
RSM	Reluctance Synchronous Motor
SOW	Slot Opening Width
SPL	Sound Power Level
SPMSM	Surface Permanent Magnets Synchronous Machine
UMP	Unbalanced Magnetic Pull

NOMENCLATURE

Symbols:

B	Magnetic flux density
B_{DC}	Amplitude of the DC flux component
B_m	Amplitude of the AC flux component
B_r	Radial flux density
B_t	Tangential flux density
c	Damping coefficient
c_o	Speed of sound
$[C]$	Damping matrix
E	Range of ε_n
F	Force
f	Frequency
f_e	Excitation frequency
f_m	Mechanical rotational frequency of motor
f_r	Electromagnetic force density radial component
f_t	Electromagnetic force density tangential component
H	Magnetic field intensity
I	Range of $I_{pk,m}$
I_{pk}	Peak current
i	Electric current
i_a, i_b, i_c	Phase current
K_{DC}	Coefficient to consider the DC flux bias effects
K_c	Eddy-current loss coefficient
K_e	Excess loss coefficient
K_h	Hysteresis loss coefficient
k	Elastic constant
$[K]$	Elasticity matrix

$[k]$	Modal elasticity matrix
L	Inductance
m	Mass
$[M]$	Mass matrix
$[m]$	Modal mass matrix
N	Number of coils
n	Rotational speed
P_c	Eddy current losses
P_e	Electric power
P_{ex}	Excess losses
P_h	Hysteresis losses
P_m	Mechanical power
P_{SC}	Power dissipated by stator copper losses
P_v	Core losses
p	Number of poles
q	Displacement vector
R_C	Coil electric resistance
$r_{rotor,o}(\beta)$	Rotor outer radius as a function of β
r_s	Stator bore radius
T	Motor torque
T_{avg}	Average motor torque
T_e	Period related to the excitation current frequency
T_{rip}	Torque ripple
T_s	Default total simulation time
t_{in}	Force modal participation factor
t_s	Default simulation time step
V_i	Induced phase voltage
Vib	Average vibration acceleration
$\overline{v_{mn}^2}$	Mean square velocity

Greek symbols:

β	Angle relative to d-axis of the rotor
Γ	Range of γ_j
γ_j	Location of slit in polar coordinates
Δ	Range of δ_i
δ	Optimization angle
$\delta(\beta)$	Air gap length as a function of β
δ_i	Shape of slit
δ_d	Air gap length in d-axis
ε_n	Excitation angle
$\mathcal{E}$	Electromotive force
$[\zeta]$	Modal viscous damping matrix
η	Efficiency
Λ	Range of λ_h
λ	Flux linkage
λ_h	Circumferential width of slit
λ_i	Eigenvalues
μ	Magnetic permeability of a general material
μ_0	Magnetic permeability of air
ξ_i	Modal participation factor
ρ_0	Air density
σ_{mn}	Sound radiation efficiency
τ_p	Pole pitch
φ	Magnetic flux
φ_i	Eigenvectors
ϕ_i	Phase angle
ω_s	Synchronous rotational speed
ω	Resonance frequency
Ω	Range of ω_k

CHAPTER 1
INTRODUCTION

1.1. Background

Over the last decade, as a result of the increased environmental awareness of the general public and the growth of car ownership, a significant trend in the automotive industry has been that of electrification and search for alternatives to the traditional internal combustion engine, with the objective of reducing pollution generated by vehicles [1], [2], [3].

In the wake of this current, researchers in the field have been focused on studying which technologies yield the best results in terms of costs of implementation, energy efficiency, and performances. Of the various solutions that have been considered, a sizeable percentage includes the utilization of electric motors as either the only or a complementary source of propulsion, fueling the growth of several categories of vehicles such as:

- Battery-powered Electric Vehicles (BEVs). This category of vehicles is characterized by a purely electric powertrain, which can be composed by one or more electric traction motors, supplied by one or more battery packs housed within the vehicle.
- Fuel Cell-powered Electric Vehicles (FCEVs). These vehicles are also propelled by electric traction motors, but they are different from BEV's in the fact that the motors are not fed by energy stored in a battery: the electric current used to drive them is generated on the vehicle by a Hydrogen Fuel Cell, which produces it by converting the potential energy contained in the chemical bonds of the gaseous fuel stored in a pressurized tank in the vehicle.
- Hybrid Electric Vehicles (HEV), which can be further classified by powertrain configuration [4], utilize both an ICE and one or more electric motors:
    - Series: also known as "range extender", in which the ICE is not directly connected to the wheels, but it generates power for the electric traction motor and the batteries, as shown in Figure 1.1a.

- Parallel, in which both the electric motor(s) and the ICE provide power to the wheels, as illustrated in Figure 1.1b.
- Combined, which are characterized by both a mechanical coupling and hybrid electrical connections, drawing from both the parallel and series architecture.

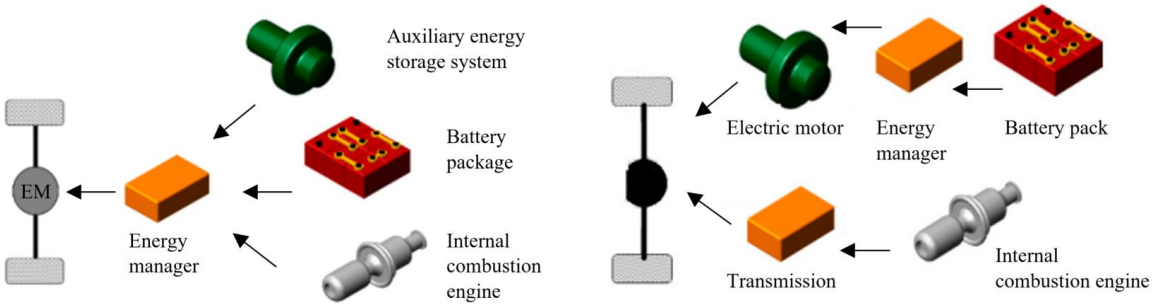

(a) (b)

Figure 1.1. Hybrid Configurations: (a) series hybrid configuration. (b) Parallel hybrid configuration [4].

As a result, the electric motor has seen a big surge in interest from the automotive industry, and consequently, its various possible architectures have been studied to find the most suitable one for this type of application.

By considering the mass production industry for the general public, we can identify two main different motor architectures that have been employed so far in the automotive field:

- Permanent Magnet Synchronous Machines (PMSMs)
- Induction Motors (IMs)

Both of these technology have their perks and drawbacks, which can be summarized in the following table [1], [3]:

TABLE 1.1. COMPARISON OF DIFFERENT MOTOR ARCHITECTURES.

Motor architecture	Advantages	Disadvantages
PMSM	High efficiency and power density, low noise and vibration, mature technology	High cost and complexity
IM	Moderate cost, robust and mature technology, good efficiency and vibrational behavior	Low power density, difficult cooling

1.2. Motivation

Considering how competitive the automotive industry has become in recent years, as the result of ever more stringent regulations on efficiency, performances, emissions, costs, and environmental sustainability, it is of utmost importance for manufacturers to be able to predict possible issues in the design and performance of the components used in their final assembly, in as much advance as possible. This set of constraints makes the use of computer-aided engineering (CAE) virtually unavoidable for original equipment manufacturers (OEMs). Specifically, the ability to predict the noise and vibration harshness (NVH) behavior of an electric drive used in EV's, without having to run experimental simulations, can generate incredible benefits for a company in terms of time and resource savings. Furthermore, developing a virtual model able to replicate the performances of the physical machine enables researches to run parametric studies and optimization cycles, which allow them to identify the best-performing set-up for any specific application, without having to run countless experimental tests which would require costly and time consuming modifications on the machine.

Parametric and optimization practices based on virtual models grant the opportunity of analyzing a very large number and diverse set of design versions, before having to commit resources to the production of any of them. This allows engineers to obtain the best performance out of complex machines, where the interdependence and combined effect of multiple design parameters is not always easy to predict, even when the target involves the compromise between different aspects of performance.

As this thesis has been developed in collaboration with researchers from a manufacturer, who supplied the data necessary for the simulation and analysis, the focus of this work will be on a permanent magnet synchronous machine, which is the architecture of a motor used as the primary traction source in a battery electric vehicle produced by the company. As mentioned previously, although the electric motor is not a recent invention, its mainstream application in the automotive industry has only been significant in recent times, which has renewed the interest of the scientific community in its characteristics and opportunities for optimization.

In [3], Tianfu Sun reviews the aforementioned different architectures employed in the industry, comparing their characteristics and giving a more detailed overview of the PMSM, which is the most commonly employed technology for propulsion purposes in vehicles [5]. Permanent magnet synchronous machines can be further split into different categories based on the arrangement of the magnets inside the motors:

- Flux direction:
  - Axial flux PMSM
  - Radial flux PMSM
    - External rotor PMSM
    - Internal rotor PMSM
      - Surface-mounted PMSM, or SPMSM
      - Interior Permanent Magnets Synchronous Machine, or IPMSM

In their very inclusive summary work [2], Deng and Zuo give a fairly detailed overview of these different architectures, highlighting differences related to the vibrational behavior of each of them.

Figure 1.3 shows two different configurations for PMSM; as they are being employed more and more frequently in the industry due to their advantages [3], such as in the case of the machine provided by the manufacturer, the focus of the study presented in this thesis will be on an interior permanent magnet synchronous machine.

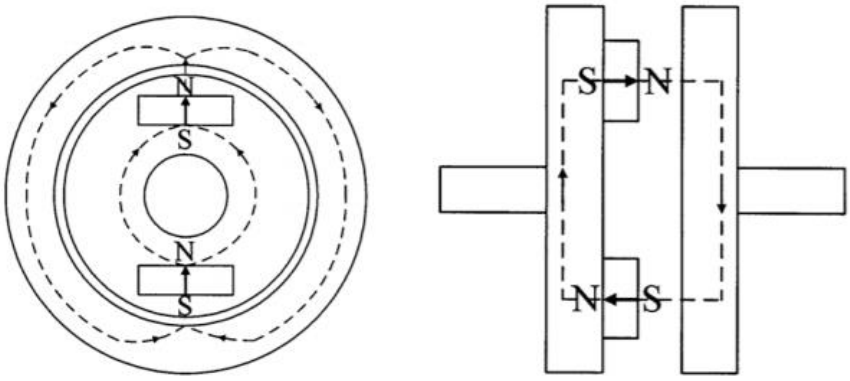

(a) (b)

Figure 1.2. PMSM flux directions. (a) Radial. (b) Axial [2].

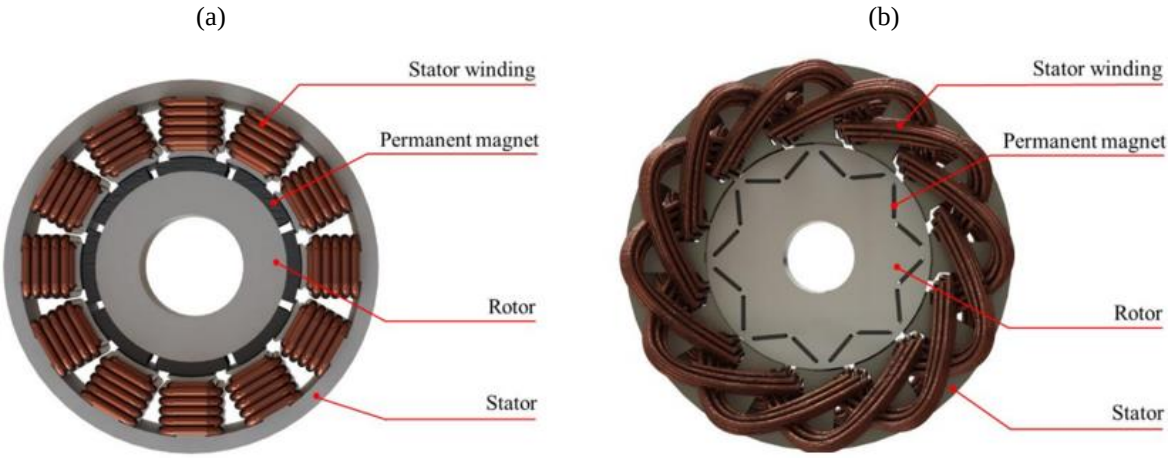

Figure 1.3. PMSM Architecture. (a) Schematic of SPMS. (b) Schematic of IPMSM [3].

1.2.1. Why an Interior Permanent Magnets Synchronous Machine ?

Following the development of permanent magnet materials and electric machine driving techniques of the last decades, PMSMs have become more and more prominent in industrial utilization, filling roles that were previously assigned to induction motors, as the former type provides advantages in both efficiency and size [6].

As mentioned before, PMSMs are mostly built with either of two architectures depending on the position of the magnets in the rotor: due to the susceptibility to centrifugal force of SPMSM, which prevents them from operating above a certain rotational velocity, IPMSMs and permanent magnets assisted reluctance synchronous motors (PM-RSMs) are the most commonly employed architectures in EVs [6].

Within the IPMSM category, there are different possible layouts that can be implemented, as they all offer different advantages in specific applications. In Figure 1.4, it is possible to see the layout of several types of electric machines belonging to the aforementioned category, appreciating the different positioning of the permanents magnets inside the rotor.

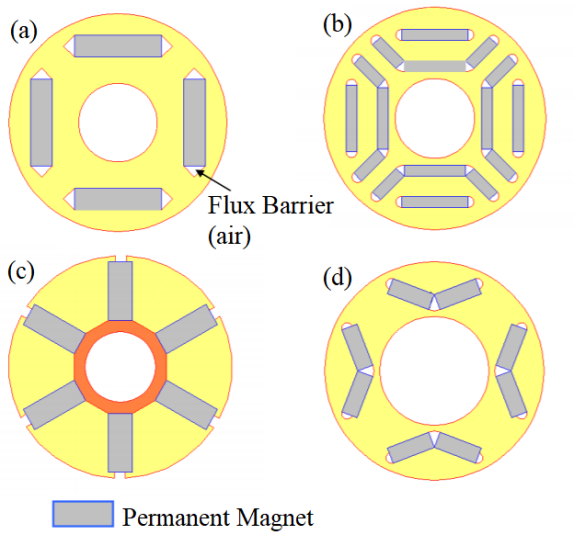

Figure 1.4. Different IPMSM Architectures. (a) Single layer type. (b) Double layer type. (c) Flux-concentrating type. (d) Modified single layer type [6].

As in all PMSMs, these machines have an internal rotor containing the magnets which produce the magnetic field, and a stator which houses the electric wire windings necessary to transfer the excitation current that powers the machine.

Within Figure 1.4, it is interesting to notice the double layer configuration (b), which is able to produce more torque and operate in a wider efficiency range when compared to the basic single layer type (a); in the flux-concentrating design (c) instead, the magnet pole area is able to produce a higher air-gap flux density than the magnet flux density [6].

1.3. Thesis Structure

Excluding the current introductory chapter, which helps the reader with an overview of the entire research project, this dissertation is structured in the following way:

- Chapter 2 is composed of three main parts: in the first one, the main theoretical concepts behind the developed analysis are presented and explained, while the second one contains a literature review of several major contributions developed by the scientific community during recent times, aimed at analyzing and reducing the vibrations produced in IPMSMs by the electromagnetic (EM) forces acting inside the machine during operating conditions. In this section, the primary sources of vibration in synchronous motors are identified and analyzed; different methods for vibration

predictions are surveyed, as well as some techniques that can be implemented to reduce vibration in synchronous motors by altering the architecture or the control technique of the electric motor, and several optimization techniques are compared and evaluated to develop the study presented in this dissertation. Lastly, the novelty introduced with this study is proposed and explained.

- Chapter 3 explains the procedure used for modelling of the PMSM in all of its different physical aspects, the set of assumptions and boundary conditions that have been employed in the simulation used to compute the electromagnetic force distribution, as well as the multiphysics model used to link vibration generation to the electromagnetic excitation.

- Chapter 4 describes the strategy used for the multi-parameter optimization, the setup of the Design of Experiments (DoE) and the Response Surface Method (RSM). The first section covers how the parametrization of core geometry was formulated, and the sensitivity analysis, which is the technique used to select a few parameters to use for the optimization procedure starting from the large initial set. The second and third section describe the parametric study, with the former talking about the DoE, and the latter about the RSM, together with the logic and structure of their implementation.

- Chapter 5 shows the results obtained from the parametric study, which are then explained and commented.

- Chapter 6 concludes the dissertation with some final remarks and suggestion for future developments.

1.4. Objectives

The objectives of this research have been established by taking into account the perspectives, necessities, and requirements dictated by both the industrial and the academic side.

Therefore, one of the first needs that was highlighted during the definition of the research scope for this project, was to conduct a comprehensive literature that would define the state of the art in the methodology for electromagnetic force analysis in internal

permanent magnet synchronous motors, the identification of a theoretical vibrational model based on the excitations caused by such forces, and an evaluation of the techniques used in the past for design optimization aimed at improving the vibration performances. This aspect will be tackled in Chapter 2, where several articles, papers, and dissertations have been analyzed to survey the most important contributions to the topic that have been developed by the international scientific community over the past decades.

The main objective of this research is, however, to run a parametric investigation procedure on a set of geometric variables that characterize the motor core, aimed at obtaining the best possible NVH behavior while taking into account performance and design constraints, using the simulation software Ansys Maxwell, RMxprt, Workbench, and Mechanical. As experimental simulation is often cumbersome and time-expensive to run, it is of key importance for manufacturer in today's competitive industry to be able to get predictive information about sensitive parameters via CAE, to obtain the best performing design version of a machine even before production begins. Starting from the results obtained from the force distribution analysis, the scope of this dissertations includes the identification or development of a multiphysics model suitable for the prediction of the vibrational behavior of the analyzed machine, to assess the sensitivity of the machine to the variation of the geometric parameters that are studied in the design improvement process.

.

CHAPTER 2
PRE-EXISITNG WORK

This chapter is divided into two main parts: the first one presents a summary and concise explanation of the main theoretical concepts and techniques used to set up the model and the analysis, while the second one provides an overview of several studies that have been conducted in the scientific community with the aim of understanding, characterizing, and improving the vibrational behavior of PMSMs. Some sources are specifically focused on the application to the automotive field while others explain important concepts and models that have been used in the development of this dissertation. Moreover, the proposed novelty introduced with study is proposed in the last section.

2.1. Theoretical Background

This first section of the chapter presents a brief summary of the main concepts that act as theoretical backbone of this study.

2.1.1. Principles of Electromagnetism

Electric motors are electromechanical machines, which are used for the conversion of electrical energy into mechanical energy. The foremost categories of AC motors are asynchronous and synchronous motors. The asynchronous motors are also called singly excited machines, that is, the stator windings are connected to AC supply whereas the rotor has no connection from the stator or to any other source of supply. The power is transferred from the stator to the rotor only by mutual induction [7]. In PMSMs, the rotor windings are replaced by permanent magnets, but the interaction between the magnetic fields generated by magnets in the rotor and windings in the stator is fairly similar to that between two sets of windings.

To understand this phenomenon, which is the basic principle behind the functioning of electric motors, we must understand some concepts about electromagnetism.

2.1.1.1. Ampere's Law and Magnetic Flux

The magnetic-field intensity H produced by current-carrying conductors can be obtained by means of Ampere's Law, which in its simplest form states that, at any time, the line (contour) integral of the magnetic field intensity along any closed path equals the total current enclosed by this path.

This is shown in Figure 2,1, where $\oint$ represents a contour or a closed-line integration. Note that the scalar H (measured in Henry [H]) in Equation (2.1) is the component of the magnetic field intensity (a vector field) in the direction of the differential length $d\ell$ along the closed path [8].

$$\oint H\, d\ell = \sum i \tag{2.1}$$

From any given H field, it is possible to derive the flux density B (measured in Tesla [T]), which depends on the permeability μ of the material in which the field is acting. When we measure the flux density in air, we use its characteristic magnetic permeability μ_0 [8]:

$$B = \mu H \qquad \mu_0 = 4\pi \cdot 10^7 \left[\frac{H}{m}\right] \tag{2.2}$$

Magnetic flux lines form closed paths; by selecting an area that is crossed by one or more of these lines, it is possible to compute the magnetic flux through the area:

$$\phi = BA\cos\vartheta \tag{2.3}$$

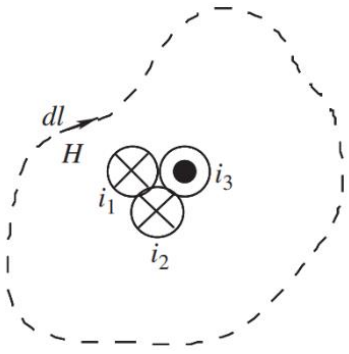

Figure 2.1. Magnetic field [8].

where A is the area subject of the computation, and ϑ is the angle between the flux lines and the normal of the selected area. If all the N turns of a coil are linked by the same flux ϕ, then the coil has a flux linkage λ [8]:

$$\lambda = N\phi \tag{2.4}$$

Moreover, it is possible to relate the flux linkage of the coil to the current flowing through it with a parameter defined as inductance of the coil L

$$L = \frac{\lambda}{i} \tag{2.5}$$

2.1.1.2. Faraday's Law and Induced Voltage

Faraday's Law dictates that the time-rate of change of flux-linkage equals the voltage across the coil at any instant:

$$\mathcal{E}(t) = \frac{d}{dt}\lambda(t) = N\frac{d}{dt}\phi(t) \tag{2.6}$$

This assumes that all flux lines link all N turns such that $\lambda = N\phi$. The polarity of the electromotive force (EMF) $\mathcal{E}(t)$ and the direction of $\phi(t)$ in the above equation are yet to be justified [8].

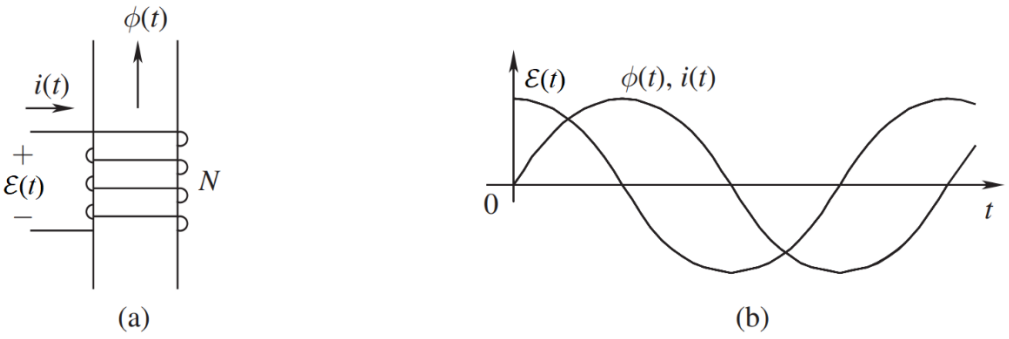

Figure 2.2. Voltage, current, and flux: (a) circuit scheme. (b) Waveform in time [8].

From Equation (2.5), we can express the same relationship with a dependence on time:

$$\lambda(t) = i(t)L \tag{2.7}$$

Therefore, combining it with Equation (2.4) and assuming that the entire flux links all N turns, we obtain:

$$\phi(t) = \frac{L}{N} i(t) \tag{2.8}$$

And substituting this into equation (2.6) gives

$$\mathcal{E}(t) = N \frac{d}{dt} \phi(t) = L \frac{di}{dt} \tag{2.9}$$

Equations (2.8) and (2.9) relate $\mathcal{E}(t)$, $\phi(t)$, and $i(t)$ which are plotted against time in Figure 2.2b.

In PM electric motors, these phenomena result in the generation of back electromotive force (BEMF), which is the voltage induced in the windings by the variation in time of the magnetic field to which they are subject, caused by the rotation of the permanent magnets in the rotor, when no load is applied to the machine.

2.1.1.3. Electromagnetic Losses

Losses in an IPMSM can be summarized into 4 categories [9]:

- Stator Copper Losses
- Iron Losses
- Stray Losses
- Mechanical Losses

Out of these 4 types, the first 3 are connected to electromagnetic principles.

Stator coils are constructed with copper, which has an inherent electric resistance. Due to Ohm's Law, when a current is coursing through the coils, there will be a power loss proportional to the coil resistance and the square of the current. In a 3 phase motor, assuming the coils of each phase to be identical, the total stator copper loss will be:

$$P_{sc} = 3\, i^2 R_c \tag{2.10}$$

where i is the current in the coils of each phase, and R_c is their electric resistance [9].

Iron losses have their origin in phenomena happening on a microscopic scale, which does not provide a practical meaning to calculate them [10]. In general, iron losses are usually treated as the summation of three different types, which are the hysteresis loss, eddy current loss, and the excess eddy current loss [9]:

- Hysteresis losses result from Barkhausen effects, which happen where small domain wall segments rapidly shift their position between local minima of the system's free energy, giving rise to localized eddy currents around the jumping segments [9].

- Eddy current losses are caused by a net change in magnetization in the magnetic material of the electric machine. As seen before, due to Faraday's Law, a variation in time of the magnetic field is able to induce currents into metallic materials. Moreover, since every material has an electric resistance, the current coursing through them will cause a power loss, similarly to what happens for stator core losses [9].

- As Roshen describes the phenomenon of iron losses, "The origins of this mechanism are the magnetic domains that exist inside a magnetic material. Inside each magnetic domain the magnetization is uniform. The magnetic domains are separated from each other by a transition region called "domain walls" in which the direction of magnetization changes from that of one domain to that of the adjacent domain. One of two mechanisms for change in the magnetization state of material is through the motion of these walls in response to an applied field, which changes magnetization only in or near the domain walls, leaving the magnetization inside the bulk of magnetic domains unchanged. Since domain walls occupy only a very small fraction of the total volume, the change in the magnetization in and around has to be very large compared to the average (over volume of the sample) magnetization. Hence, the induced eddy-current losses are much higher than those calculated on the basis of uniform magnetization. These additional losses are termed anomalous or excess eddy-current losses" [11].

Stray losses are conventionally defined as the difference between the total power loss and the rest of conventional losses once the motor is loaded. Origins of stray losses are varied and sometimes uncertain, but they are mostly attributed to saturation, manufacturing imperfections, space harmonics, and fringing and leakage flux. However, they are mostly

negligible, and so they are usually either ignored or set to 0.5% of the total power input of the motor [9].

2.1.2. Electric Motors and PMSMs Structure and Working Principle

PMSMs

are permanent magnet synchronous motors. This type of machine requires an AC supply to generate a rotating magnetic field in the windings of the stator, and normally, a DC supply to generate a constant magnetic field in the windings of the rotor. In PMSMs however, the rotor windings are substituted with permanent magnets, which generate a constant magnetic field due to their material properties. This type of configuration gives to PMSMs the advantage of being power-dense and energy-efficient [7].

In synchronous motors, the rotor spins at the same speed as the rotating field generated by the excitation current flowing through the windings. This angular velocity n is therefore obtained from the current excitation frequency f_e $[Hz]$, the number of poles in the rotor p [7]:

$$n = \frac{120\ f_e}{p}\ [rpm] \tag{2.11}$$

As seen in the previous chapter, PMSMs can either have axial or radial flux. The machine studied in this dissertation is of the second type, which is what this section will be focused on. For sake of simplicity, a 2-pole, 3-phase PMSM is chosen as an example [9]:

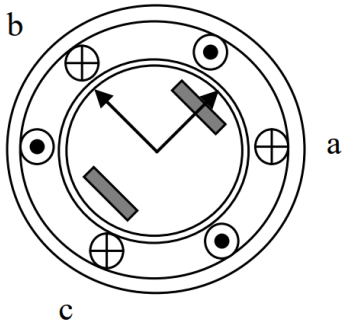

Figure 2.3. Simplified geometry of 2-pole, 3-phase PMSM [9].

In these machines, the 3-phase current excitation has waveforms described by the following equations:

$$i_a = I_{pk}\sin(2\pi f_e)$$

$$i_b = I_{pk}\sin(2\pi f_e - 2\pi/3) \tag{2.12}$$

$$i_c = I_{pk}\sin(2\pi f_e - 4\pi/3)$$

The rotating magnetic field generated by the current described in equation (2.12), spins with respect to the stator at the synchronous speed ω_s

$$\omega_s = \frac{4\pi f_e}{P} \tag{2.13}$$

The constant magnetic flux produced by the permanent magnets will try to align itself to the rotating field, effectively producing a torque on the rotor [9]. This torque can be expressed as:

$$T = r_s i l B_{PM}\sin\vartheta \tag{2.14}$$

where:

- r_s is the radius of the stator bore
- i is the current in the windings
- l is the length of the rotor
- B_{PM} is the flux density of the permanent magnets
- ϑ is the angle between B_{PM} and the magnetic field induced by stator currents [9].

It is also possible to analyze force and torque production by using another approach. Applying the Maxwell stress tensor method, EM forces acting on the stator can be split in their tangential component, which will be responsible for torque generation, and their radial component, which is the main cause of vibration in the stator [12], [13]. By using this approach, the local components of force density in the air gap of the machine can be expressed as [12]:

$$f_t = \frac{1}{\mu_0} B_r B_t \tag{2.15}$$

$$f_r = \frac{1}{2\mu_0}\left({B_r}^2 - {B_t}^2\right) \tag{2.16}$$

where:

- f_t is the tangential component of force density $\left[\frac{N}{m^2}\right]$
- f_r is the radial component of force density $\left[\frac{N}{m^2}\right]$
- μ_0 is the permeability constant of free space
- B_r is the radial component of the magnetic flux density
- B_t is the tangential component of the magnetic flux density

2.1.3. Vibration Theory

Vibration happens when there is the possibility for energy in a system to be converted from one form to another. In mechanical systems, this mostly happens in the exchange between the kinetic energy of motion and the potential energy stored in a compressible body such as a spring [14].

2.1.3.1. Equation of Motion

The simplest form of vibrational behavior can be explained with a single degree-of-freedom (DOF) system, pictured in Figure 2.4. This system is formed by a mass m, attached with a spring (with elastic constant k) to a fixed support. Moreover, the mass is constrained in a way that only allows translational motion along the axis of the spring (X axis); therefore, the position of the mass in the system is unequivocally described by a single quantity x, hence the name single DOF. If the mass is displaced and then left free to move without any external intervention, it is said to have free vibrations [15].

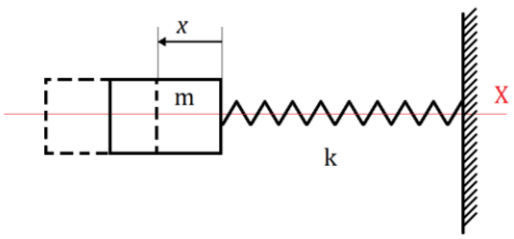

Figure 2.4. Single DOF system.

In its most basic form, the equation of motion along the X axis of such system, in which the equilibrium position corresponds to $x = 0$, is the following:

$$m\ddot{x} + kx = 0 \tag{2.17}$$

However, this type of equation is not sufficient to portray all real phenomena: to do so, it is necessary to add damping and an external source of excitations. Damping is the means by which energy is lost in elastic bodies, and dampers are characterized by c, the damping coefficient. Introducing these two new elements to the system in Figure 2.4, we obtain the following:

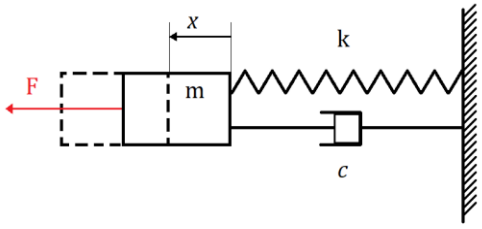

Figure 2.5. Damped single DOF system with forced oscillations.

Assuming that the period excitation can be described with $F = F_0 \sin \omega t$, the equation of motion for the system in Figure 2.5 is [15]:

$$m\ddot{x} + c\dot{x} + kx = F = F_0 \sin \omega t \tag{2.18}$$

The response to vibration of a structure is the description of the motion of the mass excited by the external force [15], which can be obtained solving the equation of motion.

2.1.3.2. Modal Analysis

The analysis of the response to a periodic excitation is studied by a branch of physics called vibroacoustic, through modal analysis [16]. While the systems analyzed in the previous section were characterized by a single degree of freedom, modal analysis usually deals with complex structures with multiple DOF's; hence, the equation of motion (2.18) is expressed in matrix form [16]:

$$[M]\{\ddot{q}\} + [C]\{\dot{q}\} + [K]\{q\} = \{F\} \tag{2.19}$$

where:

- M is the matrix which describes the mass properties of the structure (mass matrix)

- C is the damping matrix
- K is the elasticity matrix
- q is the displacement vector
- F is the excitation vector

Considering the undamped system and the associated homogeneous equation, expressed by (2.20) and (2.21) respectively, we can assume its solution to be harmonic (2.22), and rewrite its equation of motion as (2.23) [16]:

$$[M]\{\ddot{q}\} + [K]\{q\} = \{F\} \tag{2.20}$$

$$[M]\{\ddot{q}\} + [K]\{q\} = 0 \tag{2.21}$$

$$\{q\} = \{\varphi\}e^{st} \tag{2.22}$$

$$\{[M]s^2 + [K]\}\{\varphi\} = 0 \tag{2.23}$$

Equation (2.23) can be expressed in the form of eigenvalues and eigenvectors:

$$\{[M]^{-1}[K] - \lambda[I]\}\{\varphi\} = 0 \tag{2.24}$$

$$\det([M]^{-1}[K] - \lambda[I]) = 0 \tag{2.25}$$

$$s = \pm j\omega = \pm j\sqrt{\lambda} \tag{2.26}$$

Excluding the trivial solution $\{\varphi\} = 0$, which represents a still structure, the rest of the solutions to this problem are found in the n eigenvalues λ_i, which can be inserted in equation (2.24) to obtain their respective eigenvectors φ_i. From a physical point of view, eigenvalues and eigenvectors of the system represent, respectively, the natural frequencies of the structure and their associated mode shapes [16].

Since the mode shapes are orthogonal, when the mass and stiffness matrices are real and symmetric, we can obtain the following relationships:

$$\{\varphi\}[M]\{\varphi\}^T = [m] \tag{2.27}$$

$$\{\varphi\}[K]\{\varphi\}^T = [k] \tag{2.28}$$

In which $[m]$, the modal mass matrix, and $[k]$, the modal stiffness matrix, are diagonal, which implies that the equations of motions of the undamped system are uncoupled, which allows us to show that the displacement vector can be obtained as the linear combination of mode shapes [16]:

$$\{q\} = \{\varphi_1\}\xi_1 + \{\varphi_2\}\xi_2 + \cdots + \{\varphi_n\}\xi_n \tag{2.29}$$

$$\{q\} = [\varphi]\{\xi\}^T \tag{2.30}$$

where ξ_i are called modal participation factors, and indicate the contribution of each mode shape to the displacement vector. By combining (2.30) into (2.21), and multiplying each term by $[\varphi]^T$, we can express the dynamic equation of motion into modal coordinates (2.31), in which $[t_{in}]$ is the force modal participation factor, which correlates how much each mode is excited by external forces [16]:

$$[m]\{\ddot{\xi}\}^T + [k]\{\xi\}^T = [t_{in}]\{F\} \tag{2.31}$$

Lastly, in the case of a lightly damped system, it is possible to introduce the effect of viscous damping with the diagonal matrix $[\zeta]$. However, the influence of this matrix is only significant in correspondence of resonance peaks. By combining this term to equation (2.31), and using the relationship between stiffness and mass in natural frequencies expressed in (2.32), we obtain the dynamic equation describing the system as written in (2.33) [16].

$$\omega_{0,i} = \sqrt{\frac{k_i}{m_i}} \tag{2.32}$$

$$\{\ddot{\xi}\}^T + 2[\zeta][\omega_0]\{\dot{\xi}\}^T + [\omega_0]^2\{\xi\}^T = [t_{in}]\{F\} \tag{2.33}$$

Having solved each of these equations separately, it is possible to superimpose them to obtain the solution to the original system:

2.1.3.3. Harmonic Response and Modal Superposition Method

As Clough and Penzien write in their book, "for the purpose of dynamic-responses analysis, it is often advantageous to express this position in terms of the free-vibration mode

shapes. These shapes constitute n independent displacement patterns, the amplitudes of which may serve as generalized coordinates to express any set of displacements. The mode shapes thus serve the same purpose as the trigonometric functions in a Fourier series, and they are used for the same reasons; because they possess orthogonality properties, and they are efficient in the sense that they usually can describe all n displacements with sufficient accuracy employing only a few shapes" [17].

The previous section explained the theory behind mode shapes; this one illustrates why and how the superposition method is a convenient choice to solve harmonic response problems like the one that is the subject of this dissertation. When studying a system in which the excitation source is harmonically well defined, and acting on a limited range of frequencies, modal superposition can prove to be more computationally efficient than direct integration. This is true as long as the dynamic behavior of the excited structure can be effectively reproduced with only a restricted set of vibration modes which means that the elastic properties and behavior of the structure itself are constant in time [18].

As shown in equations (2.27) and (2.28), modal coordinates matrices are $n \times n$ diagonal matrices, where n is the number of the DOF's of the system they are describing. Modal superposition exploits the orthogonality properties of mode shapes (2.34) to uncouple each degree of freedom and obtain a system described in n linear equations of the type of (2.35) [17].

$$\{\varphi_i\}[M]\{\varphi_j\}^T = 0, \qquad \{\varphi_i\}[C]\{\varphi_j\}^T = 0, \qquad \{\varphi_i\}[K]\{\varphi_j\}^T = 0 \quad \forall\, i \neq j \tag{2.34}$$

Where $\{\varphi_i\}$ and $\{\varphi_j\}$ are the i^{th} and j^{th} columns of the matrix $[\varphi]$.

Using m_i to identify the i^{th} term of the diagonal of the mass matrix in modal coordinates $[m]$, and using the same convention for damping and stiffness matrices $[\zeta]$ and $[k]$, as well as for the modal participation factor matrix $[t_{in}]$, and indicating as F_i the i^{th} element of the vector of external excitations $\{F\}$, each of the n linear equations will be in the following form [17]:

$$\ddot{\xi}_i + 2\zeta_i \omega_{0,i} \dot{\xi}_i + \omega_{0,i}^2 \xi_i = t_{in,i} F_i \tag{2.35}$$

Having obtained a solution from each of the n linear equations, it is possible to superimpose them to compute the solution of the original system:

$$q(t) = \{\varphi_1\}\xi_1(t) + \{\varphi_2\}\xi_2(t) + \cdots + \{\varphi_n\}\xi_n(t) \tag{2.36}$$

It is worth mentioning that for most cases of dynamic loading, the displacement contributions are usually most significant in the lower modes, and tend to decrease for higher ones, becoming negligible after a while; therefore, it is not necessary to always include all the higher modes of vibration in the solving process, but it is sufficient to truncate the summation once the desired degree of accuracy has been reached [17].

The vector of displacement in time $q(t)$ is often considered the basic measure to evaluate the overall response of a structure to harmonic loading. Other parameters of response behavior like acceleration, stress, and forces can be evaluated starting from the displacement, and can help in judging the structural qualities of the system [17].

2.2. Literature Review

As mentioned in the beginning of the chapter, this section provides a summary of several studies which have contributed in developing knowledge and insights about the subject this dissertation, serving as the base for the study carried out and described in later chapters.

2.2.1. General Overviews

In [2], Deng and Zuo carry out a quite extensive analysis of the usage of PMSMs in the automotive industry, with specific attention to their vibration and noise performances. Their work has been crucial to the development of this dissertation and is therefore heavily referenced throughout this document. In their paper, they identify three main types of noise that can be generated by an electric motor:

- Mechanical noise: generated by mechanical components of the machine, such as bearings and fasteners; it is mostly present as low frequency noise and extensive research has been done on its identification and characterization methodology.

- Aerodynamic noise: this type of noise usually comes from the cooling fan of the motor; however, most PMSMs employed in vehicles are fan-less, as they are air or water-cooled.

- Electromagnetic noise: the noise generated by the normal EM force acting on the surface of stator teeth and permanent magnets is the most significant component of the total noise, and it is linked to the electromagnetic parameters and control strategy of the motor.

Moreover, they survey different methods for prediction of electromagnetic noise and vibration, dividing them in three categories:

- Analytical method: sound power level Π can be computed with the following equation

$$\Pi = \sum_{m,n=0}^{\infty} \sigma_{mn} \rho_0 c_0 S < \overline{v_{mn}^2} > \tag{2.37}$$

  Where

  - σ_{mn} is the sound radiation efficiency
  - ρ_0 is the air density
  - c_0 is the speed of sound
  - S indicates the area of the noise radiating surface
  - $< \overline{v_{mn}^2} >$ is the special averaged mean square velocity

  It is possible to see that the analytical approach requires an accurate computation of the surface vibration velocity and the sound radiation efficiency; since the noise radiation mechanisms are intrinsically different for axial and radial PMSMs, the authors identify two different methods for analytic prediction; however only the one for radial flux machines is relevant to this study and is therefore reported here.

  As the annular stator shell has been identified as the principal source for noise radiation in radial flux motors, it is advised to compute its modal shapes and frequencies, and then the sound radiation efficiency. Regarding modal analysis, the authors identify the finite length cylindrical shell model to be the best suited to represent most motors, when compared to the ring and the spherical models.

- Numerical modeling method: this technique exploits Finite Element Analysis (FEA) software to predict noise and vibration, and its main benefit is that even the most complex shapes and geometries can be taken into account, allowing for higher precision in the results; however, this methodology is often demanding in terms of time and computing resources.

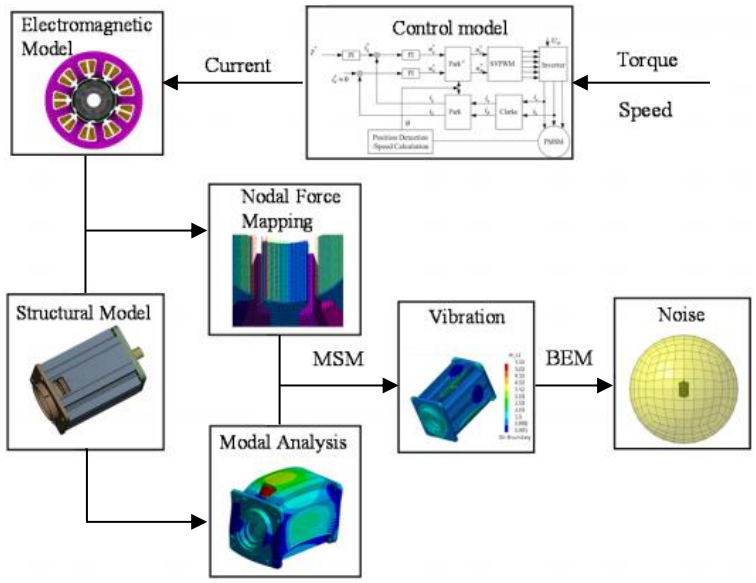

Figure 2.6. General flow chart of the vibration and noise calculation with numerical method [2] © IEEE 2019.

As shown in the figure above, different working conditions describes in terms of torque and speed are used as inputs of the control model to obtain the phase of the driving current of the motor, which is used in the electromagnetic virtual model to compute the EM force with EM analysis software such as ANSYS Maxwell. Another advantage of finite element method (FEM) computation is that the structural model on which the modal analysis is based is an assembly that represents the whole machine and not only the stator; this allows for better precision in the analysis as it is possible to simulate the interactions between different parts, and better represent the physical constraints that hold the machine in place during utilization in real life applications. Once everything has been set up properly and the results of the EM force distribution on stator teeth has been obtained, the vibrational and acoustic response of the motor can be calculated with modal superposition method (MSM) or boundary element method (BEM).

In their paper, Deng and Zuo also suggest methods to separate mechanical and aerodynamic noise from the electromagnetic one during data collection from experimental testing, through methods such as fans removal and sudden power-off. They also highlight two main obstacles in the prediction process for noise and vibration:

- Acquisition of equivalent orthotropic material parameters of stator core and windings: as the stator core of the motor is composed by stacked silicon sheets, laid down in the axial direction, and windings are composed by coils wound around stator teeth, it is easy to see that the mechanical properties of stator core and windings are not isotropic; however, simulating their exact composition in the FEA software would be quite difficult and resource-consuming. However, this problem can be overcome by obtaining the orthotropic properties with one of the two following ways:
    - Direct measurement of material properties by ultrasonic method, which, however, requires some very specific equipment for data collection.
    - Approximation of modal frequencies by adjustment of orthotropic parameters in FE model: by exploiting symmetry of the structure and assuming a negligible effect of the Poisson's ratio on modal frequencies, it is possible to reduce the necessary information to four independent variables: E_x, E_z, G_{xy}, G_{xz}, where z is the axial direction of the motor and x is the radial one.
- Loading of the distributed electromagnetic force on stator teeth – Even though studies have shown that the EM force can be adequately represented by application to the center of stator teeth [19], [20], [21], the real force is distributed on a much larger surface.

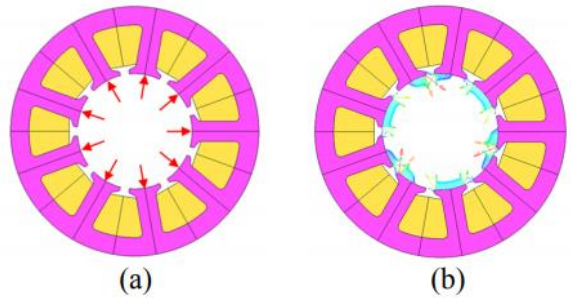

Figure 2.7. Loading method of electromagnetic force. (a) Concentrated force. (b) Distributed force [2] © IEEE 2019.

However, since the concentrated equivalent method might introduce significant errors in the computation, it is suggested to use a nodal transfer force method instead. With this technique, the nodal force calculated by the EM model is mapped into the structural model following interpolation through the use of commercial software, giving better results.

- Semi-analytical model: to get past the drawbacks of both the numerical and the analytic solution, a common practice is to combine them in one method. Several studies show that it is possible to obtain appreciable results in shorter time by computing the electromagnetic force via FEA, but then use an analytic approach to obtain the vibration and acoustic radiation. Even better accuracy can be obtained by computing the sound radiation efficiency with a numerical solution.

In their paper, Deng and Zuo also survey different methods to improve the vibrational and acoustic performance of PMSMs:

- Modal programming: this technique aims at moving the modal frequencies of the structure away from those of the electromagnetic force by adjusting structural parameters and characteristics.

- Electromagnetic force amplitude reduction: once the spatial order and the frequency of the EM force component that contributes the most to noise generation has been identified, it is possible to reduce its amplitude in several ways:

    - Optimization of electromagnetic parameters: those structural parameters which are most influential in noise generation are:

        - Slot opening width
        - Air gap length
        - Pole-arc coefficient
        - Thickness of permanent magnets

- Injection of compensation current: by injecting an appropriate compensation current, the armature reaction filed generated by it will create an electromagnetic force characterized by the same frequency and spatial order as the original one, but opposite phase and angle, which will weaken the amplitude of the former one. It is suggested to ascertain which spatial order and frequency of the EM force contribute the most to noise generation, which can be done via fast Fourier transform.

- Structure modification: this approach includes several modification techniques aimed at reducing noise and vibration, such as:

  - Stator skewing
  - Rotor skewing
  - Step and Harringbone skewing
  - Chamfering
  - Notching
  - Tooth shape modification

Moreover, the authors also address two additional issues related to noise generation in PMSMs:

- High-frequency tone noise: in addition to the EM noise mentioned up to now, there is another source of noise in PMSM driven by space vector pulse width modulation (SVPWM), which is generated by the sideband electromagnetic force induced by sideband currents due to inverter switching. This type of noise is extremely discomforting to the human ears and must therefore be addressed in automotive applications. Three different strategies are suggested to solve this issue:

  - Random modulation technique: this includes random carrier frequency modulation (RCFM), random pulse width modulation (RPWM), and hybrid random modulation, which is a technique able to simultaneously randomize pulse width and carrier frequency.

- Periodic modulation technique: this approach refers to Periodic Carrier Frequency Modulation (PCFM), which can be applied in different ways, among which are triangular modulation, sinusoidal modulation, square modulation, etc.

- Selective noise cancellation at specific frequency – whereas the two previous techniques aim at spreading the current spectrum, selective noise cancellation is implemented to create a gap around a specific frequency in the spectrum, either in the audible or non-audible range.

- Sound quality: most studies refer to the A-weighted sound power level (A-WSPL) as an indicator of noise performance for electric motors. However, this parameter presents some issues, such as:

  - A-WSPL is obtained by superposition of the sound power coming from the entire frequency range: while two different spectra may have the same A-WSPL, the human ear can perceive them in totally different ways, which means that the indicator is unable to reflect the perception of human beings, which is one of the most critical factors in this application. An alternative is to evaluate the sound pressure level instead of the power level, which better relates to human perception.

  - When PMSM's are driven by SVPWM, the inverter may cause a high-frequency noise which can affect human beings in a way the A-WSPL cannot reflect. Sound quality is instead better suited to this task, allowing the description of noise in terms of loudness, sharpness, roughness, articulation index, tonality and fluctuations.

Another major source of information for the development of this dissertation is [22]; in Varghese's work, the author further details the mechanisms responsible for electromagnetic noise generation, identifying four main distinct sources:

1. Effect of slotting: due to the repetitive nature of how permanent magnets, stator teeth, and windings slots are arranged in the motor, the magnetomotive force is periodically disturbed by the variation in the magnetic circuit reluctance due to the presence air gap, which results in strongly harmonic variations.

2. Iron magnetic saturation: this property of the metallic material results in a non-uniform distribution of the magnetic flux, which generates more harmonic components in the electromagnetic force.

3. Harmonics in voltage supply: due to the periodic nature of the signal used for PWM control of the motor, the voltage source is strongly characterized by harmonic components, which are consequently reflected in the EM force.

4. Rotor and stator eccentricity: as any small deviation from the ideal cylindrical shape of the air gap can cause a distortion in its permeance, eccentricity between rotor and stator would cause a non-uniform thickness in the air-gap, and therefore create periodic fluctuations in the electromagnetic force.

In addition, Varghese considers the noise evaluation task as a multi-physics problem, as it requires the involvement of multiple branches of physics to be solved; specifically, he defines the following magnetic-mechanical-acoustic system:

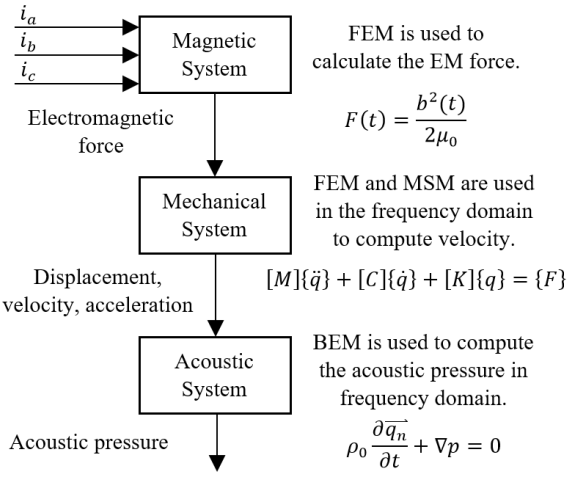

Figure 2.8. Magnetic-Mechanical-Acoustic System [22].

in which i_a, i_b, i_c represent the currents that introduce harmonics in the motor, and interact with the fundamental magnetic field by producing electromagnetic forces that excite the system in the same frequency range. As a result, the machine starts vibrating, generating a velocity pattern on the surface of the stator: these flexural waves interact with the surrounding air and generate audible sound.

Regarding excitations caused by eccentricities and deformations of rotor and stator, Li *et al*. [23], carry out an in-depth analysis of possible sources of core deformation for an IPMSM. Excluding excitations coming from the road profile, which are not strictly pertinent to this research as its subject is not an in-wheel motor, Li et al. describe several causes for air gap deformation:

- Eccentricities: several things may lead to eccentricity in IPMSM's, such as manufacturing tolerances, assembly quality, demagnetization faults, operating conditions etc. These defects can be present both in the radial and axial direction, but the former ones are much more common, and they can be grouped under three types: static, dynamic, and mixed.
- Stator deformation: excluding road excitations, the stator is subject to the radial vibrations at the second harmonic frequencies and the slot harmonics effect on the magnetic pull, which will cause the stator to deform into an elliptical shape after prolonged use; stator deformations have been found to significantly increase the vibration level of particular orders.
- Rotor deformation
    - Thermal deformation: caused by high operating temperatures.
    - Shoe pole deformation: caused by high centrifugal forces, it has a high degree of complexity and uncertainty.

2.2.2. Noise and Vibration Analysis Methods

Several works have been done in the past to study the NVH performance of IPMSMs:

- In the overview paper [13], the author proposes an extensive classification of mechanisms of noise generation in IPMSMs, which is key to understand how the design of the motor is linked to its vibrational behavior.

- In [24], both the numerical method and the analytic one are used: the former one to conduct a modal analysis of the stator, while the latter one is employed to compute the electromagnetic field and predict a response to electromagnetic excitation.

- In [25], the modal analysis is again conducted via FEM, but here also an experimental validation procedure is provided.

- In [26], the analytical model is used for the whole analysis, and it is coupled to numerical and experimental validation; the model presented in this paper goes as far as to predict sound power levels (SPL) of the noise generated by the motor. The radial pressure is computed with an integral over the cylindrical surface to which the stator is approximated. Radial displacement is computed based on material properties and strain due to the radial pressure in the structure. The SPL is obtained with a formula which combines the excitation frequency, some geometrical parameters of the motor, and the radial strain computed previously.

- Similarly, in [27] the analytical modelling technique is employed for every step of the analysis: it is used to characterize the EM force and also predict the natural modes of the stator; moreover, a numerical validation for the analytical model is provided. Vibration is evaluated by measuring minimum and maximum displacement in different vibrational modes, as well as by computing radial stress through radial force density, which is computed from the radial and tangential components of the magnetic flux through Maxwell stress tensor formula.

- In [28], analytical modelling is used to predict the SPL, while natural resonance frequencies are computed with FEA; moreover, this study evaluates the performance of a skewed stator and verifies the proposed model with experimental validation. Maxwell stress tensor is again used in the computation, but in this study the radial and tangential component of the magnetic flux filed are formulated in a way that takes into account the skew factor of the stator.

- The analytical approach is also used by Shin et al. in [29], where an extensive characterization of most electromagnetic quantities, such as magnetic field, 2D permeance function, back-electromotive force (back-EMF), torque ripple, and radial

force, is presented. Then, the results are validated with FEM, which is also used to obtain the results for the modal analysis and the vibration measurements.

- Another example of theoretical analysis is presented in [30], where the radial electromagnetic force wave form is developed analytically and then validated with experimental results.

- In [31], what the authors define as a "hybrid" computation method is used to predict noise and vibration in PMSM:

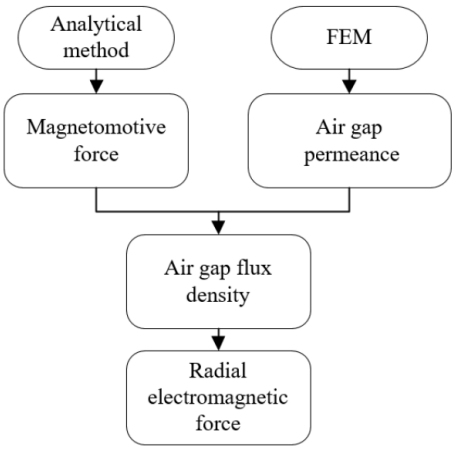

Figure 2.9. Hybrid calculation method [31].

By comparing the results of the hybrid method to the traditional FEM it is possible to see that the novel approach manages to achieve a good accuracy of results while saving considerable time when compared to a FEA-only approach.

- In [32], only numerical analysis is used to predict noise and vibration, by following this scheme:

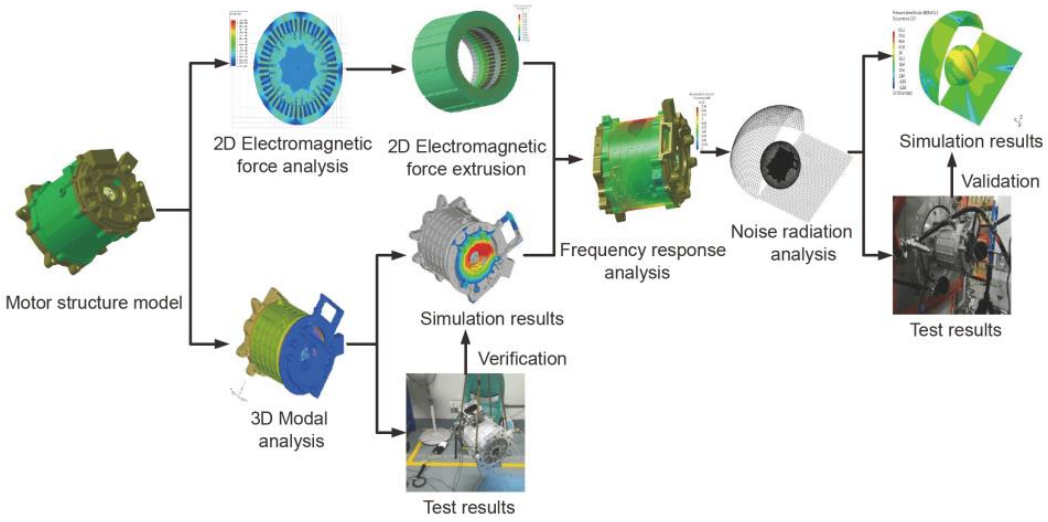

Figure 2.10. The study diagram on noise and vibration prediction of PMSM [32].

Moreover, this paper introduces a possible path for optimization, by studying the performance of a step-skewed rotor.

- In [33], the authors compute vibrational performance with a traditional FEM analysis, while also employing the principle of transfer path analysis to study how noise propagates from the motor. Qian *et al*.[33] suggest that the motor surface should be split into several smaller areas, each of which to be considered a source of noise, causing the air transfer path to the interior of the cabin different from the case in which the whole motor is considered the only point of origin. With this method, the electromagnetic excitation previously obtained with FEA is projected on the mesh of the motor, and radiated electromagnetic vibration acceleration is computed with the modal superposition method to define each small area of the motor as its own noise source. Then, a contribution analysis is carried out to evaluate which areas of the motor are most responsible for noise production, with the upper motor surface and motor junction box being the primary contributors.

- In [34], Lin *et al*. take into account a phenomenon that has so far been mostly neglected in the analysis of electromagnetic sources of noise: current harmonics. An analytical approach is used to characterize EM forces considering current harmonics, and then FEA is used to predict the vibration and noise behavior of the motor. It is then explained how current harmonics can change the vibration and noise peak value.

- In [35] and [36], the effect of magnetostriction on PMSM vibration is taken into account. In the first paper, Zhu *et al*. [35] conduct a numerical analysis based on a variational principle, which helps determining the non-negligible contribution of magnetostriction to stator deformation. In [36], the authors use a non-conforming mesh to improve the accuracy of the numerical solution, coupled with a magnetoelastic model.

- In [37] the concept of Unbalanced Magnetic Pull (UMP) is introduced as one of the main sources of electromagnetic vibration in PMSM, and an analytical model based on the Maxwell stressed tensor is proposed and then validated with numerical and experimental results. The UMP is caused by an asymmetric air gap between stator and rotor, and it increases rotor and stator eccentricity, introducing nonlinear vibrations.

- In [38], the radial EM force is analyzed, together with torque ripple and cogging torque for four different topologies of PMSM, to evaluate which is able to yield the best performances. The analysis is carried out both from a theoretical standpoint, for what concerns the electromagnetic characterization of the motors, and with a numerical approach, since the radial force distribution is computed through FEA. The results show that the 18/6 (18 slot/ 6 poles) topology obtains the best torque quality, while the 27/6 machines exhibits the lowest radial forces.

- Lin *et al*. also consider eccentricity between rotor and stator in [39], where they analytically derive the expression for the radial force as a function of static or dynamic eccentricity. Moreover, FEA is also carried out to validate the results, and to predict noise and vibration under different eccentricity types and lengths. Lastly, experimental data are collected to validate the prediction.

2.2.3. Optimization Techniques

In this section, the focus is on several strategies of optimization or improvement. They are analyzed to understand how to approach the issues of parameters selection and range definition in the current study.

- As mentioned before, in [32] the author proposes an optimization strategy based on the use of step-skewing. This technique uses a tridimensional model to study how the

skewing of core parts affects the performance of the motor and the NVH aspect. Even though this strategy can lead to significant improvement, it has not been chosen for this study because it is not applicable to a 2D model. A 3D model implies much higher computational times which were not compatible with the time frame of the project.

- Another idea for optimization is studied in [40], where two different solutions are proposed after a semi-analytical model is used to study radial force density:
  - The first approach introduces the method of sinusoidal rotor field poles, where the two equations (2.38) and (2.39) are used to determine how to alter the rotor surface. This technique uses the d-q reference frame to position the notches. The d-q model is a 2-phase equivalent circuit that is used to analyze synchronous machines, in which, for a simplified 2-poles motor such as the one in Figure 2.3, the direct axis (d-axis) is parallel to the rotor magnetic field, while the quadrature axis (q-axis) precedes it by 90˚ in the direction of rotation [41].

$$\delta(\beta) = \frac{\delta_d}{\cos\left(\frac{\pi}{\tau_p}\beta\right)} \tag{2.38}$$

$$r_{rotor,o}(\beta) = r_{rotor,o} + \delta_d - \delta(\beta) \tag{2.39}$$

    Where:

    - δ_d is the air-gap length in the d-axis
    - τ_p is the pole pitch
    - β is the angle relative to d-axis of the rotor
    - $\delta(\beta)$ is the air-gap length
    - $r_{rotor,o}(\beta)$ is the rotor outer radius dependent on β.

  - The second method is notching the rotor surface about the d- and q- axes, as shown in Figure 2.11:

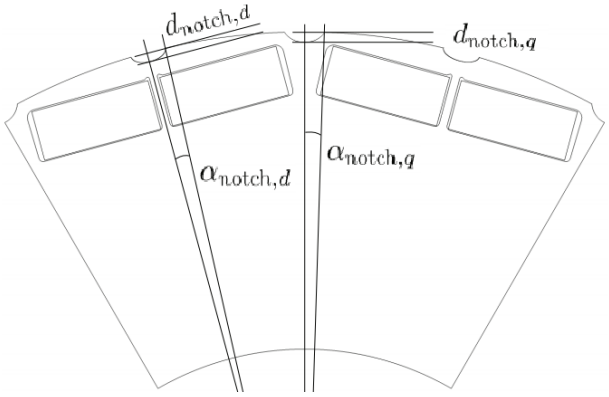

Figure. 2.11. Notch on *d*- and *q*- axes [40] © IEEE 2016.

- In [42], adjustment of slot opening is proven to be an effective way to improve vibrational behavior. Specifically, Slot Opening Width (SOW) is found to have a correlation with force harmonics, which allows to achieve a considerable reduction in noise when there is only one dominant peak resulting from high-permeance harmonics.

- In [43], optimization is carried out by acting on the shape and dimension of flux barriers. The model, presented in Figure 2.12, uses as parameters of the optimization problem the polar coordinates of the highlighted points of the flux barrier. The scope of the analysis is to find the best trade-off between torque, NVH, and structural strength. Results show that several solutions have to be invalidated as they do not provide the required structural strength. The analysis shows that the thickness of the bridge above the flux barriers is one of the most critical optimization aspects.

- Another approach is employed by Jiang *et. al*. in [44], where a very thorough optimization process is conducted about the introduction of slits on rotor circumference. The main objective of their work is to reduce the magnitude of the 48^{th} order harmonic component of the radial force, which is recognized as the main source of vibrations.

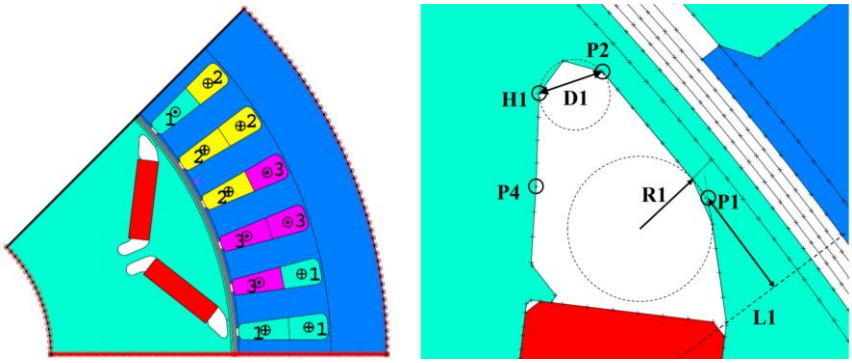

(a) (b)

Figure 2.12. Electromagnetic model used for optimization. (a) Electric machine pole model. (b) Parameters for study [43].

Moreover, this analysis in conducted over a range of six rotational speeds with 250 rpm increments, as to better simulate real working conditions for the machine. The problem is centered on minimizing the following function:

$$\Re_0 - \Re_j(\delta_i, \lambda_h, \gamma_j, \omega_k, \iota_m, \varepsilon_n) \qquad (2.40)$$

Where $\Re_0$ is the original magnitude of the 48th component, and $\Re_j$ is the magnitude relative to the j^{th} model of motor, as a function of the six following variables (where capital Greek letters symbolize the set of possible values they can take):

- Geometric variables
  - $\delta_i \in \Delta$ is the shape of the slit
  - $\lambda_h \in \Lambda$ is the circumferential width of the slit
  - $\gamma_j \in \Gamma$ is the location of the slit in polar coordinates
- Operating variables
  - $\omega_k \in \Omega$ is the rotational speed of the motor
  - $I_{pk,m} \in$ I is the amplitude of the peak current
  - $\varepsilon_n \in$ E is the excitation angle

The analysis is split into two phases:

- At first, a preliminary analysis is run for a few priority points to save time, to quickly identify which parameters have the most significant impact on the radial force reduction.

- Consequently, a more thorough analysis is run with 1920 operating points, which are studied with the help of a Matlab code that is written to compile scripting files, run the simulation, extract FEA results, and evaluate motor performances.

Even though it is very thorough, this type of approach is computationally heavy, as the high-dimensional analysis alone required almost 1300 hours of runtime to be completed.

- In [45] instead, the subject of the study is magnet positioning. The location of the two magnets for each pole is parametrized by using four variables, which are the subject of the optimization problem. Two objective functions are defined in the following way:

$$f_1 = T_{avg} \tag{2.41}$$

$$f_2 = T_{avg} - T_{rip} - 2 \cdot Vib \tag{2.42}$$

Where:

- T_{avg} is the average motor torque
- T_{rip} is the average torque ripple
- Vib is the average vibration acceleration
- 2 is a numerical coefficient deemed appropriate by the authors

Objective function 2 is used to reduce torque ripple and vibration acceleration without penalizing performance (motor torque). The four optimization parameters, shown in Figure 2.13 are studied by using the response surface methodology (RSM), in which they are combined into a quadratic equation defined by 81 coefficients. The algorithm increments the range of the parameters of 5% each step looking for the optimal point within the solution space. With this method, the best solution out of the 81 case studies achieves an average torque that is 105% of the original one, torque ripple is reduced to 81%, and vibration acceleration to 66%.

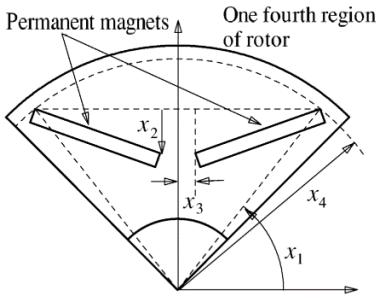

Figure 2.13. Parameters defining shape and location of PMs in the rotor [45] © IEEE 2011.

2.3. Novelty Introduction

As seen in section 2.2 of this chapter, the study of vibration sources and mechanisms in IPMSMs is a complex topic, but it has significantly been explored in the past, as the motor is not a recent technical invention. On the other hand, its application to the automotive industry on a scale such as the one we are experiencing nowadays requires some aspects to be developed to a degree that might not have been considered as important for other kinds of applications in the past.

Specifically, the very nature of the car industry, which is strictly tied to the harsh laws and trends of its market, makes the optimization of every aspect of each part introduced in a car essential to the success of the final product itself. For this reason, computer-aided design (CAD) and CAE are as prominent as ever, and the main method used to research and develop new technologies and procedures in most of the studies discussed so far, as they enable OEMs to save time and resources with respect to physical experimentation with the production and use of prototypes. Moreover, the application of PMSM technology to passenger cars as traction motors requires them to function in a varied range of working conditions, which is significantly different from that of the rest of common applications of this architecture. Other than temperature, which can influence the magnetic properties of the PMs and therefore motor performance, the use of IPMSM as traction motors implies that they must work, and perform well for that matter, in a wide range of speeds, and not only at their rated one.

Based on what has been developed in the literature so far, it is worth noting that even though optimization of core geometry has been considered and analyzed in several studies,

the vast majority only considered the motor to be running at its rated speed, which does not correctly portray the actual working conditions. Furthermore, most studies focused their optimization process on a limited area of the rotor or stator, such as flux barriers or teeth profile, without considering the variation of other geometric parameters and therefore failing to evaluate the effect of possible interactions between the different variables.

The novelty proposed in this study is to apply current state of the art procedures for vibration reduction to a limited set of geometric parameters that have a relevant influence on NVH performance, to study the interactions between them over a range of rotational speeds that simulates real working conditions for an electric propulsion motor in passenger cars.

The proposed methodology allows to act on few very influential design parameters to minimize vibration generation while guaranteeing satisfactory performance. This is achieved exploiting the accuracy provided by the FEM applied to a multiphysics system within the ANSYS platform, which is also able to simulate real working conditions by developing the analysis not only for the rated speed of the motor, but for a range of rotational speeds suitable for this application.

CHAPTER 3
MODEL SET UP AND PRELIMINARY ANALYSES

As mentioned before, the particular nature of the problem tackled in this dissertation requires a multiphysics approach, which means that several models have to be set up to accurately portray all the different physical phenomena. In this chapter, the different models used for the simulation are presented, applied to the different software used to implement them.

3.1. Electromagnetic Model

The first physical aspect of the model that needs to be portrayed is the electromagnetic one. This is done in two steps, with two different tools of the suite Ansys Electromagnetics.

The initial step is the generation of the electric machine with RMxprt. This software application is used to develop the geometry of several types of machines, and it can also be used to evaluate some preliminary performance indicators to approximately determine the quality of the design. Moreover, the program is considerably helpful due to its capabilities of determining several geometric and configuration parameters that the user can leave unspecified.

The machine used in this dissertation is defined by the following characteristics:

- It is an interior permanent magnet synchronous machine driven by a Y3 circuit fed by a 3 phase AC current.
- It has an external stator characterized by 48 slots of the shape depicted in Figure 3.1a. Stator geometric parameters include:
    - Outer diameter
    - Inner diameter
    - Length
    - Steel type
    - Press board thickness (null)

- Magnetic press board (null)
- Skew width (null)
- Lamination Sectors (null)

- The winding configuration in the stator is defined by the following parameters:
  - Winding layers
  - Winding type
  - Parallel branches
  - Conductors per slot
  - Coil pitch
  - Number of strands (auto-designed)
  - Wire size (auto-designed)
  - Conductor material

- The rotor is internal and characterized by 8 interior permanent magnet poles of the type depicted in Figure 3.1b. The geometric parameters used to define the rotor are:
  - Outer diameter
  - Inner diameter
  - Length
  - Stacking factors
  - Steel type
  - Pole type (also shown in Figure 3.1b)

Once enough parameters have been defined, RMxprt generates the geometry of the machine, automatically filling in those variables left blank for auto-determination. The result is visible in Figure 3.2, where the machine core geometry and the winding pattern are shown.

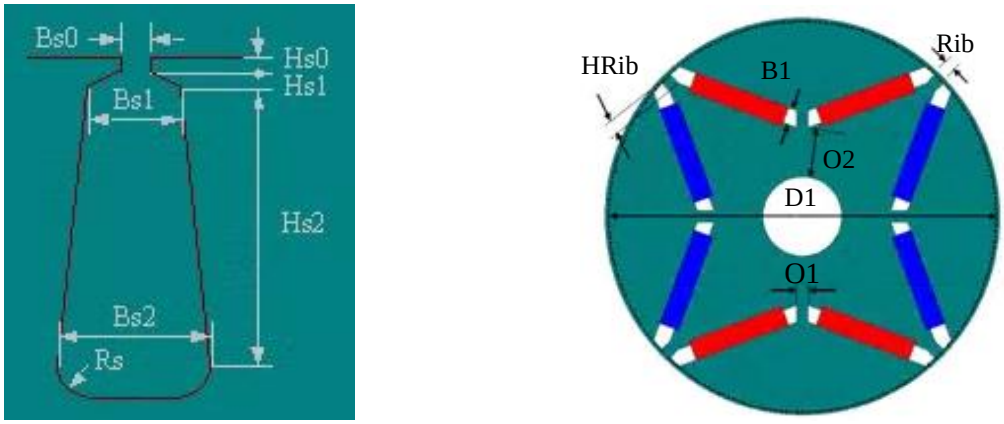

(a) (b)

Figure 3.1. Geometric parametrization of core. (a) Stator slot. (b) Rotor poles.

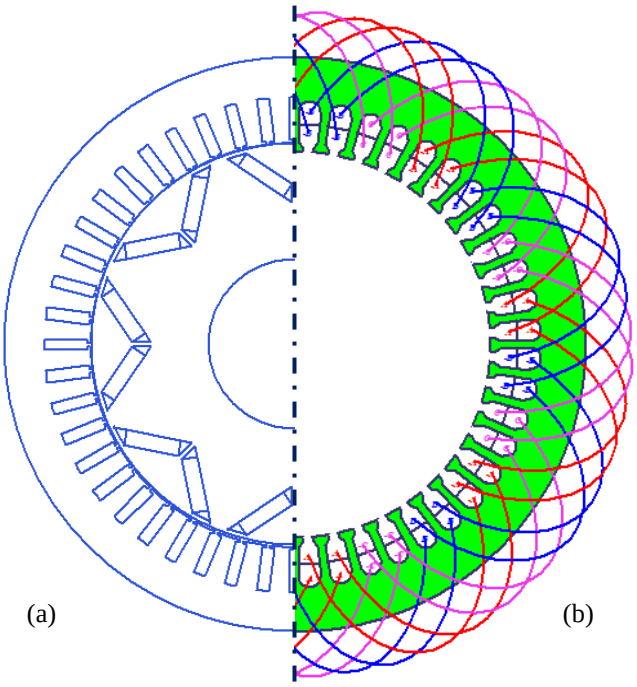

(a) (b)

Figure 3.2. RMxprt model. (a) Geometry of core. (b) Winding connection.

From this basic model, it is possible to generate a more complex one that will be analyzed within the Maxwell environment. For this dissertation, since the geometry and properties of the machine are constant along its axis, it was possible to choose a 2D simulation set up. Not only does RMxprt generate a two-dimensional model according to the given inputs, but it also creates the equivalent electric circuit for the motor, as visible in Figure 3.3.

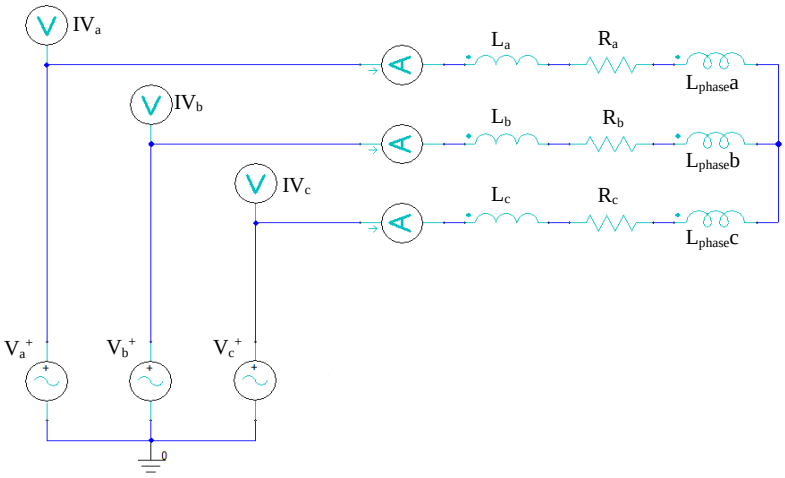

Figure 3.3. Electric motor equivalent circuit developed by RMxprt.

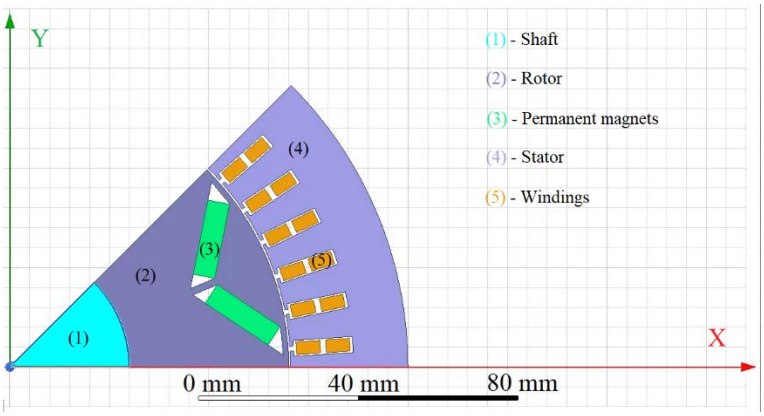

Figure 3.4. Maxwell 2D representation of one-pole model (1/8 of motor).

The 2D electromagnetic model of one pole is shown in Figure 3.4, where each part is highlighted by a different color. All of the parts are characterized by material properties which depend on the material assigned during the design of the electric machine in RMxprt. Referring to the denomination of Figure 3.4, the assigned materials are:

(1) Vacuum (since the shaft is excluded from the electromagnetic analysis of the motor)
(2) Electric steel – M19_29G
(3) Permanent magnet – VACODYM 764AP 20℃
(4) Electric steel – M19_29G
(5) Copper

Their most relevant material properties are presented in Table 3.1, while Figure 3.5 and 3.6 show the magnetization curve of the electric steel and the permanent magnet material.

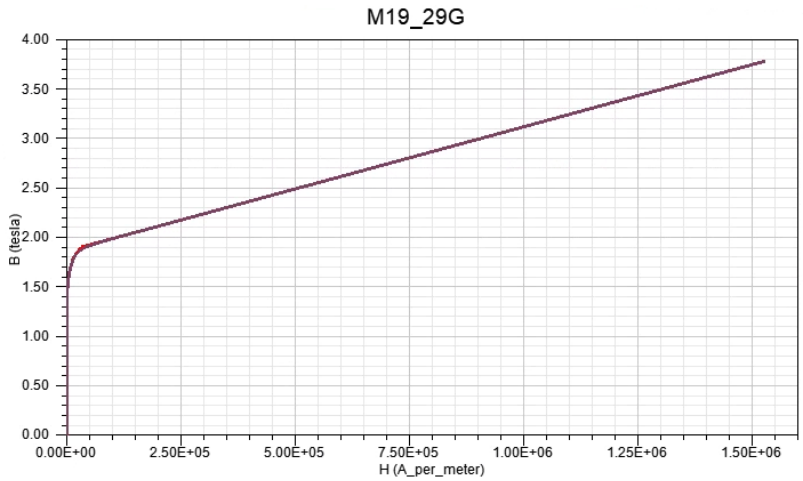

Figure 3.5. BH curve of electric steel M19_29G.

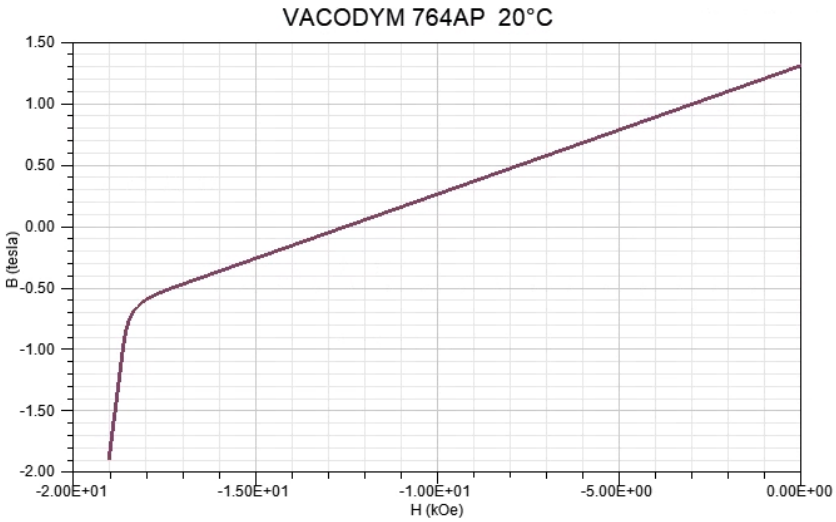

Figure 3.6. BH curve of permanent magnet VACODYM 764AP.

TABLE 3.1. ELECTROMAGNETIC AND OTHER PROPERTIES OF PMSM MATERIALS.

Property	**Electrical Steel**	**Permanent Magnet**	**Copper**
Mass Density [kg/m^3]	7650	7600	8933
Specific Heat [J/(kg ℃)]	Not defined	450	385
Relative Permeability	Nonlinear, see Figure 3.5	Nonlinear, see Figure 3.6	Simple 0.9999991
Bulk Conductivity [siemens/m]	1960000	714286	58000000
Magnetic Coercivity [kOe]	(0, 0, 0)	(0, 0, -12.5029)	(0, 0, 0)
Core Loss Model [W/m^3]	Kh = 164.2 Kc = 0.409 Ke = 0	None	None

In ANSYS Maxwell, core losses for electrical steel under sinusoidal flux conditions are computed in the following way [46]:

$$P_v = P_h + P_c + P_{ex} = K_h f (B_m)^2 + K_c (f B_m)^2 + K_e (f B_m)^{1.5} \tag{3.1}$$

If a DC component exists in the flux density, then the formula must be modified to

$$P_v = C_{DC} K_h f (B_m)^2 + K_c (f B_m)^2 + K_e (f B_m)^{1.5} \tag{3.2}$$

where

- K_h is the hysteresis loss coefficient
- K_c is the eddy-current loss coefficient
- K_e is the excess loss coefficient
- f is the frequency
- B_m is the amplitude of the AC flux component
- $C_{DC} = 1 + K_{DC} {B_{DC}}^2$, in which:
    - B_{DC} is the amplitude of the DC flux component
    - K_{DC} is the coefficient to consider the DC flux bias effects

Once created, it is possible to assign several boundary conditions to the model, which are necessary to accurately simulate the specific electromagnetic phenomena we want to investigate. Specifically, the following conditions are established:

- For the permanent magnets, a null current excitation is defined, and eddy current losses are enabled.
- For the rotor and the stator, core losses are enabled.
- For the windings, the driving current excitation is defined, with waveform as expressed in equation (3.3).

$$I_{s,i}(t) = I_{peak} \cdot \sin(2\pi \cdot f_e \cdot t + \delta - \phi_i) \quad (3.3)$$

Where:

- $i = a, b, c$ is the phase
- $I_{peak} = \sqrt{2} \cdot I_{rms}$ is the peak current
- $I_{rms} = 500\ A$
- $f_e = \frac{f_m \cdot p}{2} = \frac{n \cdot p}{120}$ is the electrical excitation frequency
- f_m is the mechanical rotational frequency of the motor
- $p = 8$ is the number of poles
- n is the rotational speed of the motor shaft
- $\delta = 40°$is the optimization angle to exploit saliency to obtain maximum torque
- $\phi_i = 0°, 120°, 240°$ is the phase angle

Once these operations have been completed, it is possible to analyze the performance of the motor. This is done with magnet transient analysis set up, in which the time step and analysis time are obtained from the frequency of the motor:

- $T_e = \frac{1}{f_e}$ is the period related to the excitation current frequency
- $T_s = 10\ T_e$ is the default total simulation time
- $t_s = T_e/100$ is the default simulation time step

Several characteristics related to performance can be investigated to evaluate the quality of the electromagnetic model. Some of these are:

- Moving torque: the mechanical torque measurable at motor shaft produced by the electromagnetic force moving the rotor.
- Cogging torque: mechanical torque measured at the shaft when the motor is running in no load conditions.

- Back-electromotive force (BEMF): is the voltage measurable in the windings when the motor is run at no load (no current or voltage excitations). This phenomenon is caused by the interaction of the moving magnetic field generated by the magnets with the copper coils in the stator, and it is responsible for a force that opposes the rotation of the motor.

- Efficiency: this parameter measures how much of the electrical power spent to drive the machine is converted into mechanical power delivered by the shaft. It is computed in the following way:

$$\eta = \frac{P_{out}}{P_{in}} = \frac{P_m}{P_e} \tag{3.4}$$

  where:

  - $P_m = T \cdot \omega$ is the mechanical power
  - $P_e = \sum_{i=1}^{3} I_i \cdot V_i$ is the electric power
  - I_i current of phase *i*
  - V_i induced voltage in phase *i*

The following figures show the waveforms in time of the performance parameters described above; for sake of brevity and clarity, the time axis is limited to 10ms as the motor reaches steady state quite quickly, and it would be redundant to show the graphs for the duration of the whole simulation.

Another detail that it is important to highlight is the definition of bands and inner and outer areas necessary to correctly set up the mesh for the EM analysis. The software needs the user to specify which part of the motor moves during operation, so that it can create the proper mesh in that area. This is done by creating different surfaces that enclose the physical parts of the motor.

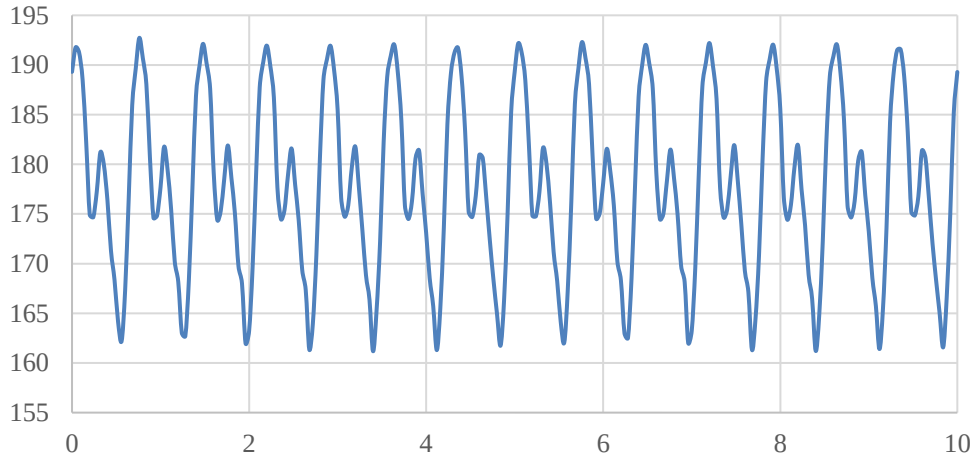

Figure 3.7. Moving torque [Nm] over time [ms].

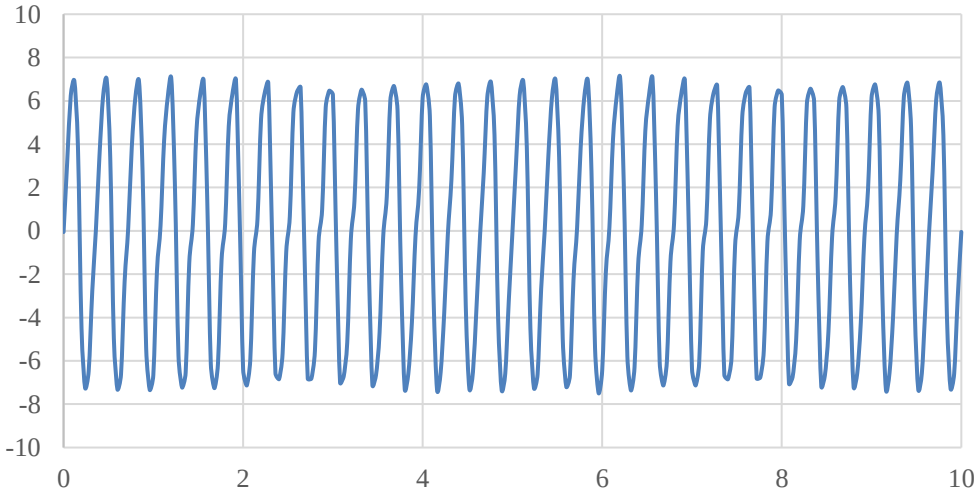

Figure 3.8. Cogging torque torque [Nm] over time [ms].

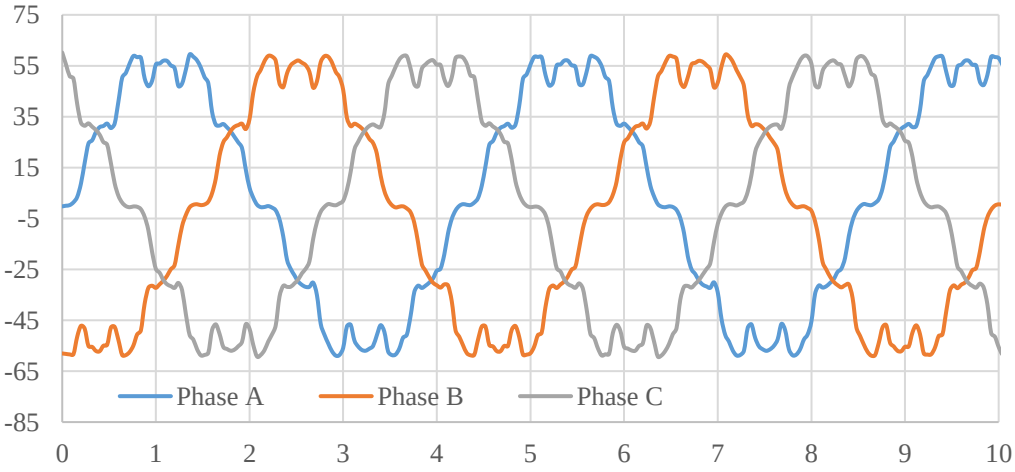

Figure 3.9. BEMF [V] over time [ms].

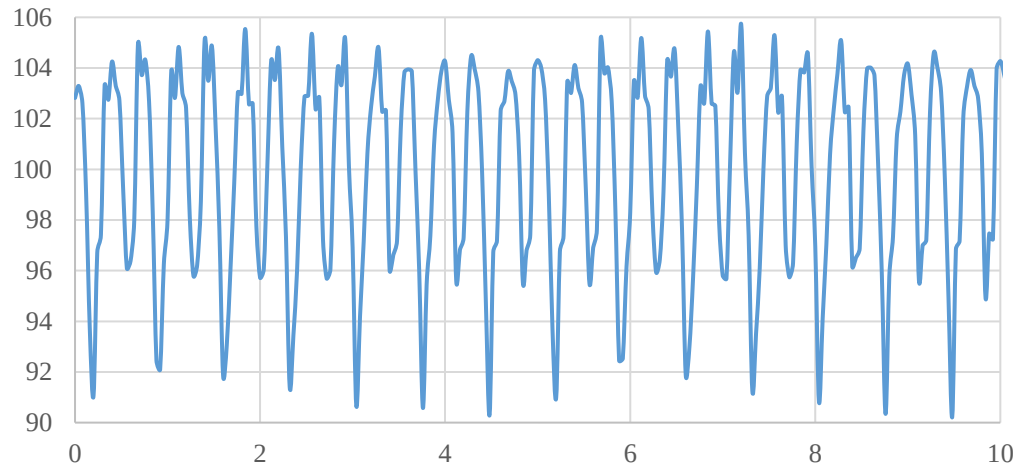

Figure 3.10. Efficiency [%] over time [ms].

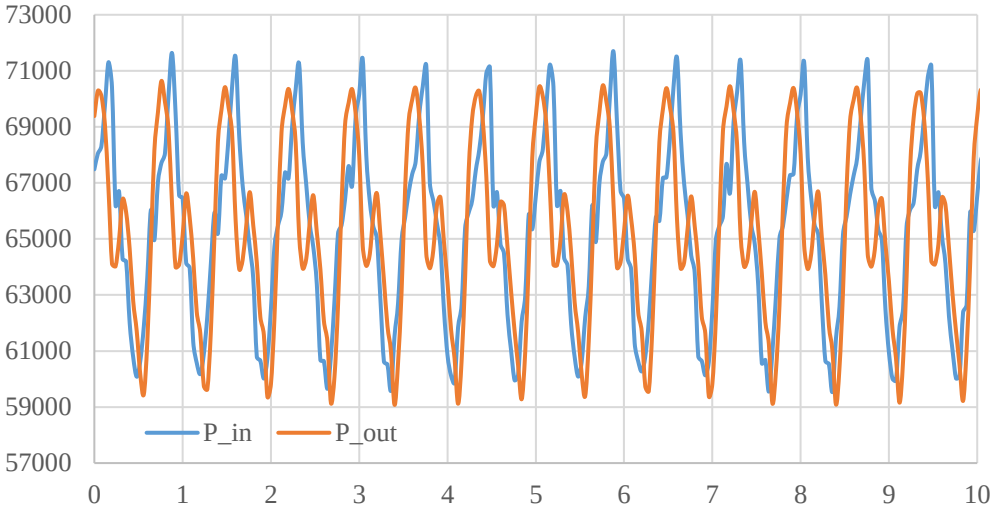

Figure 3.11. Input and output power [W] over time [ms].

Moreover, to improve the mesh scaling in the air gap in the radial direction, which improves accuracy, it is possible to set up multiple intermediate bands. These model objects do not actively take part to the simulation, but they are simply used to control and improve the meshing of for the FEA of the machine. The different bands are shown in Figure 3.12a.

Once the base setup is completed and the performance values have been evaluated to make sure they are satisfactory, it is possible to enable the simulation of electromagnetic forces. This tool, embedded in the Maxwell 2D application, allows to compute the EM acting on one or more surfaces or bodies of the model. Since, as it was seen in Chapter 2, it has been proven that the part that is most subject to vibration in IPMSMs is the stator, that

is where the forces will be computed. Specifically, our focus will be on the edge of the stator teeth, which are the areas highlighted in red in Figure 3.12b.

The role of the electromagnetic model is to simulate the EM forces, which act as external excitation in the dynamic analysis of the harmonic response of the stator. Once the EM model has been correctly setup to compute the forces on the stator, it is then possible to proceed to the next step in the multiphysics system, which is the model generated for the modal analysis, which will also be used to compute the harmonic response, as they both deal with the same structure, and physical aspects.

The overall scheme of the multiphysics simulation is visible in Figure 3.13, which represent the setup generated in Ansys Workbench, which is the software designed to couple different kinds of physical systems together. In it, it is possible to see the 2D electromagnetic system, solved in Maxwell, and the modal analysis and harmonic response systems, which are both solved within Ansys Mechanical.

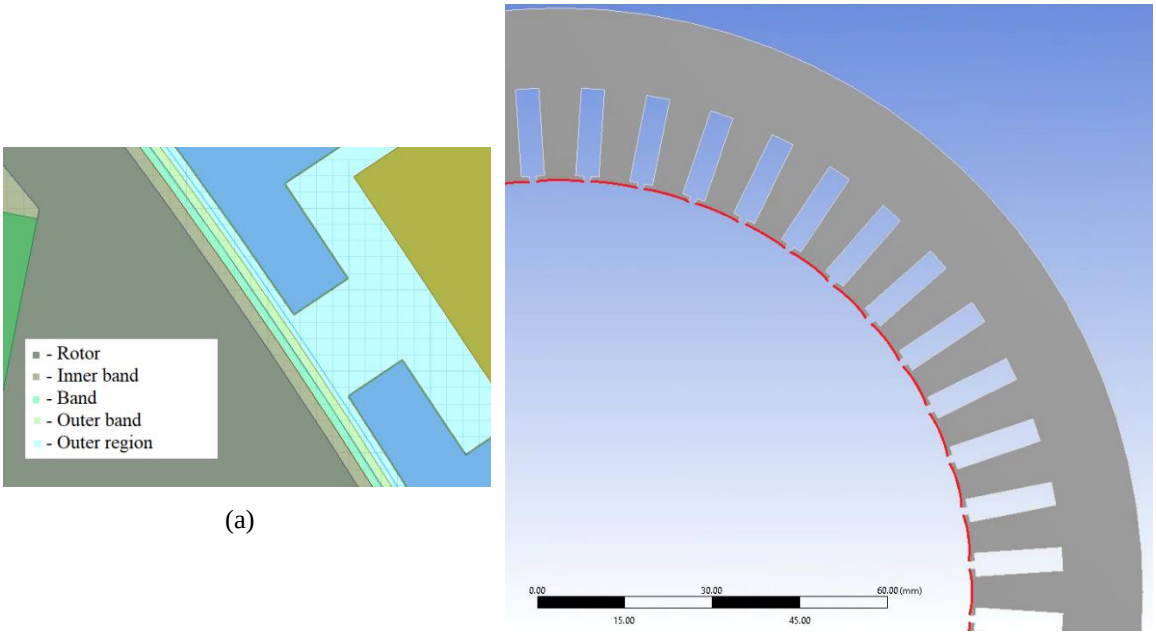

(a)

(b)

Figure 3.12. Electric motor core model details. (a) Definition of bands. (b) Stator teeth edges.

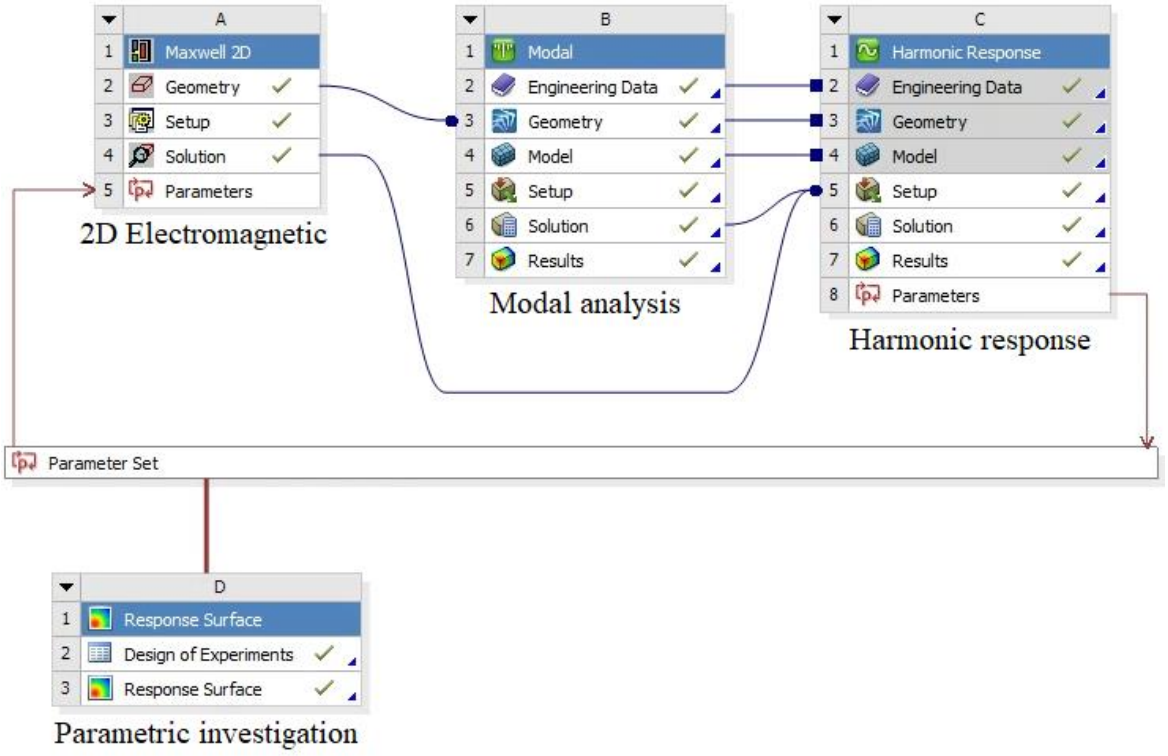

Figure 3.13. Multiphysics system setup in ANSYS Workbench.

3.2. Modal Analysis Model

As mentioned previously, the second part of the multiphysics system is the model that is used for the modal analysis. It is built on the geometry of the stator of the motor, but since the analysis requires the geometry of a whole structure, it is not sufficient to use what can be imported from the existing EM model. Therefore, as it will be explained later on, the housing geometry is added to that of the stator ring, to allow for the simulation of constraints.

Furthermore, it is necessary to define the material properties of stator, for which I choose to use structural steel, and for the housing, which is made of an aluminum based alloy, for which specific data was not available; therefore, the material employed for the housing was a generic aluminum alloy which was available in the software libraries. This decision is based on the fact that the motor on which the EM model is based, is built of electric steel, which is a material that has enhanced EM properties when compared to structural steel, but is similar enough from a structural point of view [48]. The properties

used for the analysis can be found in Table 3.2a. For the housing, instead, the lack of information on the properties of the alloy and the limited impact they have on the simulation results, justify the choice of simply using aluminum. Similar to steel, its properties are described in Table 3.2b.

Once the materials are chosen and their properties defined, it is possible to start setting up the modal analysis. Since the solver uses FEM to compute the natural resonance frequencies and mode shapes of the stator, it is necessary to apply a mesh to its surface. For this computation, a mixed mesh with both triangular and quadrangular elements, with element size of 1mm and program-controlled element order is chosen. Such element size is sufficiently small to obtain a mostly regular mesh, as it can be seen in Figure 3.9. Moreover, since the thickness of the model is uniform across its surface, it is sufficient to use a two-dimensional mesh, to which is added a thickness value that represents that of the original motor geometry, as defined in the previous section of the chapter.

TABLE 3.2A. MATERIAL PROPERTIES OF STRUCTURAL STEEL.

Material Property	**Value**	**Unit**
Density	7850	kg/m^3
Coefficient of Thermal Expansion	$1.2 \cdot 10^{-5}$	$(°C)^{-1}$
Young's Modulus	$2 \cdot 10^{11}$	Pa
Poisson's Ratio	0.3	
Bulk Modulus	$1.667 \cdot 10^{11}$	Pa
Shear Modulus	$7.692 \cdot 10^{10}$	Pa

TABLE 3.2B. MATERIAL PROPERTIES OF THE ALUMINUM ALLOY.

Material Property	**Value**	**Unit**
Density	2770	kg/m^3
Coefficient of Thermal Expansion	$2.3 \cdot 10^{-5}$	$(°C)^{-1}$
Young's Modulus	$7.1 \cdot 10^{10}$	Pa
Poisson's Ratio	0.33	
Bulk Modulus	$6.9608 \cdot 10^{10}$	Pa
Shear Modulus	$2.6692 \cdot 10^{10}$	Pa

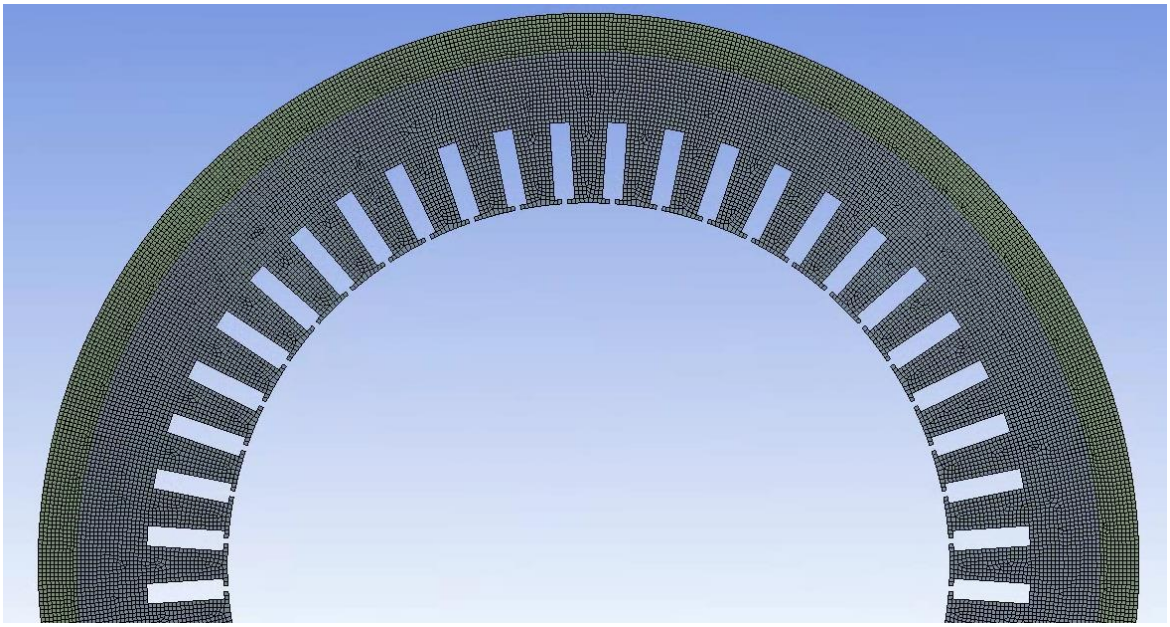

Figure 3.14. Mesh of stator surface (internal, grey) and housing ring (external, green).

Another important step is to create the selection of geometry that will be used to assign the external excitation, which is, in this case, the EM force coming from the 2D model. Since the force is distributed along the inner edge of the stator teeth, as seen in Figure 3.12, it is necessary to group together the edges of all the stator teeth. To do so, the software allows us to create an item called "Named Selection" which can be used to group together several individual geometric entities. To this named selection will be then applied the load in the harmonic response analysis.

The next step is to define the initial conditions and the modal analysis parameters. Specifically, after having defined material properties and mesh characteristics, it is necessary to define:

- Pre-stress conditions: since the analyzed part, which is the stator ring of the motor core, is not subject to any static loading, there is no pre-stress to be applied. Electric motors are usually fastened to a support structure through their housing, but the stator does not share any of the fastening loads. The modelling of the housing is explained later, together with how their interaction is simulated in this analysis.

- Analysis setting: the main parameters to be specified in this section are related to the natural modes. For the purpose of the simulation, 100 modes were deemed enough to

portray the desired effects, and therefore the search was limited to that number. Moreover, it was also possible to limit the search of natural frequencies within the 50000 Hz range. This decision was based on the spectrum analysis of the harmonic excitation. As seen in equation (2.16), the radial component of the force acting on the stator teeth is proportional to the magnetic flux; therefore, by analyzing the frequency spectrum of the latter, it is possible to obtain information about the former. By analyzing the waveform of the magnetic flux in a random point of the air gap (Figure 3.15, obtained with a time step equal to $1/100f_e$), it is possible to obtain information about its frequency spectrum using the Fast Fourier Transform (FFT). The distribution of the signal over the frequency range, shown in Figure 3.16, highlights that bandwidth of the excitation is internal to the 0 to 12000 Hz range, with the most significant components being below 4000Hz. This suggests that, even by raising the rotational speed of the motor, which would imply an increase in the frequency of the EM excitation, the effect of the most significant modes would still be taken into account up to a rotational speed that is three times the base one.

For the purpose of giving a thorough explanation, the results of the modal analysis of the stator in its nominal design version are presented here. The first 20 natural modes are shown to better understand the concept of mode shape deformation. The summary of the results can be found in Table 3.3 and Figure 3.17, where the table contains the list of natural modes and their respective resonance frequencies, while the figure shows the mode shapes and their deformation. It is important to point out that the figure only portrays a partial aspect of the deformation of the stator, since the phenomena, which happens in a tridimensional space for an unconstrained structure, is only captured in 2 dimensions. The actual modal analysis is instead carried out on the whole structure, so stator plus housing; however, the results are not shown here since the housing acts as a constraint on the stator deformation, which is therefore only visible in the teeth, while a free stator is free to deform in its actual mode shapes. Mode shapes are pattern of structural deflection which correspond to natural resonance frequencies. A freely vibrating structure deforms therefore in all the three dimensions.

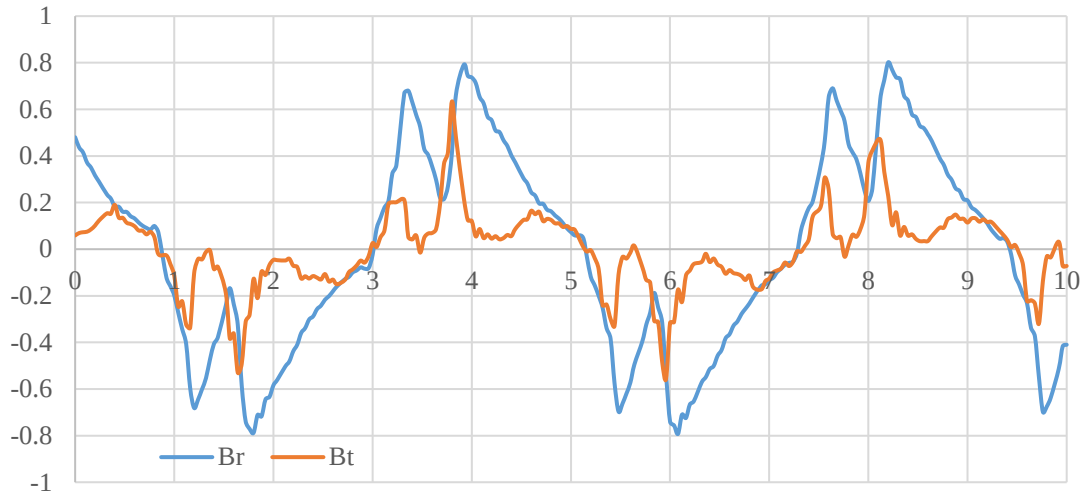

Figure 3.15. Magnetic flux in the air gap [T] over time [ms].

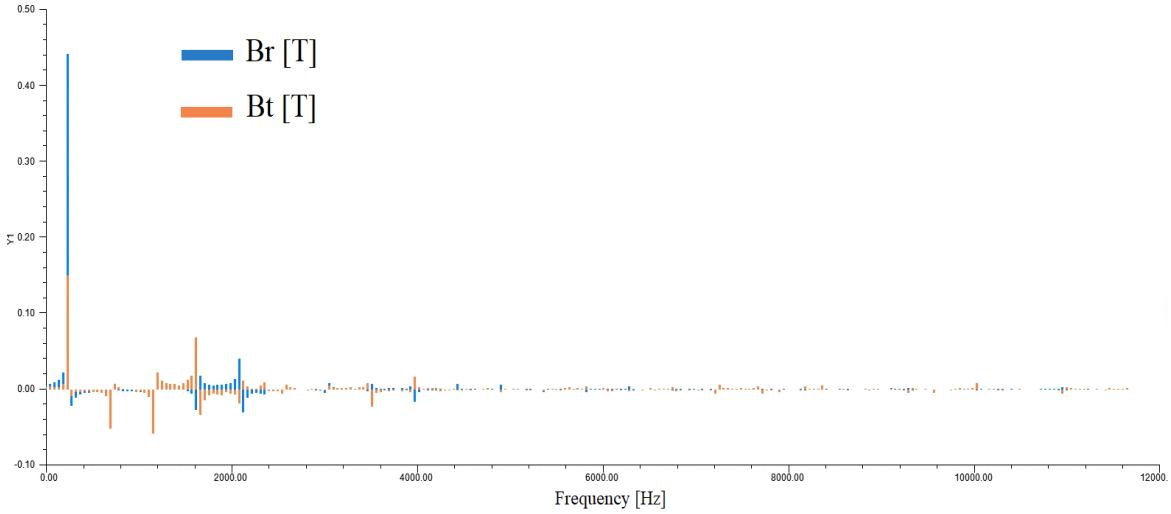

Figure 3.16. FFT of magnetic flux waveform in the time domain.

TABLE 3.3. FIRST 20 STATOR NATURAL MODES AND THEIR RESONANCE FREQUENCIES.

Mode	Frequency [Hz]	Mode	Frequency [Hz]	Mode	Frequency [Hz]	Mode	Frequency [Hz]
1	0.00250	6	2077.2	11	5375.8	16	9724.1
2	0.00475	7	2077.2	12	6827.5	17	9984.2
3	0.00594	8	3780.4	13	7779.5	18	9984.3
4	767.77	9	3780.4	14	7779.5	19	11393
5	767.77	10	5375.8	15	9724	20	11393

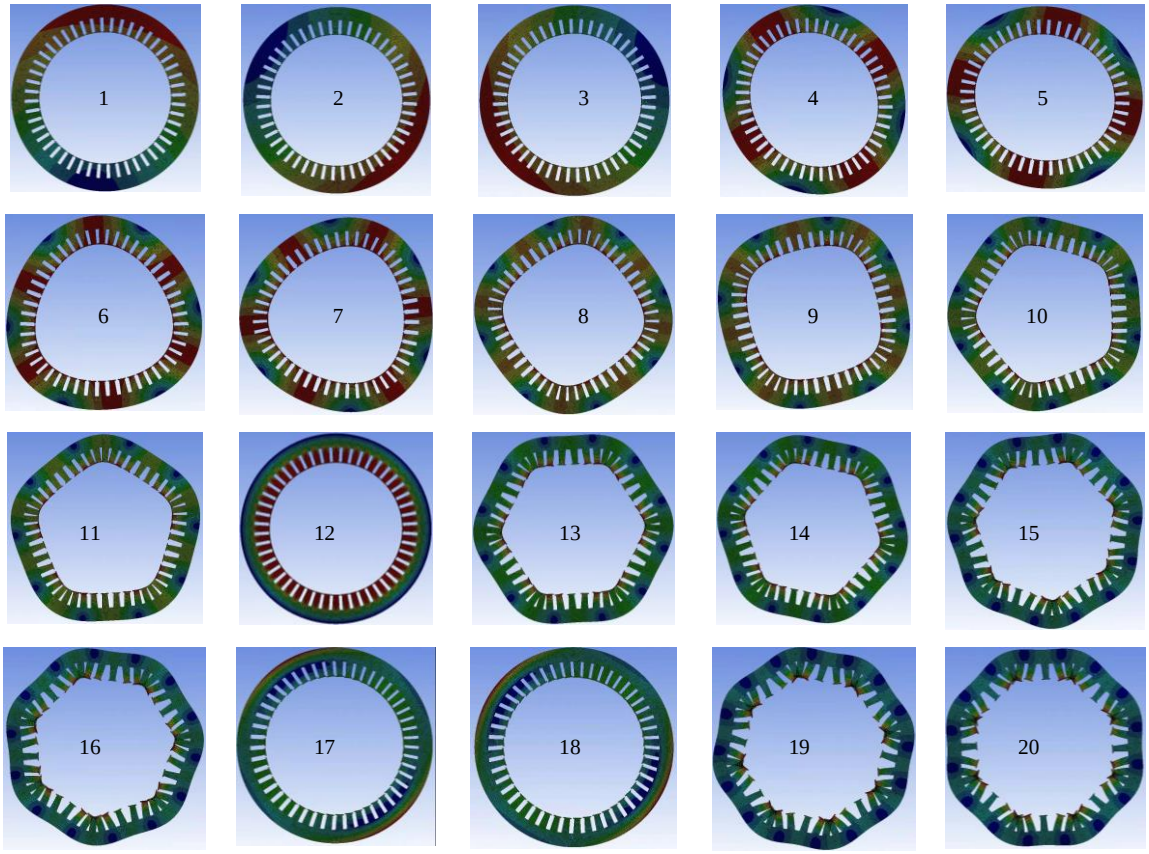

Figure 3.17. Natural mode shapes of the unconstrained stator.

To properly meausre vibration however, it is important to define all the boundary conditions of the simulation. In this case, adding constraints to the stator is the main task to be performed, as other parameters such as ambient temperature, pressure, and humidity are hardly relevant for this type of analysis.

As in most common architecturs for PMSMs, the stator is constrained by an external body called housing, which is also used to protect and isolate the core from the external environment. The housing acts as an external sleeve which holds the stator in place. For the scope of this project, it was decided not to simulate the whole body, which would have required a 3D analysis, and in turn much longer computation times; instead, the housing is modeled as an annulus ring which represents the section of the piece directly in contact with the stator. The choice of keeping consistency with the bidimensionality of the EM modal was made because the radial effect strongly prevail on the axial ones, and therefore it was worth compromising in order to save computational time. Moreover, a 3D model would

have required more detailed geometric specification about the housing strucutre which was not available from the manufacturer. Basing the model on the architecture of air-cooled IPMSMs, the cylindrical sleeve that constraints the stator often includes fins used to dissipate heat, and the fastenings to the chassis. For the scope of this project, the fins are not simulated since they do not influence the vibration sources, while fastenings are simulated with a fixed support assigned to the external surface of the housing. The contact between the housing and the stator, which is responsible for keeping the stator in place, is simulated with a “no separation connection”, since data about friction and other characteristcs of surface interaction was not available. The two boundary conditions applied on the model are visible in Figure 3.18.

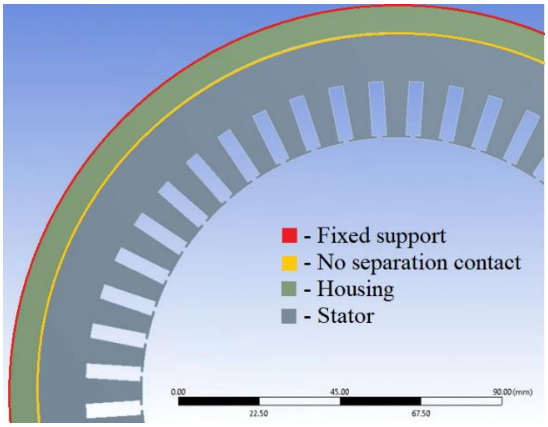

Figure 3.18. Boundary conditions in mechanical model.

3.3. Harmonic Response Model

In Ansys Workbench, it is possible to create a harmonic response simulation that shares the model with the one used for the modal analysis, as it can be seen in Figure 3.8. This means that the material properties, the geometry of the stator, as well as the mesh generated previously are all shared to the model for the harmonic response analysis.

Moreover, it is possible to link both the solutions of the electromagnetic and the modal analysis to the setup stage of the harmonic response system, to exploit the results of those simulations. This feature is essential to the analysis as it gives the foundations for the multiphysics system and it enables to solve the computation of vibrations with the modal superposition method. Specifically, by linking the three simulations as described until now

and pictured in Figure 3.8, the information regarding the natural resonance modes and frequencies of the stator, contained in the solution of the modal analysis, is shared to the harmonic response solver, while the information about the external excitation is obtained from the solution of the 2D EM analysis of the motor.

As mentioned before, the electromagnetic forces, computed by the software using the Maxwell stress tensor method (explained in section 2.1.2), are extracted from the EM solution and mapped to the internal edge of stator teeth in the Mechanical model. The forces are computed on the EM model, and to map them onto the geometry of the mechanical model, it is necessary to modify the former one. Specifically, an arc is created in the air gap and then split into several segments in correspondence of the stator teeth tips, as it can be seen in Figure 19.a. For this study, the loads are evaluated and then mapped as concentrated forces, meaning that the pressure on each stator tooth tip is taken into account as a single force (and torque, if present).

Once the loads are imported and generated onto the stator teeth edges, it is possible to proceed with defining the characteristics of the analysis. Specifically, the solver allows the user to determine which strategy to employ in the selection of frequencies to use for the evaluation of output parameters such as deformation, velocity, or acceleration of the stator surface.

Since the solution method chosen for this analysis is the modal superposition method, the evaluation of results should include the natural resonance frequencies computed in the modal analysis. To do so, it is possible to use the option “cluster frequencies”, which solves for the output parameters at all the natural frequencies. Moreover, to take into account resonance peaks, the solver computes solutions for a set of frequencies centered around the natural ones; the size of the set is defined cluster number.

Last, damping is defined for the stator structure with a constant damping ratio appropriate for the material properties and the analysis type. Since the stator is made of solid steel, and there are no fluids simulated in the model, nor any other elastic structure nor material, damping is strictly caused by the hysteresis and internal frictions effects of the material of the stator.

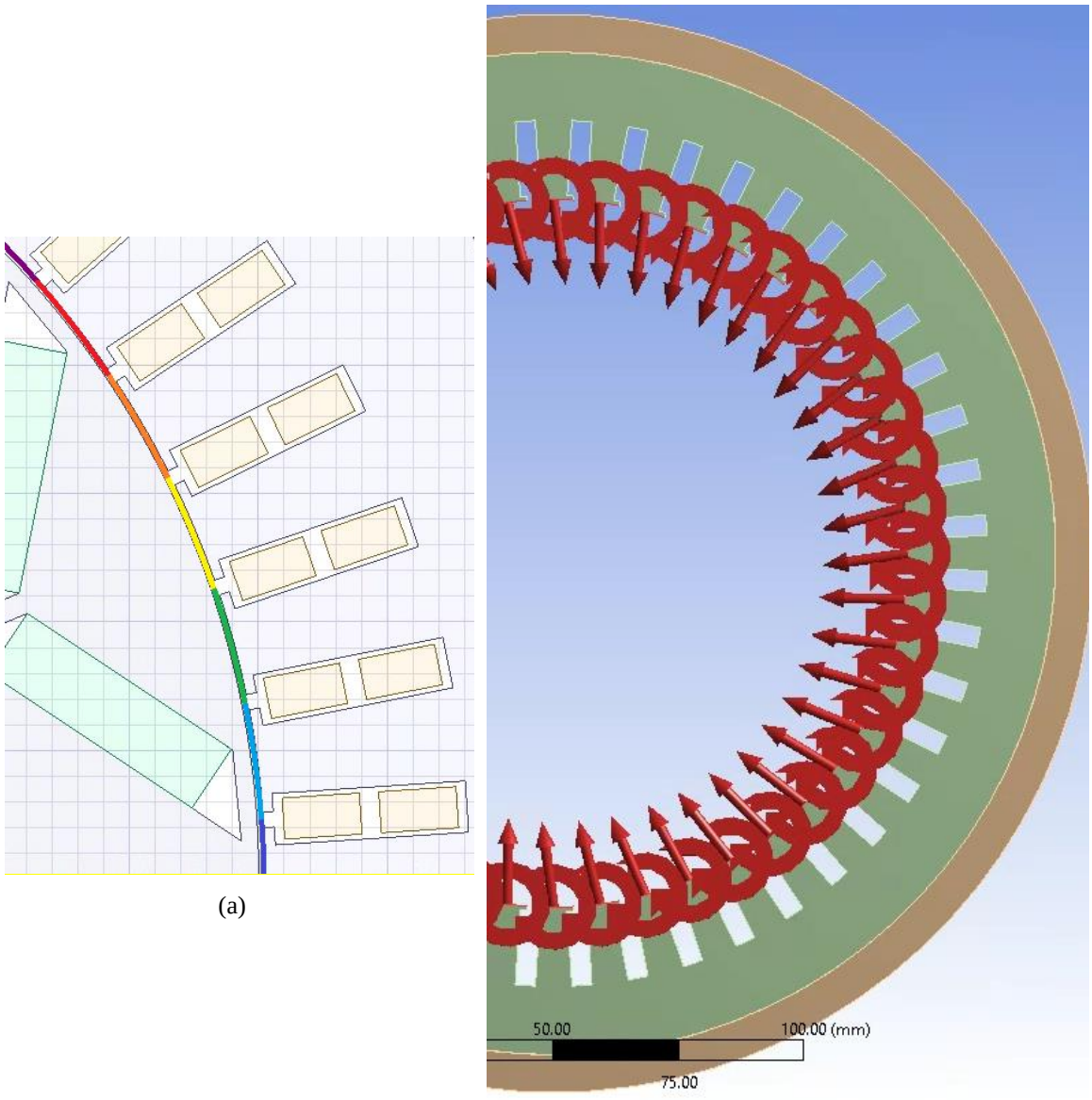

(a)

(b)

Figure 3.19. EM Force mapping. (a) Segmentation of pole arc. (b) Loads imported in mechanical solver.

CHAPTER 4
PARAMETRIC INVESTIGATION

4.1. Sensitivity Analysis

When trying to reduce the vibrations generated by the electromagnetic forces acting in the motor core, it is possible to adopt two main strategies. The first one is to act on the control algorithm of the source current to modify the harmonic content of the EM excitation and mitigate the vibration source. The second is to modify the motor structure and geometry of its parts to make it less responsive to the excitations. Several such methods have been employed in the past, some of which are reviewed in chapter 2, but most studies tend to only focus on an area of the motor core as the subject of the variations for optimization, such as notching of the core surface [32], adjustment of slot opening [42], and shape modification of flux barriers [43].

To obtain a more comprehensive understanding of which factors have the greatest influence on the generation of vibration through EM forces, a sensitivity analysis is carried out on 17 geometric parameters that define the topology of the core, which are shown in Table 4.1 and refer to the pole and slot geometry described in Figure 3.1 at the beginning of the previous chapter.

Thanks to the parametrization tools available in Maxwell, it is possible to define the geometry of the core in the following way:

$$l_i = l_{n,i} + x_i \tag{4.1}$$

where:

- l_i is the total length of variable i, in mm
- $l_{n,i}$ is the nominal length of variable i in mm, as per Table 4.1
- x_i is the adjustment term of variable i, which will be varied in the analysis

therefore, the original design version is obtained with $x_i = 0 \ \ \forall i$, where i is the number of the variable, as per Table 4.1.

TABLE 4.1. GEOMETRIC PARAMETERS FOR SENSITIVITY ANALYSIS.

Variable number	Core part	Variable name (as in Figure 3.1)	Nominal value [mm]
1	Stator	Inner diameter	141.1
2	Slot	Hs0	0.8
3		Hs1	0
4		Hs2	15
5		Bs0	1.2
6		Bs1	4
7		Bs2	4
8		Rs	0
9	Rotor	Outer diameter	140.1
10	Pole	D1	137.5
11		O1	1.7
12		O2	19.44
13		B1	5.5
14		Rib	5.96
15		Hrib	0
16	Magnet	Magnet thickness	5.5
17		Magnet width	38

The analysis is aimed at selecting a small number of variables from this larger set which nevertheless are the most relevant in influencing the electromagnetic forces which cause vibrations. Since, as seen in [13], the most important component of the EM forces responsible for vibrations is the radial Maxwell force, which is connected to the magnetic flux, as seen in section 2.1.2, the sensitivity analysis is based on the computation of 3 output parameters: the average motor torque, the maximum radial magnetic flux and the maximum tangential magnetic flux. The first parameter is used to monitor the performance of the motor, while the latter ones are used to evaluate the influence of each parameter on the magnetic flux generation.

4.1.1. Single Variable Sensitivity

The first step in the sensitivity analysis is to study the response of the magnetic flux and torque to the variation of each parameter, one at a time. Moreover, this study helps to identify the boundaries of the range of possible values each variable can assume due to the geometric constraints of the structure. To better explain, each variable has a limited set of values that result in a feasible design: for example, if the stator inner diameter becomes

smaller than the rotor outer diameter, the design cannot be generated, therefore the value used in such iteration for the stator diameter is not feasible.

The extrema of the variation range of each variable were also found by taking into account performance constraints, through the monitoring of the average motor torque value. The threshold for acceptability was chosen to be 95% of the value corresponding to the nominal design version. The results of the analysis are presented in Table 4.2, where the percentages refer to the values of the nominal design, and Figure 4.1. From the table, it is possible to see which variables affect more the torque generation and the two components of the magnetic flux (radial and tangential), as well as the range boundaries and the step size for the analysis. In Figure 4.1, it is possible instead to understand the proportionality between the variation of each geometric parameter and the components of the magnetic flux. We can see that, even though few variables are characterized by a strictly direct or inverse proportionality, it is possible to distinguish a set of parameters that have a significantly stronger influence on the flux than the rest. The characterization of the proportionality between the two components of the flux and the geometric parameters is summarized in Table 4.3

TABLE 4.2 FIRST ROUND SENSITIVITY ANALYSIS RESULTS.

Name of variable	Step size [mm]	Lower limit [mm]	Upper limit [mm]	Torque variation [%]		Br variation [%]		Bt variation [%]	
x_1	0.29	-0.71	0.14	97.7	106.3	102.7	116.5	34.8	106.0
x_2	0.22	-0.56	1.00	98.6	99.9	93.9	111.7	79.1	111.0
x_3	0.17	-1.00	0.50	99.6	100.0	91.7	101.8	96.9	100.4
x_4	1.00	-7.00	2.00	95.8	103.2	84.4	102.7	99.7	100.7
x_5	0.22	-1.00	1.00	99.4	100.0	101.1	104.5	85.6	121.2
x_6	0.56	-3.00	0.89	96.6	104.6	95.1	106.8	76.5	110.6
x_7	0.56	-3.00	2.00	95.2	103.3	99.7	104.1	99.8	102.6
x_8	0.30	0.00	3.00	97.0	100.0	100.6	101.8	95.7	102.6
x_9	0.33	-0.33	0.67	95.7	104.6	84.4	105.4	93.0	113.8
x_{10}	0.14	-0.23	1.00	99.6	101.2	101.4	103.5	98.2	100.9
x_{11}	0.11	-1.00	0.26	99.6	101.0	101.8	103.1	99.8	102.0
x_{12}	0.55	-5.00	-0.09	97.1	99.9	93.4	101.8	100.5	106.3
x_{13}	0.27	-2.50	-0.05	95.5	99.9	89.0	101.6	99.9	104.0
x_{14}	0.27	-2.50	0.23	96.2	100.3	98.3	102.0	100.1	100.5
x_{15}	0.08	0.00	1.00	99.0	99.9	91.7	101.7	97.6	100.4
x_{16}	0.41	-0.36	2.50	97.1	101.3	100.9	102.7	100.4	100.7
x_{17}	1.05	-2.63	-0.53	96.2	99.1	97.2	102.5	100.6	105.7

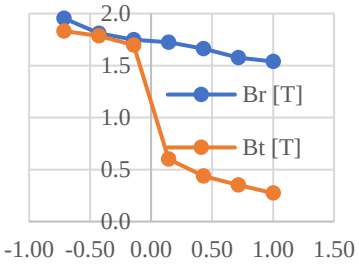

(1)

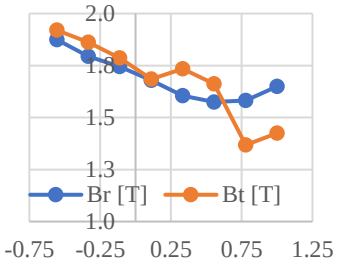

(2)

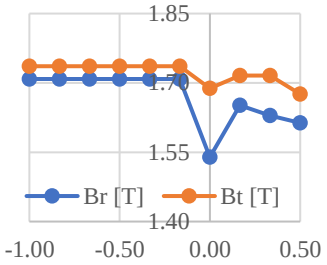

(3)

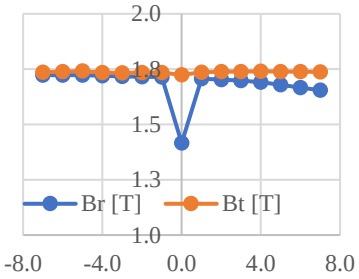

(4)

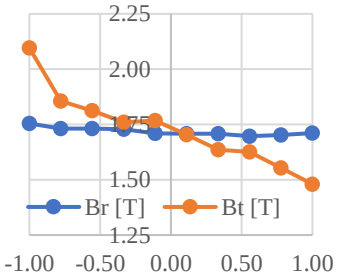

(5)

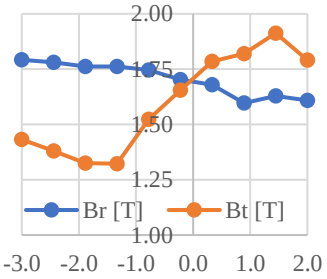

(6)

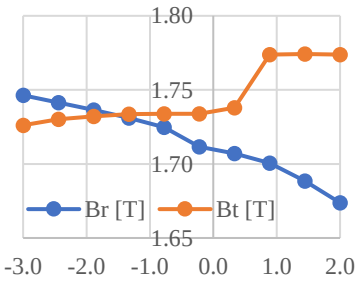

(7)

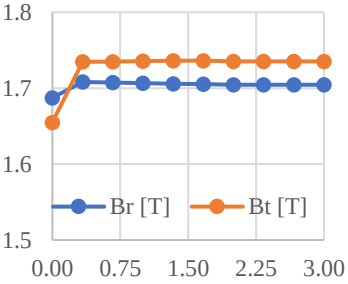

(8)

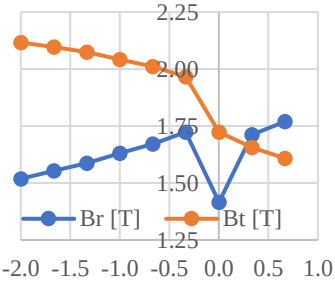

(9)

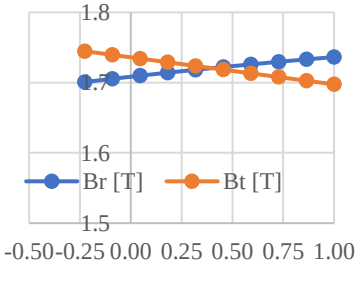

(10)

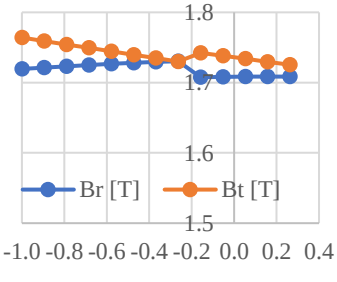

(11)

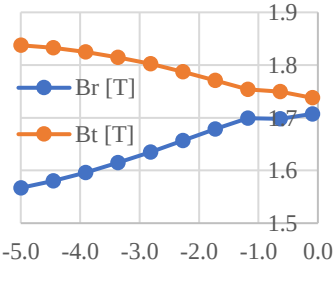

(12)

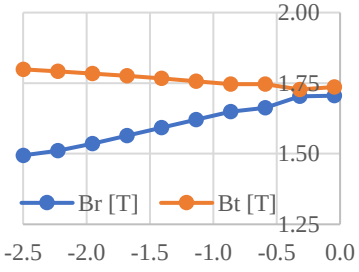

(13)

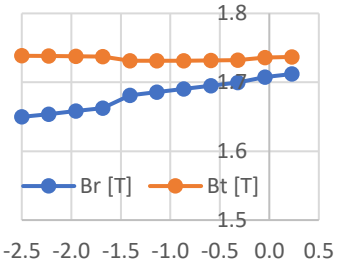

(14)

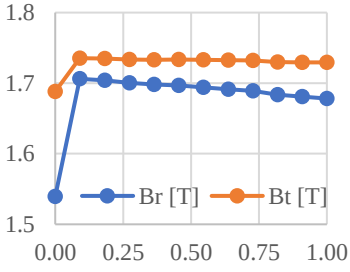

(15)

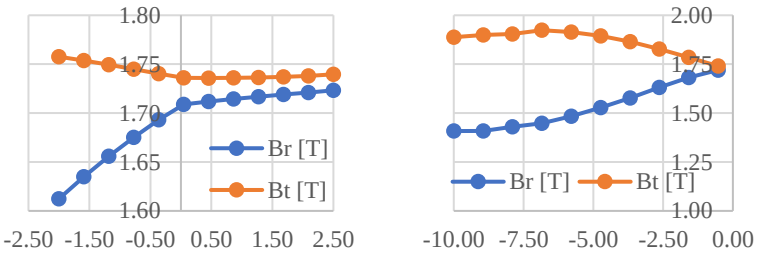

(16) (17)

Figure 4.1. Results of first round sensitivity analysis. Magnetic flux in the air gap [T] over variation of geometric parameters x_i [mm].

TABLE 4.3. RELATIONSHIP BETWEEN MAGNETIC FLUX COMPONENTS AND VARIATION OF GEOMETRIC PARAMETERS.

	Proportionality of radial flux Br	**Proportionality of tangential flux Bt**
x_1	Mostly inverse	Mostly inverse, significantly piecewise
x_2	Mostly inverse	Mostly inverse
x_3	Absence of general trend	Absence of general trend
x_4	Absence of general trend	Mostly negligible proportionality
x_5	Mostly negligible proportionality	Mostly inverse
x_6	Mostly inverse	Mostly direct, significantly piecewise
x_7	Mostly inverse	Mostly direct, significantly piecewise
x_8	Mostly negligible proportionality	Mostly negligible proportionality
x_9	Mostly direct, significantly piecewise	Mostly inverse, significantly piecewise
x_{10}	Mostly direct	Mostly inverse
x_{11}	Absence of general trend	Mostly inverse, significantly piecewise
x_{12}	Mostly direct	Mostly inverse
x_{13}	Mostly direct	Mostly inverse
x_{14}	Mostly direct	Mostly negligible proportionality
x_{15}	Mostly negligible proportionality	Mostly negligible proportionality
x_{16}	Mostly direct, significantly piecewise	Mostly inverse, significantly piecewise
x_{17}	Mostly direct	Absence of general trend

From this first round of analysis, it was possible to conclude that variables 7, 8, 10, 11, and 14-17 are mostly negligible when it comes to influencing the magnetic flux, and can therefore reasonably be ignored when investigating the sources of vibration.

4.1.2. Multiple-Variable Sensitivity

Since the optimization procedure becomes significantly more computationally heavy the more variables are used in it, it is necessary to further reduce the pool of geometric parameters to be considered from the analysis. The second step in the process is to consider interactions between related variables.

First, a series of 2-variable sensitivity analyses was carried out for variables related to each other from a geometric point of view. For example, variables 1 to 6 all describe the geometry of the stator, with variables 2 to 6 defining slot dimensions. This procedure highlights which variable is predominant over the others in determining the magnetic flux density. In the next page, Table 4.4 shows the evaluation of the aforementioned group of variables, using x_2, which is the slot aperture, as the base variable and studying the interactions of the others with it.

Another technique was also used to investigate the relationships between smaller groups of variables. In these two cases, one for rotor and one for stator, 3 parameters of each component are evaluated together with a full factorial technique, in which each parameter has 6 levels within its range. For the stator, variables 3, 4, and 5 are investigated together, while for the rotor, variables 9, 12, and 13 were used.

As visible in Tables 4.4-6, it is possible to exploit conditional formatting to investigate which variable has a predominant effect on each output parameter. In the first table, the average motor torque and the maximum radial and tangential flux densities are evaluated, while in the second table the efficiency is also computed. Each column is formatted so the color scale shows the relative position of the cell when compared to the others displaying the same physical quantities. This allows to study the color gradient patterns and determine which parameter has the strongest influence on a physical quantity. Moreover, it is important to specify that those cells in the motor torque column which have underlined values, are those design versions in which the torque does not satisfy the performance criterion, which is to generate at least 95% of the nominal design motor torque. As a last note on how to read this group of tables, it is necessary to explain that those cells

containing “nan” in Table 4.4, indicate that the computation was not possible because the geometry resulting from that combination of parameters is not feasible.

For example, in Table 4.4, to determine whether a geometric parameter x_i is more influential than the reference x_2, it is possible to look at the color gradient of a column: if the cells are mostly uniformly fading to the same shade over the whole column, then the influence of the reference is stronger than that of the analyzed variable; on the other hand, if the color scale has a pattern which somewhat repeats every 6 cells, which is the number of levels of each variable, then the reference is weaker than the analyzed variable. With this approach it is possible to determine, for instance, that x_1 and x_6 have the strongest influence on torque and Br, while x_5 and x_6 have the strongest influence on Bt.

Similarly, by applying the same logic to Tables 4.5 and 4.6 it is possible to further reduce the set of variables that will be used for the optimization strategy and the DoE. Specifically, it was possible to determine that variables 3, 4, and 12 are not as important as the rest when it comes to affecting magnetic flux density. To obtain a set of 5 variables, which was the target size set at the beginning of the sensitivity analysis, parameters x_1 and x_9 are dropped.

This choice is made because these two parameters affect the dimension and position of the air gap, which is where the EM forces are measured for mapping. By moving or changing the air gap, there is a very high risk that the EM model defined so far would not be suitable for the accurate computation of the forces, since the bands (defined in Section 3.1), and the arc on which the forces are measured would stay in the same location as they do in the nominal design version, which might not be compatible with the dimensions generated by varying parameters x_1 and x_9.

The origin datasets for Tables 4.5 and 4.6 can be found in Appendix A.

TABLE 4.4. 2-VARIABLE INTERACTIONS OF STATOR GEOMETRIC PARAMETERS.

x2 [mm]	x3 [mm]	Br_{max} [T]	Bt_{max} [T]	Torque [Nm]	x4 [mm]	Br_{max} [T]	Bt_{max} [T]	Torque [Nm]	x5 [mm]	Br_{max} [T]	Bt_{max} [T]	Torque [Nm]	x6 [mm]	Br_{max} [T]	Bt_{max} [T]	Torque [Nm]	x1 [mm]	Br_{max} [T]	Bt_{max} [T]	Torque [Nm]
-0.50	-0.20	1.826	1.911	175.78	-7.00	1.835	1.901	179.41	-1.00	1.904	2.129	175.92	-3.00	1.785	1.680	185.26	-1.00	nan	nan	nan
-0.50	-0.06	1.826	1.911	175.78	-5.20	1.831	1.895	178.95	-0.60	1.877	2.107	175.94	-2.20	1.835	1.645	186.08	-0.76	2.155	1.137	188.26
-0.50	0.08	1.804	1.852	175.98	-3.40	1.830	1.911	178.42	-0.20	1.857	1.952	175.85	-1.40	1.850	1.681	184.15	-0.52	2.098	2.455	184.59
-0.50	0.22	1.764	1.764	176.23	-1.60	1.827	1.902	177.54	0.20	1.819	1.812	175.70	-0.60	1.819	1.658	180.06	-0.28	1.989	2.102	180.64
-0.50	0.36	1.747	1.707	176.26	0.20	1.826	1.912	175.45	0.60	1.792	1.695	175.51	0.20	1.822	2.012	174.09	-0.04	1.834	1.964	176.53
-0.50	0.50	1.716	1.643	176.31	2.00	1.821	1.914	170.62	1.00	1.816	1.619	175.28	1.00	1.770	2.090	165.19	0.20	1.834	0.568	171.07
-0.20	-0.20	1.727	1.818	176.46	-7.00	1.754	1.818	180.96	-1.00	1.777	2.123	176.05	-3.00	1.782	1.535	183.95	-1.00	nan	nan	nan
-0.20	-0.06	1.727	1.818	176.46	-5.20	1.756	1.825	180.44	-0.60	1.759	1.921	176.48	-2.20	1.782	1.456	185.12	-0.76	2.030	2.034	187.97
-0.20	0.08	1.719	1.771	176.45	-3.40	1.751	1.819	179.86	-0.20	1.745	1.816	176.52	-1.40	1.762	1.327	183.87	-0.52	2.007	1.945	184.63
-0.20	0.22	1.689	1.697	176.43	-1.60	1.750	1.823	178.68	0.20	1.723	1.750	176.37	-0.60	1.750	1.599	180.43	-0.28	1.851	1.889	181.03
-0.20	0.36	1.640	1.703	176.45	0.20	1.727	1.819	176.03	0.60	1.710	1.659	176.08	0.20	1.731	1.865	174.78	-0.04	1.735	1.837	177.16
-0.20	0.50	1.620	1.857	176.28	2.00	1.734	1.822	170.20	1.00	1.717	1.506	175.69	1.00	1.665	1.876	166.74	0.20	1.735	0.553	171.77
0.10	-0.20	1.651	1.684	176.45	-7.00	1.666	1.683	182.01	-1.00	1.685	2.045	175.27	-3.00	1.774	1.389	182.48	-1.00	nan	nan	nan
0.10	-0.06	1.651	1.684	176.45	-5.20	1.666	1.688	181.46	-0.60	1.667	1.782	176.25	-2.20	1.749	1.311	183.87	-0.76	1.871	1.783	187.09
0.10	0.08	1.613	1.727	176.46	-3.40	1.660	1.680	180.77	-0.20	1.661	1.672	176.47	-1.40	1.726	1.300	183.02	-0.52	1.798	1.736	184.14
0.10	0.22	1.594	1.728	176.23	-1.60	1.658	1.682	179.29	0.20	1.651	1.626	176.36	-0.60	1.681	1.521	180.08	-0.28	1.759	1.671	180.78
0.10	0.36	1.581	1.694	175.95	0.20	1.651	1.684	175.93	0.60	1.650	1.568	176.04	0.20	1.628	1.711	174.94	-0.04	1.659	1.693	177.11
0.10	0.50	1.570	1.633	175.65	2.00	1.646	1.687	169.22	1.00	1.664	1.445	175.56	1.00	1.552	1.766	167.02	0.20	1.660	0.595	171.88
0.40	-0.20	1.569	1.731	176.04	-7.00	1.577	1.716	182.75	-1.00	1.570	1.844	173.91	-3.00	1.769	1.271	180.84	-1.00	nan	nan	nan
0.40	-0.06	1.569	1.731	176.04	-5.20	1.576	1.722	182.18	-0.60	1.563	1.755	175.58	-2.20	1.730	1.177	182.42	-0.76	1.752	1.643	185.93
0.40	0.08	1.562	1.702	175.86	-3.40	1.574	1.717	181.29	-0.20	1.567	1.741	176.01	-1.40	1.684	1.340	181.85	-0.52	1.736	1.585	183.31
0.40	0.22	1.553	1.634	175.51	-1.60	1.572	1.724	179.47	0.20	1.572	1.624	175.98	-0.60	1.628	1.566	179.24	-0.28	1.691	1.528	180.15
0.40	0.36	1.560	1.563	175.15	0.20	1.569	1.732	175.43	0.60	1.597	1.590	175.66	0.20	1.565	1.774	174.67	-0.04	1.579	1.707	176.67
0.40	0.50	1.576	1.485	174.75	2.00	1.562	1.745	167.77	1.00	1.644	1.387	175.12	1.00	1.519	1.747	167.14	0.20	1.600	0.715	171.79
0.70	-0.20	1.591	1.597	175.21	-7.00	1.601	1.586	183.16	-1.00	1.519	1.756	172.05	-3.00	1.765	1.171	179.04	-1.00	nan	nan	nan
0.70	-0.06	1.591	1.597	175.21	-5.20	1.599	1.578	182.53	-0.60	1.586	1.725	174.32	-2.20	1.727	1.125	180.79	-0.76	1.760	1.458	184.69

0.70	0.08	1.604	1.490	175.00	-3.40	1.597	1.580	181.44	-0.20	1.598	1.653	175.06	-1.40	1.678	1.331	180.46	-0.52	1.749	1.490	182.24
0.70	0.22	1.611	1.476	174.55	-1.60	1.595	1.588	179.25	0.20	1.593	1.511	175.16	-0.60	1.632	1.488	178.14	-0.28	1.778	1.463	179.22
0.70	0.36	1.599	1.344	174.09	0.20	1.589	1.639	174.49	0.60	1.615	1.435	174.94	0.20	1.576	1.617	173.94	-0.04	1.582	1.546	175.83
0.70	0.50	1.634	1.356	173.62	2.00	1.580	1.661	165.72	1.00	1.663	1.377	174.45	1.00	1.507	1.753	166.90	0.20	1.564	0.800	171.70
1.00	-0.20	1.636	1.415	174.22	-7.00	1.635	1.355	183.49	-1.00	1.525	1.720	169.89	-3.00	1.754	1.087	177.13	-1.00	nan	nan	nan
1.00	-0.06	1.636	1.415	174.22	-5.20	1.635	1.353	182.78	-0.60	1.658	1.726	172.82	-2.20	1.730	1.134	179.05	-0.76	1.770	1.382	183.29
1.00	0.08	1.641	1.389	173.93	-3.40	1.641	1.409	181.59	-0.20	1.645	1.650	173.90	-1.40	1.691	1.223	178.90	-0.52	1.746	1.357	181.00
1.00	0.22	1.651	1.346	173.42	-1.60	1.639	1.412	178.93	0.20	1.633	1.499	174.19	-0.60	1.643	1.302	176.86	-0.28	1.763	1.394	178.10
1.00	0.36	1.664	1.363	172.85	0.20	1.635	1.415	173.43	0.60	1.696	1.410	174.03	0.20	1.624	1.435	173.04	-0.04	1.630	1.402	174.82
1.00	0.50	1.676	1.367	172.26	2.00	1.624	1.462	163.58	1.00	1.701	1.343	173.59	1.00	1.566	1.440	166.51	0.20	1.624	0.881	170.66

TABLE 4.5. EXTRACT FROM 3-VARIABLE FULL FACTORIAL INTERACTION BETWEEN STATOR PARAMETERS.

Version #	x3 [mm]	x4 [mm]	x5 [mm]	Br_{max} [T]	Bt_{max} [T]	Efficiency [%]	Torque [Nm]
1	-1.00	-7.00	-1.00	1.732	2.096	99.78	181.55
2	-1.00	-7.00	-0.60	1.714	1.816	99.75	181.99
3	-1.00	-7.00	-0.20	1.708	1.720	99.71	181.87
4	-1.00	-7.00	0.20	1.692	1.669	99.65	181.51
5	-1.00	-7.00	0.60	1.685	1.603	99.58	180.96
6	-1.00	-7.00	1.00	1.698	1.473	99.49	180.29
7	-1.00	-5.20	-1.00	1.730	2.110	99.75	180.99
8	-1.00	-5.20	-0.60	1.714	1.820	99.73	181.43
9	-1.00	-5.20	-0.20	1.708	1.724	99.69	181.33
10	-1.00	-5.20	0.20	1.693	1.675	99.63	180.98
11	-1.00	-5.20	0.60	1.685	1.607	99.56	180.47
…	…	…	…	…	…	…	…
214	0.50	2.00	0.20	1.577	1.591	99.48	167.40
215	0.50	2.00	0.60	1.614	1.493	99.40	167.21
216	0.50	2.00	1.00	1.659	1.387	99.30	166.89

TABLE 4.6. EXTRACT FROM 3-VARIABLE FULL FACTORIAL INTERACTION BETWEEN ROTOR PARAMETERS

Version #	x9 [mm]	x12 [mm]	x13 [mm]	Br_{max} [T]	Bt_{max} [T]	Efficiency [%]	Torque [Nm]
1	-0.50	-5.00	-2.50	1.580	1.838	99.53	151.86
2	-0.50	-5.00	-2.00	1.594	1.853	99.15	154.64
3	-0.50	-5.00	-1.50	1.608	1.886	99.24	157.42
4	-0.50	-5.00	-1.00	1.610	1.932	99.80	160.27
5	-0.50	-5.00	-0.50	1.601	1.986	99.92	161.83
6	-0.50	-5.00	0.00	1.585	2.050	99.88	161.82
7	-0.50	-3.90	-2.50	1.579	1.857	99.56	153.00
8	-0.50	-3.90	-2.00	1.600	1.868	99.18	155.74
9	-0.50	-3.90	-1.50	1.613	1.899	99.31	158.53
10	-0.50	-3.90	-1.00	1.615	1.941	99.85	161.26
11	-0.50	-3.90	-0.50	1.611	1.987	99.87	162.75
…	…	…	…	…	…	…	…
214	0.50	0.50	-1.00	1.678	1.660	99.20	180.92
215	0.50	0.50	-0.50	1.667	1.656	99.10	181.52
216	0.50	0.50	0.00	1.702	1.648	99.50	182.81

4.2. Design of Experiments

The sensitivity analysis was used to reduce the size of the parameter set from 17 down to 5. These 5 geometric variables are then chosen to be the subject of the main parametric investigation study, which begins with the design of experiments. The term DoE is cost commonly used to describe a branch of applied statistics which deals with structuring and managing a set of tests aimed at evaluating some factors and their influence and control over a group or a single parameter [47].

In the case of this study, the DoE describes the technique used to generate a set of design versions from the combination of the 5 geometric variables, while also considering the variation of the rotational speed in the specified range. The objective of such study is to investigate the interaction among the various parameter and evaluate how they affect the generation of vibrations. The employment of the DoE tool of Ansys Workbench brings two main advantages:

- The first benefit of using the integrated tool is that the experimental process is automated, meaning that the user simply needs to define a strategy for the generation of

the design points, and the program is automatically able to sequentially generate a solution for all of them. A design point is the term used to define a specific combination of all the input parameters of the DoE, which in this case are the 5 geometric variables plus the rotational speed.

- The second advantage is that the DoE tool offers a choice of pre-configured strategies for the generation of the design points, which are the individual combinations of different levels of each variable. Each design point is unique as it is generated by a unique combination of values of the input parameters of the DoE. The strategy chosen for the definition of design point in this study is the Latin Hypercube Sampling method.

4.2.1. Latin Hypercube Sampling

An experimental design is characterized by p design points in d dimensions, and it can be represented by a $p \times d$ matrix $E = [r_1\ r_2\ r_3\ \dots\ r_p]^T$ where each column represents an input variable, and each row $r_i = [r_i^{(1)}\ r_i^{(2)}\ r_i^{(3)}\ \dots\ r_i^{(d)}]$ represents a design point (also referred to as sample). The Latin Hypercube design is generated in a way such that each of the d dimensions is divided into p equal levels, and there is only one sample per level [49]. An example is shown in Figure 4.2.

Other common alternatives for DoE techniques are central composite designs and D-optimal designs, but in this study the Latin Hypercube is chosen because of its benefits, such as:

- It is able to cover design spaces of any dimensions, as it has no requirements on data density and location.
- It can be optimized without in-depth statistical knowledge of the model assumptions.
- It can generate however many points the user determines appropriate.
- It is flexible, in the way that it maintains its characteristics even when dimensions are reduced [48].

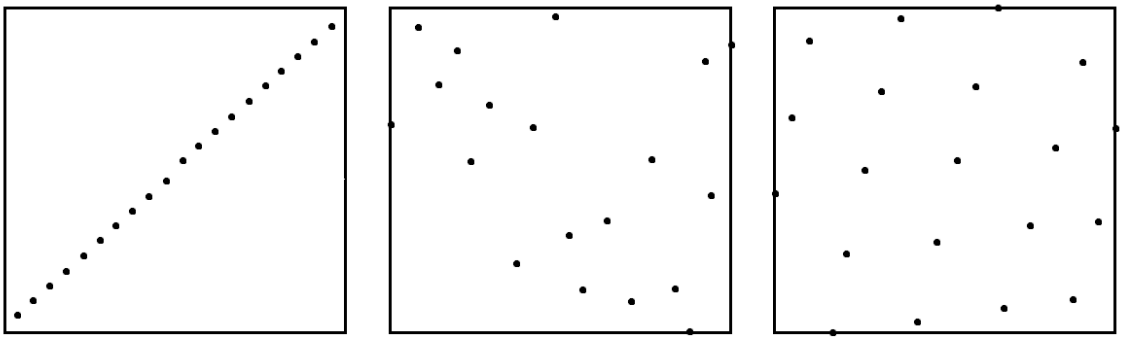

(a) (b) (c)

Figure 4.2. Examples of Latin Hypercube designs with $d = 2$ and $p = 20$. (a) Design with poor space filling properties. (b) Randomized design. (c) Design with good space filling properties [48].

The design field is originally generated with 50 DPs, each of which is the result of a unique combination of values of the 5 design variables plus the rotational speed. Latin Hypercube Sampling discretizes the range of each input parameter in as many values as DPs: therefore, in this case the variation ranges are selected 50 values which are assigned to the 50 design points. An extract from the whole design space, which can be found in Appendix B, is presented in Table 4.7.

TABLE 4.7. EXTRACT FROM DOE DESIGN SPACE.

DP number	x2 [mm]	x5 [mm]	x6 [mm]	x12 [mm]	x13 [mm]	n [rpm]
1	-0.54	-0.26	-2.73	-0.16	-2.33	4465
2	0.52	0.10	-0.47	-2.95	-2.08	2425
3	-0.11	-0.94	0.31	-4.55	-1.18	5315
4	-0.33	-0.10	-0.70	-0.26	-0.18	3955
…	…	…	…	…	…	…
30	-0.51	-0.42	0.00	-2.36	-1.93	5145
31	-0.45	0.38	0.23	-3.75	-0.53	10075
32	-0.26	0.54	-0.08	-4.75	-2.48	4635
33	-0.17	-0.22	-1.33	-1.86	-1.63	7185
…	…	…	…	…	…	…
50	0.20	-0.98	-0.78	-1.56	-0.98	7015

4.3. Response Surface

As the last step in the optimization procedure, Workbench offers the possibility to build a Response Surface starting from the DoE. RSM is a widespread technique used to model and analyze a process in which the one or more outputs of interest are affected by multiple variables, and its goal is to optimize the response of the output to the independent variables [50].

The DoE is the first step and one of the most important aspects of RSM: the mathematical model of the process and the selection of the DoE technique have a great impact in determining the quality of the surface construction. As mentioned before, the strategy chosen for the experiments design is the Latin Hypercube; for the generation of the surface, on the other hand, Ansys offers six options:

- Genetic aggregation: default technique, suitable to most DoE conditions due to high versatility. It runs an iterative algorithm to find best response surface type and settings for each output parameter, aggregating them together. Good for low/medium number of DPs. It is also capable of automatic refinement (adding of DPs until surface meets user requirements).

- Standard response surface (2^{nd} order polynomial): good fit for DoE with high number of DPs, provides satisfactory results when variation of output parameters is smooth.

- Kriging: multidimensional interpolation, provides global model of design space with good fit in any condition; however, cannot handle well “noisy” results due to inability of filtering out oscillations.

- Non-parametric regression: creates envelope around true output surface, checking that most output points are within it: good for noisy results, usually delivers good fit, but it is computationally slow.

- Neural network: uses a neural network type of algorithm to generate surface: very successful with nonlinear responses but requires a very high number of DPs.

- Sparse grid: automatically refining response surface, requires many DPs, should only be used when solving process is fast [46].

The genetic aggregation technique is employed for the analysis, since it is the one advised for models requiring long solving times which do not have a high number of design points.

The output parameters chosen for the parametric investigation are the maximum oscillation amplitude and the maximum acceleration peak in the frequency response analysis: the solver automatically computes minimum and maximum for all output variables in each DP. Both values are measured at the stator teeth tips, in the radial direction.

CHAPTER 5
RESULTS AND DISCUSSION

In the following chapter, the main results of the simulation are presented and discussed. Throughout the research process, several simulations adopting different strategies and setups were run, which have been useful to better understand the model and the analysis method. These simulations and their results are not included in this chapter for sake of brevity, but they have been nevertheless important in obtaining the final results.

Both in the RSM, and the DoE on which it is based, two output variables are computed (Key Performance Indicators, or KPIs), both in frequency response form:

- Maximum displacement amplitude of the oscillation peak, measured in mm.
- Maximum acceleration peak of the oscillations, measured in m/s^2.

The first result is significant because it gives the reader a tangible information on how much the exciting forces deform the structure, while the second one is useful to get an idea of the intensity of vibration, and also because it is what is most commonly measured in experimental tests, which could be carried out in the future to verify the simulation work presented in this dissertation.

5.1. Design of Experiments Results

The DoE produces a table which contains the definition of the 50 Design Points by specifying the values of each input variable in the point, as well as the values of the output functions in the point. The entire table is presented in Appendix B, but an extract is shown in Table 5.1 for clarity:

TABLE 5.1. EXTRACT FROM DOE RESULTS TABLE.

#	**n [rpm]**	**x2 [mm]**	**x5 [mm]**	**x6 [mm]**	**x12 [mm]**	**x13 [mm]**	**Max. Amplitude of Oscillations [mm]**	**Maximum Acceleration Peak [mm/s²]**
1	4465	-0.54	-0.26	-2.73	-0.16	-2.33	0.1711	422.31
2	2425	0.52	0.10	-0.47	-2.95	-2.08	0.3102	1957.37
3	5315	-0.11	-0.94	0.31	-4.55	-1.18	0.2089	3014.87
4	3955	-0.33	-0.10	-0.70	-0.26	-0.18	0.3120	2855.75
5	8375	0.11	-0.86	-2.11	-4.15	-0.73	0.2573	11118.15

From the table, it is possible to highlight the DP which produces the best result in term of oscillations, that is, the lowest maximum oscillation:

46	9735	0.14	0.30	-0.39	-0.56	-0.23	0.1246	3313.34

And the DP which generates the lowest peak in acceleration:

49	5825	0.17	-0.54	-0.32	-0.66	-2.13	0.1843	195.95

Since the outputs are functions of multiple variables, including the shaft rotational speed n, the low values obtained in the two previous DPs should not be taken as best results without further investigation. To better represent the transient nature of the working conditions, which require the motor to work under varying rotational speed, the 5 best DPs are examined for each output function:

TABLE 5.2. 5 BEST DESIGN VERSIONS FOR LOWEST MAXIMUM OSCILLATION AMPLITUDE.

#	**n [rpm]**	**x2 [mm]**	**x5 [mm]**	**x6 [mm]**	**x12 [mm]**	**x13 [mm]**	**Max. Amplitude of Oscillations [mm]**	**Maximum Acceleration Peak [mm/s^2]**
46	9735	0.14	0.30	-0.39	-0.56	-0.23	0.1246	3313.33
27	7525	0.73	0.46	-1.64	-1.36	-1.68	0.1274	4324.57
10	8545	0.80	-0.74	0.85	-4.45	-1.08	0.1286	1570.81
44	6505	0.45	-0.66	-1.87	-0.76	-1.58	0.1697	2675.71
1	4465	-0.54	-0.26	-2.73	-0.16	-2.33	0.1711	422.31

TABLE 5.3. 5 BEST DESIGN VERSIONS FOR LOWEST MAXIMUM ACCELERATION PEAK.

#	**n [rpm]**	**x2 [mm]**	**x5 [mm]**	**x6 [mm]**	**x12 [mm]**	**x13 [mm]**	**Max. Amplitude of Oscillations [mm]**	**Maximum Acceleration Peak [mm/s^2]**
49	5825	0.17	-0.54	-0.32	-0.66	-2.13	0.1843	195.54
1	4465	-0.54	-0.26	-2.73	-0.16	-2.33	0.1711	422.31
16	3615	0.49	0.58	0.07	-0.86	-1.83	0.2576	543.60
38	9565	0.55	0.74	-2.03	-1.26	-0.58	0.3799	852.22
34	8205	0.39	0.66	-0.24	-1.16	-2.43	0.2862	902.52

It is easy to see that while the DPs are generated from fairly scattered values of the input variables within their range, they mostly vary around similar values. This is can be better explained through the following procedure:

1. First, the average of the 5 values for each variable are taken, in each of the two lists.

2. Then, the difference between the averaged geometric parameters generating the best 5 designs in terms of oscillation amplitude (Table 5.2) and the average of the geometric parameters that produce the lowest acceleration (Table 5.3) is computed.
3. Finally, the difference obtained this way is compared to the width of the variation range of each variable.

The results of this procedure are presented in the following table:

TABLE 5.4. COMPARISON BETWEEN RESULTS OF TABLES V.II AND V.III.

	x2 [mm]	**x5 [mm]**	**x6 [mm]**	**x12 [mm]**	**x13 [mm]**
Average value from Table V.II	0.32	-0.18	-1.16	-1.46	-1.38
Average value from Table V.III	0.21	0.24	-1.05	-0.82	-1.86
Variable total range	1.53	1.96	3.81	4.89	2.44
Difference between averages with respect to total range [%]	6.94%	21.22%	2.86%	13.06%	19.59%

As it is possible to see in the last row, the difference between the two averaged values is within 22% of the variation range. Of course we must not forget that taking the average of the first 5 best values does reduce the variability, but the result still shows that the best performances are obtained with values of the geometric parameters coming from a restricted area of the total range.

To compare the outputs of the DoE with the nominal design version, the performance of six different geometries (shown in Table 5.5) is evaluated with a loop over the range of rotational speed discretized into 50 DPs. The two KPIs are measured for each rotational speed and the values obtained in each design version are compared.

As partially explained above, design versions 4, 5, and 6, are obtained by averaging the values of different sets of geometric parameters. This is done for 2 reason: the first one is to filter out any possible singularity generated by the combination of particular excitation frequencies and harmonic response peaks, as well as to try to compromise between low oscillation amplitude maximum and low maximum acceleration peak. These versions are then tested on their own, generating results as if they were regular design versions as defined in the DoE.

TABLE 5.5. FINAL DESIGN VERSIONS.

Design version description	x2 [mm]	x5 [mm]	x6 [mm]	x12 [mm]	x13 [mm]
1 - Nominal design	0.00	0.00	0.00	0.00	0.00
2 - DP #46 (lowest oscillation amplitude)	0.14	0.30	-0.39	-0.56	-0.23
3 - DP #49 (lowest maximum acceleration)	0.17	-0.54	-0.32	-0.66	-2.13
4 - Average of Table 5.2 values	0.32	-0.18	-1.16	-1.46	-1.38
5 - Average of Table 5.3 values	0.21	0.24	-1.05	-0.82	-1.86
6 - Average of values from both tables	0.26	0.03	-1.10	-1.14	-1.62

The evaluation can be carried out by studying Figure 5.1 and 5.2:

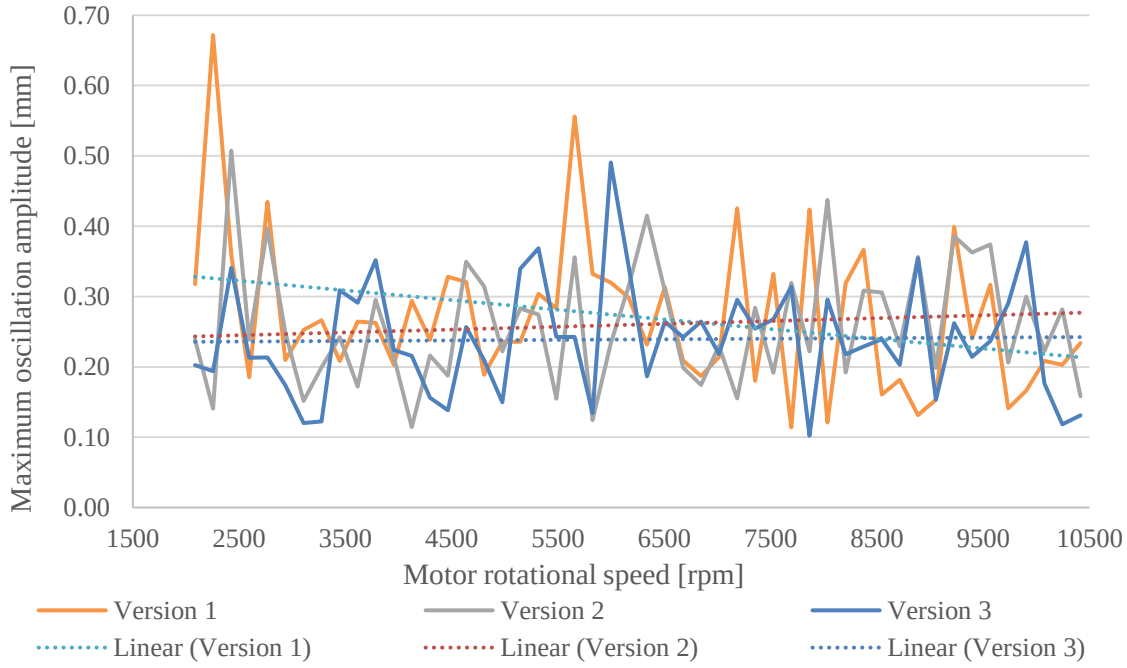

(a)

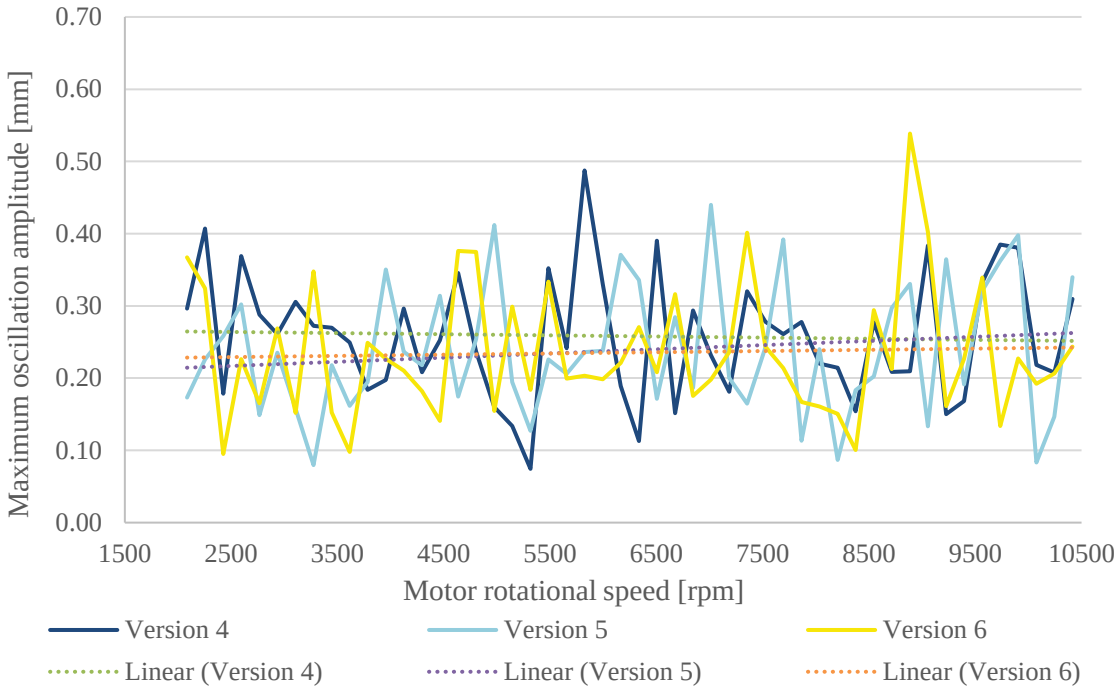

(b)

Figure 5.1. Comparison of maximum oscillation amplitudes for different design version over the range of speed. (a) Versions 1 through 3. (b) Versions 4 through 6.

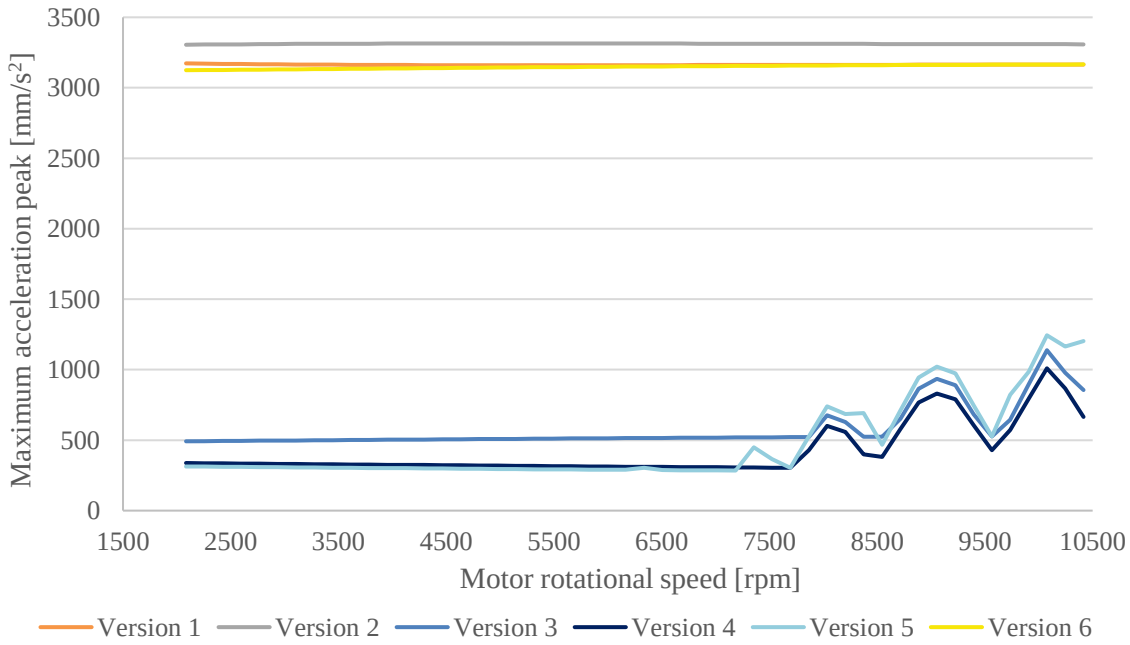

Figure 5.2. Comparison of maximum acceleration peaks for different design version over the range of speed.

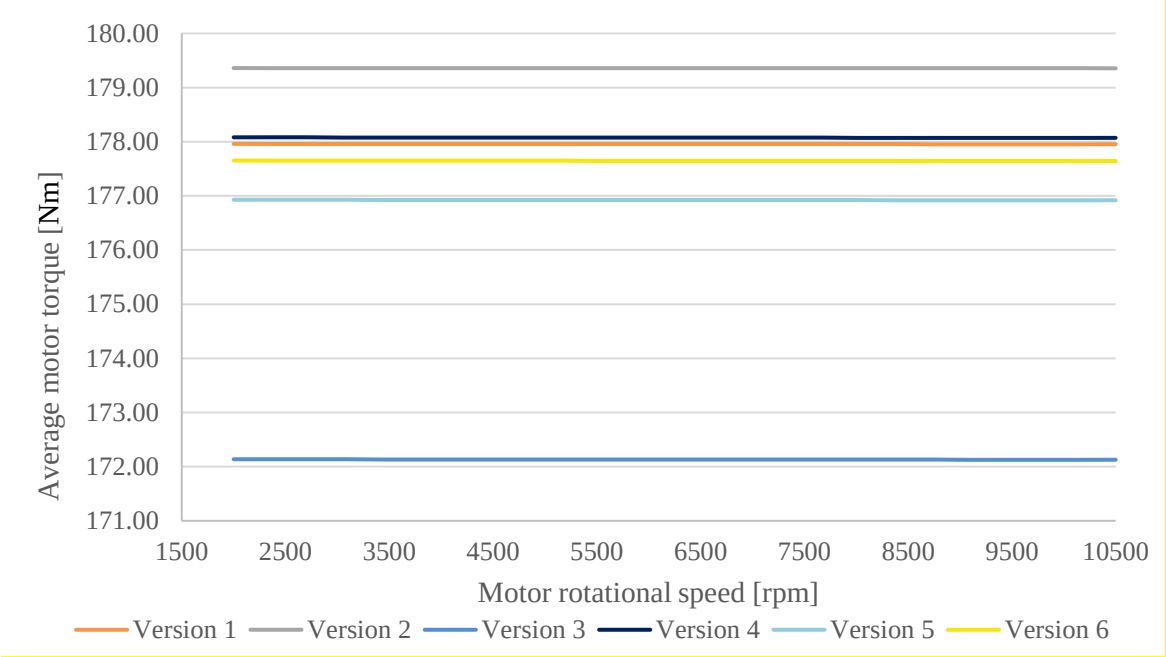

Figure 5.3. Comparison of average motor torque for different design version over the range of speed.

Figure 5.1 is split in two separate graphs to be more easily understandable to the reader. For each design version, the results are scattered, which is why it is hard to interpolate them into a linear function. Linear trends are added to give a better idea about the mean value for each geometry, since the trend is almost horizontal for all of them, meaning that there is no significant increase or decrease in oscillations along the rotational speed range. It is interesting to notice, however, that there seem to be few neighborhoods of the rotational velocity domain at which several versions have spikes, such as around 6000 rpm, for versions 1, 2, 4, and 3; and also around 2000 rpm, for versions 1, 2 and 4. Nevertheless, due to the highly scattered distribution of the results, it is easier to examine the performance of each design version by looking at the average value of maximum oscillation amplitude across the range from Table 4.1. As we can see, each version yields an improvement from the nominal, with version 6 peaking at over 13% of reduction.

For what acceleration levels are concerned, it is clear to see that the results present two separate issues:

- First, there are two recognizable trends among the results of the 6 different versions, as geometries 1, 2, and 6 yield a more or less constant maximum value for the acceleration

of stator teeth tips that across the speed range, where the remaining 3 versions have an increasing trend with oscillations in values that start above 7000 rpm. Considering that the simulation set up is the same for all the different versions, the difference in geometry is not quite enough to justify such vastly different behaviors. More on this will be explained in the Conclusions chapter of the dissertation.

- Second, and just as important, it is possible to point out that the values of maximum acceleration are incredibly high, and not realistic for the structure discussed in this study. Since the recording of vibrations has been carried out by registering the maximum value registered by the software, since the intent of the author was to take into account the worst case scenarios, it is possible that the presence of outliers in the results set has skewed the values to impossibly high values. This phenomenon could be caused by the inability of a 2D simulation to accurately represent the distortion of a complex geometry, as well as the poor accuracy in simulating the damping properties of the structure. As mentioned before, this issue will be tackled again in the last chapter of the dissertation, where possible issues are analyzed and suggestions for future research are developed.

TABLE 5.6. FINAL COMPARISON BETWEEN DIFFERENT DESIGN VERSIONS.

	Figure 5.1 average value [mm]	**Improvement from nominal [%]**	**Figure 5.2 average value [mm/s^2]**	**Improvement from nominal [%]**	**Torque Average [Nm]**	**Improvement from nominal [%]**
Version 1	0.2709	-	3163.08	-	177.96	-
Version 2	0.2601	3.98%	3311.59	-4.70%	179.36	0.79%
Version 3	0.2390	11.76%	583.60	81.55%	172.13	-3.27%
Version 4	0.2581	4.74%	422.90	86.63%	178.07	0.07%
Version 5	0.2385	11.97%	476.44	84.94%	176.92	-0.58%
Version 6	0.2354	13.10%	3148.47	0.46%	177.65	-0.17%

Therefore, although it was possible to obtain vast improvements from the nominal design version, considering that designs 2 through 5 all show a reduction in maximum acceleration of more than 80%, it is not possible to guarantee that this scenario accurately represents real worlds results, since there was no availability of experimental data to be compared with the simulation results.

5.2. Response Surface Methodology Results

The RSM produces a several different types of results. In this section, an extract of them is presented, while more can be found in Appendix C. Moreover, even though it is possible to use the RSM results to formulate considerations and comments on the analysis, it is worth noticing that the high maximum predicted error for both oscillations amplitude and even more so for acceleration peak, shown in Figure 5.4, make the results of the procedure not sufficiently reliable. That is why the final design version was based on the results of the DoE. Furthermore, it is possible to see that the calculated best value for the oscillation maximum amplitude is not far from the one computed in the DoE.

1	Name	Calculated Minimum	Calculated Maximum	Maximum Predicted Error
2	P18 - Frequency Response Frequency (Hz)	0.011023	0.012918	0.00015549
3	P19 - Frequency Response Maximum Amplitude (mm)	0.085075	0.43996	0.079673
4	P20 - Frequency Response 2 Maximum Amplitude (mm s^-2)	-278.45	4248.1	280.89
5	P21 - Frequency Response 2 Frequency (Hz)	3457.6	20000	5517

Figure 5.4. RSM results and errors.

As mentioned above, the RSM is able to produce different kinds of data, in addition to the values of minima and maxima for the output parameters. An interesting graph obtained from the analysis, for example, is that of local sensitivity of each output to the various input variables. It is interesting to notice that the sensitivity values vary based on the point at which they are measure: the local sensitivity graph at base speed for the nominal design version (Figure 5.5a) is different from those generated at the maxima and minima (Figures 5.5b and 5.5c) of the range of each input variable, and the one generated for the nominal design version at high speed (Figure 5.5d).

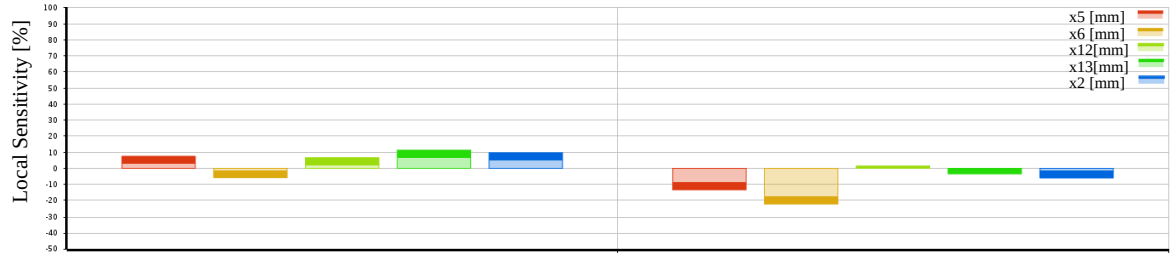

(a)

Figure 5.5. Local sensitivity results in different points. (a) Nominal version at base speed. (b) Maximum of variation range. (c) Minimum of variation range. (d) Nominal design version at maximum speed.

Several things can be observed on these graphs:

- The sensitivity of all evaluated outputs to the input variable is highly influenced by the point of measurement.
- In the second column, which describes the sensitivity of the KPI maximum oscillation amplitude, it is possible to notice that variable x_{13} is often one of the more influential ones. Variables x_5 and x_6 are also often influential.
- In the first column, which describes the sensitivity of the KPI maximum acceleration peak, it is worth noticing that even though the trends are different, variables x_5, x_6 and x_{13} are again more or less consistently the most influential ones.

Another kind of results that the RSM is able to produce, is an actual three-dimensional surface which shows how one of the desired outputs (on the z axis) changes with the variation of 2 input parameters (x and y axes). Since it is possible to generate this kind of

graph for any particular point of the 6-dimensional design space, such tool is more useful to inspect specific neighborhoods of the space rather than being used to interpret general trends. Therefore, I have included Figures 5.6a through 5.7c to give a demonstrative example of this tool, with an analysis centered around the nominal design version. More graphs can be found in Appendix C.

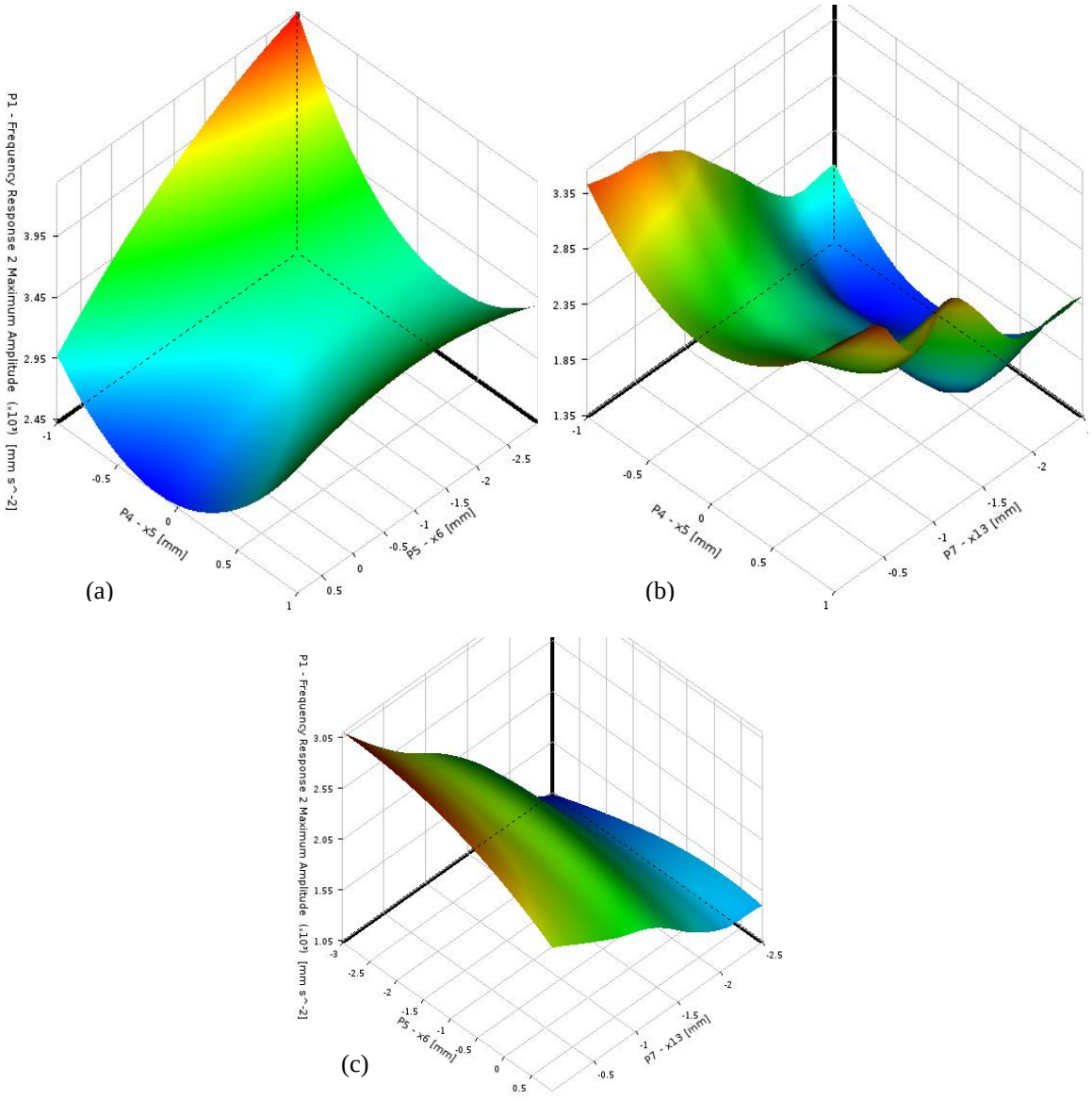

Figure 5.6. 3D response surface for maximum acceleration peak. (a) Response to x_5 and x_6 variation. (b) Response to x_5 and x13 variation. (c) Response to x_6 and x_{13} variation.

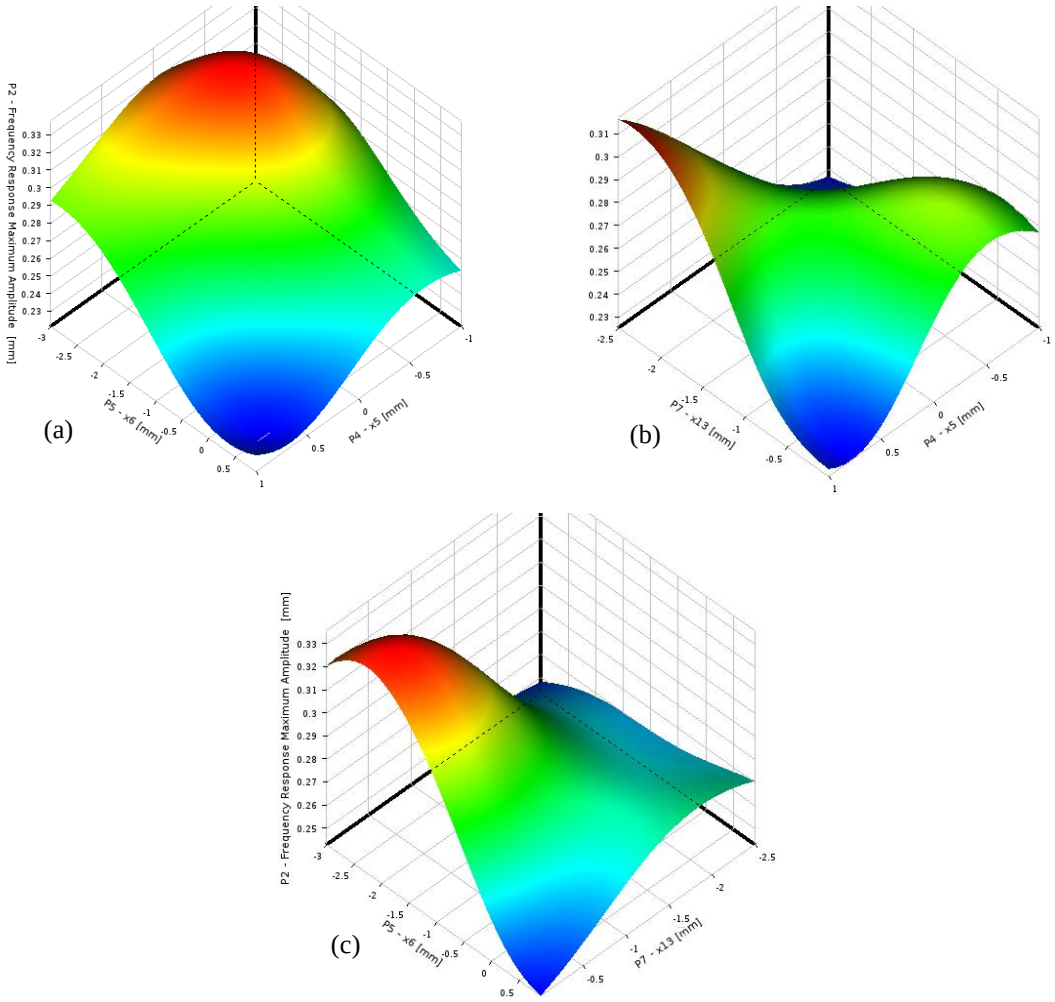

Figure 5.7. 3D response surface for maximum oscillation amplitude: (a) Response to x_5 and x_6 variation. (b) Response to x_5 and x13 variation. (c) Response to x_6 and x_{13} variation.

It is possible to notice in Figure 5.3 that 2 surfaces have a distinct concavity towards the midpoint of the range of x_5, meaning that its value in the nominal design version is already close to the optimal one. On the other hand, it is possible to highlight an opposite situation in Figure 5.4, where the center of the graph is never a local nor global minimum.

5.3. Comparison between Nominal and Final Design Version

Based on the results showcased in section 5.1, it is possible to select version 5 as the most improved geometry from the nominal design. In this section, a side to side comparison of the two is presented.

First, Figure 5.8 shows the difference in the geometry of the core. As we can see, a noticeable difference is in the shape of the slot, which is not rectangular anymore, as it now has the lateral edges converging towards the inner side. Moreover, the slot opening width is increasing. In the rotor design, the permanent magnets are shifted toward the center, and the flux barriers are more narrow. The new slot shape increases the width of the stator teeth, which most likely is a factor that contributes positively in the vibration generation behavior.

Then, a more detailed comparison is presented with the help of Table 5.7, in which it is possible to appreciate the difference both in the parameters which determine the change in geometry of the improved version, as well as the effect on the key performance indices of this study, which, as defined earlier, are the maximum oscillation amplitude and peak acceleration of the stator teeth tips in the radial direction, as well as the motor torque average value, all of which are measured over the range of rational speed simulating real driving conditions.

As it is possible to notice from the table, the majority of influential geometric parameter describe the slot opening. It is therefore possible to affirm that, for future reference and further studies, a convenient place to start optimization procedures would indeed be from the shape of the slot opening. Interestingly enough, while all of the stator-related parameters determine the geometry of elements near the air gap, the two rotor-related ones define instead the shape of elements of the rotor which are furthest from the gap.

Last but not least, it is possible to see that while the vibration behavior is significantly affected by the change in geometry obtained through the parametric investigation, the performance of the motor, characterized by its average torque production, is approximately unchanged from the nominal design version. This is a very important result since it implies that it is indeed possible to improve vibration by acting on the electromagnetic forces, since its main source is the radial EM force, while not sacrificing motor torque, which is strongly related to tangential Maxwell forces.

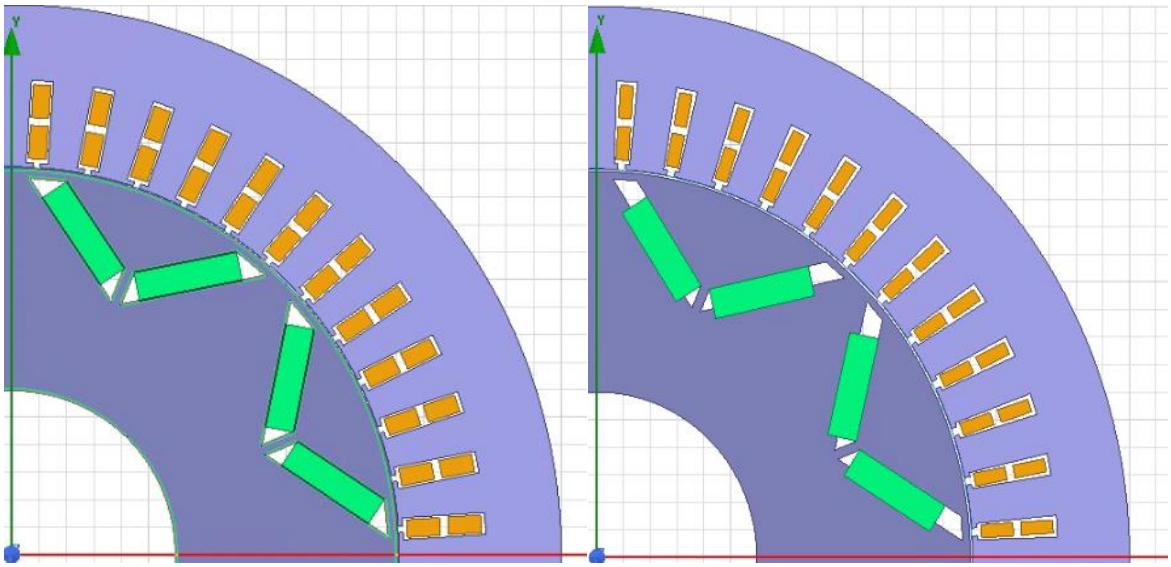

(a) (b)

Figure 5.8. Comparison of nominal and optimized designs. (a) Nominal version. (b) Final, optimized version.

TABLE 5.7. SIDE-BY-SIDE COMPARISON BETWEEN INITIAL AND FINAL DESIGN VERSIONS.

Characteristic	**Nominal design version**	**Final design version**
Hs0 – Slot opening depth	0.8 mm	1.01 mm
Bs0 – Slot opening width	1.2 mm	1.44 mm
Bs1 – Slot inner width	4 mm	2.95 mm
O2 – Back iron width	19.44 mm	18.62 mm
B1 – Magnetic flux barrier width	5.5 mm	3.64 mm
Maximum oscillation amplitude	0.2709 mm	0.2385 mm
Maximum acceleration peak	3163.08 mm/s^2	476.44 mm/s^2
Average motor torque	177.96 Nm	176.92 Nm

CHAPTER 6
CONCLUSIONS AND RECOMMENDATIONS

6.1. General Summary and Conclusions

Tying up what has been discussed so far, it is possible to review what has been achieved with this research project: from the analysis of the most commonly employed electric motor architecture for traction in passenger vehicles, the IPMSM topology was chosen to conduct a parametric investigation on the geometry of its core, which would allow to improve the vibration behaviour while maintaining satisfactory performance in terms of produced motor torque, as well as also taking into account real working conditions of the machine through the inclusion of a wide range of rotational speed, which simulates driving conditions. After a literature review, it was determined that the major causes of vibration in IPMSMs are the EM Maxwell forces which act on the stator teeth tips.

Through the development of a two-dimensional EM model of the machine with parametrized geometry, it was possible to study the influence of several variables on the radial and tangential component of the magnetic flux, which is in turn related to the EM forces through Maxwell stress tensor formulas, as well as the motor torque. 5 geometric parameters where chosen for the investigation, 3 of which describe stator properties (slot opening width and depth, internal slot width) and 2 of which describe rotor topology (PM back iron, magnetic flux barriers width).

The EM loads were then mapped into a mechanical model within the context of a multiphysics simulation including a modal analysis and a harmonic response, in addition to the 2D electromagnetic model. Using the modal superposition method to compute maximum acceleration peaks and oscillation amplitude for stator teeth tips in the radial direction, a 50 DP – DoE was developed using the Latin Hypercube Sampling strategy. The DoE was then used to build a response surface.

Due to the poor reliability of the RSM results, the data computed with the DoE was used to evaluate the performance of 5 design versions, in addition to the original nominal one, over the entire range of speed. The best performing one, which allowed for a reduction of over 10% of maximum oscillation amplitude, and over 80% of maximum acceleration

peak, while exhibiting a negligible variation in torque production, was chosen as best result, and consequently more extensively compared to the original design.

Overall, the key findings of this research project can be summarized as:

- The slot opening geometry is more important than the geometry of the outer slot in influencing the magnetic flux at the air gap, which in turn determines the pressure and excitation on the stator teeth, causing them to vibrate.
- The curvature radius of the slot fillets has a negligible contribution to the magnetic flux.
- The size of ribs and PMs in the core is also less impactful on magnetic flux when compared to other topologic features of the core, especially when comparing with stator parameters variations.
- Magnetic flux barrier width, and back iron length are instead both significantly influential in affecting EM force generation.
- The rotational speed of the motor is not as influential as previously thought on vibration, for what oscillation amplitude is concerned; on the other hand, even though due to the poor accuracy of the maximum acceleration results it is not advisable to form a conclusive statement, it is possible to speculate that maximum acceleration peaks do increase with rotational speed, as seen in the trend for versions 3, 4, and 5, as well as results of preliminary simulations that have not been included in this dissertation.
- It is indeed possible to reduce vibrations without compromising torque generation too much: as shown from the results of the final evaluation in Table 5.6, the average torque production varies almost negligibly with respect to the vibration figures, and in case of version 2 and 4, it was even increased from the value of the nominal version.

6.2. Recommendations for Future Development

The research work that has been carried out within the context of this dissertation is, although somewhat conclusive in itself, only a preliminary stage of the in depth analysis that could be performed to obtain even more accurate predictions on motor vibrations. The scope and time frame of the project has limited the simulation work to what has been

achieved and described in this report; however, several recommendations can be made for future works, based on what the author has observed throughout the research process:

1. A first step in improving the accuracy of the results would be to use materials that better represent the ones used in a physical machine. Most importantly, for the simulation of the stator, the use of the type of electrical steel of which it is made of would be suggested, to better reflect its actual material properties, even though structural steel is not too far off. The same comment can be done on the housing material, since the aluminum alloy used in the simulation may not represent the properties of the actual alloy used for the construction of the housing.

2. Another important improvement to the parametric investigation procedure can be introduced by considering the external rotor radius and the internal stator radius, which are the boundaries of the air gap, in the parametric study. As mentioned before, the way that parametrization was set up for this study did not allow to consider these two variables in the procedure without having to make big changes to the model, which were not feasible due to time constraints. Ideally, when making the electromagnetic model, the parametrization should be done so that the position and size of the air gap can be varied, to a degree, without compromising the functioning of the model. For example, a possible way to do these within the Ansys environment could be by parametrizing the diameter of the bands with variables that depend on the diameter of the air gap, so that they can follow its variations while still having their role in defining the mesh and improving its quality and scaling.

3. Within the mechanical model, an increase of accuracy level could be obtained by better simulating damping. As mentioned before, a standard coefficient was used to model hysteretic damping for the structure, but the datum did not come directly from the geometry. Especially with the case of a tridimensional model and simulation, a damping coefficient that is derived from the geometry of the structure other than just its material properties would most likely benefit the simulation, allowing to obtain more accurate results especially with respect to acceleration data.

4. The housing of the motor was simulated in a simplified way in the mechanical mode; this is because the information necessary to model it in its entirety (geometric specifications) was not provided by the manufacturer. For a two-dimensional simulation, the margin of improvement related to the modelling of the housing is obviously limited, but if future research is conducted with a 3D model, a more detailed version of the housing could benefit the accuracy of results for multiple reasons, such as allowing for more accurate computation of resonance modes, better simulation of the interaction between stator and housing, and accurate simulations of how the structure is constrained to the chassis.

5. A tridimensional model, or a least 2.5D one, would also allow to consider different kinds of improvement strategies, such as skewing. The 2.5D model is used in the EM simulation of PMSMs to study the effect of skewing without having to build a full tridimensional model. This technique is useful to accurately model skewing by using very limited computational resources [51].

6. In this research, the EM force was mapped onto the stator teeth tips as a concentrated force, meaning that each tip had one force (and torque, if present) acting on it. As it is explained in section 2.2.1 of this dissertation, a distributed force better represents the real phenomenon, allowing the model to achieve better accuracy.

7. An even further step in evaluating the vibrational behaviour of the motor with respect to passenger comfort, would be to record the acoustic noise generated by the vibrations. As explained in Chapter 2 of the dissertation, one way to achieve this is to use the Boundary Element Method to compute the sound pressure levels around the structure.

8. Yet another aspect that was not included in the scope of this study, but which nonetheless should be considered, especially when the investigation is aimed at the design of a new machine, is the structural feasibility of the motor geometry. Specifically, material stress has not been considered in the analysis, but it could be a non negligible problem when the parametric study produces design versions in which the thickness of structural elements of the core is significantly altered.

9. Finally, a paramount contribution would be added to this with the validation of the model, by comparison with data obtained experimentally in a testing facility. This kind of approach however would require the model to be based on certain specific geometries of which a physical machine is available for testing, as well as different versions to evaluate the improvement brough by the parametric investigation.

6.3. Final Remarks

Even though there are several aspects in which the model could be improved to obtain more accurate or more informative results, it is possible to notice how most suggestions for future work involve the utilization of a more complete representation of the structure of the motor, specifically, in a tridimensional sense. This is because, even though the motor core does benefit from its radial symmetry, that is not the case for its surrounding parts, such as the housing and support, which are however of non negligible influence in transmitting vibrations.

Unfortunately, it was not possible to implement this kind of set up in the mechanical simulation, due to several reasons, such as the unavailability of data related to the geometry of those components, the strict time constraints framing the projects, which did not allow for the creation of a mock up geometry that might have been sufficient to capture the aspects described previously. These are most likely the main causes for the poor quality of the acceleration results.

Based on the results obtained from the 2D simulation, and what was examined during the literary review, it is advised to carry out a structural evaluation of vibration only when enough data about the motor geometry and structural properties is available. On the other hand, it is possible to investigate the variation of EM forces generated by the motor without the need of characterizing the whole structure; this would then be a viable approach for those who do not have the aforementioned information at their disposal.

Nonetheless, this study provides important insight on the role of different geometrical parameters in affecting vibrations, as well as an overview on different analysis methods and a novel inclusion of the rotational speed range to simulate driving conditions.

REFERENCES/BIBLIOGRAPHY

[1] M. Villani, "High performance electrical motors for automotive applications – status and future of motors with low cost permanent magnets," in *Proc. 8th International Conference on Magnetism and Metallurgy*, Dresden, Germany, 2018.

[2] W. Deng and S. Zuo, "Electromagnetic vibration and noise of the permanent-magnet synchronous motors for electric vehicles: an overview," *IEEE Trans. Transportation Electrification*, vol. 5, no. 1, pp. 59–70, 2019.

[3] T. Sun, "Efficiency optimised control of interior permanent magnet synchronous machine (IPMSM) drives for electric vehicle tractions," Ph.D. thesis, University of Sheffield, Sheffield, UK, 2016.

[4] Z. Yang, M. Krishnamurthy, and I. P. Brown, "Electromagnetic and vibrational characteristic of IPM over full torque-speed range," in *Proc. International Electric Machines & Drives Conference*, Chicago, IL, USA, 2013, pp. 295–302.

[5] F. Un-Noor, S. Padmanaban, L. Mihet-Popa, M. Mollah, and E. Hossain, "A comprehensive study of key electric vehicle (EV) components, technologies, challenges, impacts, and future direction of development," *Energies*, vol. 10, no. 8, p. 1217, Aug. 2017.

[6] S. T. Lee, "Development and analysis of interior permanent magnet synchronous motor with field excitation structure," Ph.D. thesis, University of Tennessee, Knoxville, TN, 2009.

[7] A. Balashanmugham and M. Maheswaran, "Permanent-magnet synchronous machine drives," in *Applied Electromechanical Devices and Machines for Electric Mobility Solutions*, 2019.

[8] Ned Mohan, *Electric Machines and Drives: a First Course*. Hoboken, NJ: Wiley, 2012.

[9] J. Kettlewell, “Study on performance characteristics of interior permanent magnet synchronous motor due to rotor configuration,” Library and Archives Canada = Bibliothèque et Archives Canada, Ottawa, 2013.

[10] J. Reinert, A. Brockmeyer, and R. W. A. A. De Doncker, “Calculation of losses in ferro- and ferrimagnetic materials based on the modified Steinmetz equation,” *IEEE Trans. Ind. Appl*., vol. 37, no. 4, pp. 1055–1061, Aug. 2001.

[11] W. Roshen, “Iron loss model for permanent-magnet synchronous motors,” *IEEE Trans. Magn*., vol. 43, no. 8, pp. 3428–3434, Aug. 2007.

[12] W. Zhu, S. Pekarek, B. Fahimi, and B. J. Deken, “Investigation of force generation in a permanent magnet synchronous machine,” *IEEE Trans. Energy Convers*., vol. 22, no. 3, pp. 557–565, Sep. 2007.

[13] N. Remus *et al*., “Electromagnetic noise and vibration in PMSM and their sources: an overview,” in *Proc. IEEE Canadian Conference on Electrical and Computer Engineering*, London, ON, Canada, 2020.

[14] B. Stone, *Chatter and Machine Tools*. Springer International Publishing, 2014, pp. 193-195.

[15] R. E. Blake, “Chapter 2 - Basic Vibration Theory,” in *Harris’ Shock and Vibration Handbook*, New York, USA: McGraw-Hill Book Company, 2001.

[16] C. Gambino, “Vibration damping via acoustic treatment attached to vehicle body panels,” M.S. thesis, University of Windsor, Windsor, ON, Canada, 2016.

[17] R. Clough and J. Penzien, *Dynamics of Structures*, Third Edition. Berkeley, CA, USA: Computers & Structures, Inc., 2003.

[18] C. S. Horas *et al*., “Application of modal superposition technique in the fatigue analysis using local approaches,” *Procedia Eng*., vol. 160, pp. 45–52, 2016.

[19] D. Torregrossa, B. Fahimi, F. Peyraut, and A. Miraoui, “Fast computation of electromagnetic vibrations in electrical machines via field reconstruction method

and knowledge of mechanical impulse response," *IEEE Trans. Ind. Electron*., vol. 59, no. 2, pp. 839–847, Feb. 2012.

[20] F. L. M. dos Santos, J. Anthonis, F. Naclerio, J. J. C. Gyselinck, H. Van der Auweraer, and L. C. S. Goes, "Multiphysics NVH modeling: simulation of a switched reluctance motor for an electric vehicle," *IEEE Trans. Ind. Electron*., vol. 61, no. 1, pp. 469–476, Jan. 2014.

[21] M. Valavi, A. Nysveen, R. Nilssen, R. D. Lorenz, and T. Rolvag, "Influence of pole and slot combinations on magnetic forces and vibration in low-speed PM wind generators," *IEEE Trans. Magn*., vol. 50, no. 5, pp. 1–11, May 2014.

[22] S. Varghese, "Electromagnetic noise from permanent magnet motors," M.S. thesis, Royal Institute of Technology, Stockholm, SE, 2013

[23] Y. Li, F. Chai, Z. Song, and Z. Li, "Analysis of vibrations in interior permanent magnet synchronous motors considering air-gap deformation," *Energies*, vol. 10, no. 9, p. 1259, Aug. 2017.

[24] Shenbo Yu and Ren, "Electromagnetic and mechanical characterizations of noise and vibration in permanent magnet synchronous machines," *IEEE Trans. Magn*., vol. 42, no. 4, pp. 1335–1338, Apr. 2006.

[25] H. Li *et al*., "Analysis on the vibration modes of the electric vehicle motor stator," *Vibroengineering PROCEDIA*, vol. 22, pp. 81–86, Mar. 2019.

[26] R. Islam and I. Husain, "Analytical model for predicting noise and vibration in permanent-magnet synchronous motors," *IEEE Trans. Industry Applications*, vol. 46, no. 6, pp. 2346–2354, Nov. 2010.

[27] F. Andrei-Toader and H. Radu-Petru, "Multiphysics modeling of a permanent magnet synchronous machine," *Journal of Electrical and Electronics Engineering*, vol. 5, no. 2, p. 55-58, Oct. 2012.

[28] Z. Han, J. Liu, C. Gong, and J. Lu, “Influence mechanism on vibration and noise of PMSM for different structures of skewed stator,” *in Proc. 20th International Conference on Electrical Machines and Systems*, Sydney, Australia, Aug. 2017.

[29] H.-J. Shin, J.-Y. Choi, H.-I. Park, and S.-M. Jang, “Vibration analysis and measurements through prediction of electromagnetic vibration sources of permanent magnet synchronous motor based on analytical magnetic field calculations,” *IEEE Trans. Magn*., vol. 48, no. 11, pp. 4216–4219, Nov. 2012.

[30] L. Gao, H. Zheng, L. Zeng, and R. Pei, “Evaluation method of noise and vibration used in permanent magnet synchronous motor in electric vehicle,” *in Proc. IEEE Trans. Electrification Conference and Expo*, Detroit, MI, USA, Jun. 2019. pp. 1–4.

[31] T. Dai, H. Li, and J. Li, “A hybrid calculation method of radial electromagnetic force based on finite element method and analytic method in a permanent magnet synchronous machine,” *in Proc. 22nd International Conference on Electrical Machines and Systems*, Harbin, China, Aug. 2019.

[32] Q. Dong, X. Liu, H. Qi, C. Sun, and Y. Wang, “Analysis and evaluation of electromagnetic vibration and noise in permanent magnet synchronous motor with rotor step skewing,” *Science China Technol. Sciences*., vol. 62, no. 5, pp. 839–848, May 2019.

[33] K. Qian, J. Wang, Y. Gao, Q. Sun, and J. Liang, “Interior noise and vibration prediction of permanent magnet synchronous motor,” *Journal of Vibroengineering*, vol. 20, no. 5, pp. 2225–2236, Aug. 2018.

[34] F. Lin, S. Zuo, W. Deng, and S. Wu, “Modeling and analysis of electromagnetic force, vibration, and noise in permanent-magnet synchronous motor considering current harmonics,” *IEEE Trans. Ind. Electron*., vol. 63, no. 12, pp. 7455–7466, Dec. 2016.

[35] Lihua Zhu, Qingxin Yang, Rongge Yan, Yongjian Li, and Weili Yan, “Magnetoelastic numerical analysis of permanent magnet synchronous motor

including magnetostriction effects and harmonics," *IEEE Trans. Appl. Supercond*., vol. 24, no. 3, pp. 1–4, Jun. 2014.

[36] L. Zhu, B. Wang, R. Yan, Q. Yang, Y. Yang, and X. Zhang, "Electromagnetic vibration of motor core including magnetostriction under different rotation speeds," *IEEE Trans. Magn*., vol. 52, no. 3, pp. 1–4, Mar. 2016.

[37] X. Chen, Z. Deng, J. Hu, and T. Deng, "An analytical model of unbalanced magnetic pull for PMSM used in electric vehicle: numerical and experimental validation," *Int. J. Appl. Electromagn. Mech*., vol. 54, no. 4, pp. 583–596, Jul. 2017.

[38] F. Pop-Piglesan, F. Jurca, C. Oprea, and C. Martis, "Permanent magnet synchronous machine design for low-noise drive systems," *in Proc. 26th International Conference on Noise and Vibration Engineering*, Leuven, Belgium, 2014.

[39] F. Lin, S. Zuo, and W. Deng, "Impact of rotor eccentricity on electromagnetic vibration and noise of permanent magnet synchronous motor," *J. Vibroengineering*, vol. 20, no. 2, pp. 843–857, Mar. 2018.

[40] A. K. Putri, S. Rick, D. Franck, and K. Hameyer, "Application of sinusoidal field pole in a permanent-magnet synchronous machine to improve the NVH behavior considering the MTPA and MTPV operation area," *IEEE Trans. Industrial Applications*, vol. 52, no. 3, pp. 2280–2288, May 2016.

[41] D. Y. Ohm, "Dynamic model of pm synchronous motors," Drivetech, Inc., Blacksburg, Virginia, 2000.

[42] F. Lin, S.-G. Zuo, W.-Z. Deng, and S.-L. Wu, "Reduction of vibration and acoustic noise in permanent magnet synchronous motor by optimizing magnetic forces," *J. Sound Vib.*, vol. 429, pp. 193–205, Sep. 2018.

[43] J. Nägelkrämer, A. Heitmann, and N. Parspour, "Multi-objective optimization of the rotor design to improve the acoustic behavior of high power density interior permanent magnet synchronous machines," *in Proc. EVS30 Symposium*, Stuttgart, Germany, Oct. 2017.

[44] J. W. Jiang, B. Bilgin, A. Sathyan, H. Dadkhah, and A. Emadi, "Noise and vibration reduction for IPMSM by using rotor circumferential slits," *in Proc. IEEE International Electric Machines and Drives Conference*, Miami, FL, USA, May 2017.

[45] T. Ishikawa, M. Yamada, and N. Kurita, "Design of magnet arrangement in interior permanent magnet synchronous motor by response surface methodology in consideration of torque and vibration," *IEEE Trans. Magn.*, vol. 47, no. 5, pp. 1290–1293, May 2011.

[46] Ansys® Electromagnetic Suite, Release 19.2, Help System, Maxwell Help, ANSYS, Inc.

[47] P. Roy, M. Towhidi, F. Ahmed, S. Mukundan, H. Dhulipati, and N. C. Kar, "A novel hybrid technique for thermal analysis of permanent magnet synchronous motor used in electric vehicle application," *in Proc. SAE World Congress Experience Conference*, Detroit, MI, April 21-23, 2020.

[48] K. Bower, "What is design of experiments," asq.org. https://asq.org/quality-resources/design-of-experiments (accessed May 27, 2020).

[49] F. A. C. Viana, "A tutorial on Latin Hypercube design of experiments," *Qual. Reliab. Eng. Int.*, vol. 32, no. 5, pp. 1975–1985, Jul. 2016.

[50] A. Y. Aydar, "Utilization of response surface methodology in optimization of extraction of plant materials," in *Statistical Approaches with Emphasis on Design of Experiments Applied to Chemical Processes*, V. Silva, Ed. InTech, 2018.

[51] P. Ponomarev, J. Keränen, M. Lyly, J. Westerlund, P. Råback, Peter, "Multi-slice 2.5D modelling and validation of skewed electrical machines using open-source tools," *in Proc. IEEE Conf. Electromagnetic Field Computation*, United States, 2016.

APPENDICES

Appendix A – 3-Variable interaction study

In this first appendix, the results of the two 3-variable interaction evaluations, one for the rotor and one for the slot parameters, are presented in their entirety.

Slot parameter interactions evaluation table with conditional formatting:

Version #	x3 [mm]	x4 [mm]	x5 [mm]	Br_{max} [T]	Bt_{max} [T]	Efficiency [%]	Torque [Nm]
1	-1.00	-7.00	-1.00	1.732	2.096	99.78	181.55
2	-1.00	-7.00	-0.60	1.714	1.816	99.75	181.99
3	-1.00	-7.00	-0.20	1.708	1.720	99.71	181.87
4	-1.00	-7.00	0.20	1.692	1.669	99.65	181.51
5	-1.00	-7.00	0.60	1.685	1.603	99.58	180.96
6	-1.00	-7.00	1.00	1.698	1.473	99.49	180.29
7	-1.00	-5.20	-1.00	1.730	2.110	99.75	180.99
8	-1.00	-5.20	-0.60	1.714	1.820	99.73	181.43
9	-1.00	-5.20	-0.20	1.708	1.724	99.69	181.33
10	-1.00	-5.20	0.20	1.693	1.675	99.63	180.98
11	-1.00	-5.20	0.60	1.685	1.607	99.56	180.47
12	-1.00	-5.20	1.00	1.697	1.476	99.47	179.80
13	-1.00	-3.40	-1.00	1.725	2.115	99.72	180.21
14	-1.00	-3.40	-0.60	1.707	1.812	99.69	180.71
15	-1.00	-3.40	-0.20	1.700	1.717	99.66	180.66
16	-1.00	-3.40	0.20	1.686	1.666	99.60	180.35
17	-1.00	-3.40	0.60	1.679	1.600	99.53	179.87
18	-1.00	-3.40	1.00	1.691	1.470	99.44	179.24
19	-1.00	-1.60	-1.00	1.723	2.113	99.65	178.58
20	-1.00	-1.60	-0.60	1.705	1.814	99.63	179.21
21	-1.00	-1.60	-0.20	1.698	1.718	99.61	179.25
22	-1.00	-1.60	0.20	1.683	1.668	99.57	179.02
23	-1.00	-1.60	0.60	1.677	1.603	99.49	178.60
24	-1.00	-1.60	1.00	1.689	1.472	99.41	178.04
25	-1.00	0.20	-1.00	1.719	2.087	99.57	175.06
26	-1.00	0.20	-0.60	1.698	1.816	99.58	175.88
27	-1.00	0.20	-0.20	1.691	1.719	99.56	176.05
28	-1.00	0.20	0.20	1.676	1.670	99.52	175.94
29	-1.00	0.20	0.60	1.671	1.605	99.45	175.64
30	-1.00	0.20	1.00	1.683	1.474	99.37	175.20
31	-1.00	2.00	-1.00	1.713	2.083	99.59	168.27
32	-1.00	2.00	-0.60	1.693	1.829	99.59	169.27
33	-1.00	2.00	-0.20	1.686	1.722	99.58	169.57

34	-1.00	2.00	0.20	1.671	1.673	99.53	169.59
35	-1.00	2.00	0.60	1.666	1.608	99.46	169.43
36	-1.00	2.00	1.00	1.678	1.477	99.38	169.14
37	-0.70	-7.00	-1.00	1.732	2.096	99.78	181.55
38	-0.70	-7.00	-0.60	1.714	1.816	99.75	181.99
39	-0.70	-7.00	-0.20	1.708	1.720	99.71	181.87
40	-0.70	-7.00	0.20	1.692	1.669	99.65	181.51
41	-0.70	-7.00	0.60	1.685	1.603	99.58	180.96
42	-0.70	-7.00	1.00	1.698	1.473	99.49	180.29
43	-0.70	-5.20	-1.00	1.730	2.110	99.75	180.99
44	-0.70	-5.20	-0.60	1.714	1.820	99.73	181.43
45	-0.70	-5.20	-0.20	1.708	1.724	99.69	181.33
46	-0.70	-5.20	0.20	1.693	1.675	99.63	180.98
47	-0.70	-5.20	0.60	1.685	1.607	99.56	180.47
48	-0.70	-5.20	1.00	1.697	1.476	99.47	179.80
49	-0.70	-3.40	-1.00	1.725	2.115	99.72	180.21
50	-0.70	-3.40	-0.60	1.707	1.812	99.69	180.71
51	-0.70	-3.40	-0.20	1.700	1.717	99.66	180.66
52	-0.70	-3.40	0.20	1.686	1.666	99.60	180.35
53	-0.70	-3.40	0.60	1.679	1.600	99.53	179.87
54	-0.70	-3.40	1.00	1.691	1.470	99.44	179.24
55	-0.70	-1.60	-1.00	1.723	2.113	99.65	178.58
56	-0.70	-1.60	-0.60	1.705	1.814	99.63	179.21
57	-0.70	-1.60	-0.20	1.698	1.718	99.61	179.25
58	-0.70	-1.60	0.20	1.683	1.668	99.57	179.02
59	-0.70	-1.60	0.60	1.677	1.603	99.49	178.60
60	-0.70	-1.60	1.00	1.689	1.472	99.41	178.04
61	-0.70	0.20	-1.00	1.719	2.087	99.57	175.06
62	-0.70	0.20	-0.60	1.698	1.816	99.58	175.88
63	-0.70	0.20	-0.20	1.691	1.719	99.56	176.05
64	-0.70	0.20	0.20	1.676	1.670	99.52	175.94
65	-0.70	0.20	0.60	1.671	1.605	99.45	175.64
66	-0.70	0.20	1.00	1.683	1.474	99.37	175.20
67	-0.70	2.00	-1.00	1.713	2.083	99.59	168.27
68	-0.70	2.00	-0.60	1.693	1.829	99.59	169.27
69	-0.70	2.00	-0.20	1.686	1.722	99.58	169.57
70	-0.70	2.00	0.20	1.671	1.673	99.53	169.59
71	-0.70	2.00	0.60	1.666	1.608	99.46	169.43
72	-0.70	2.00	1.00	1.678	1.477	99.38	169.14
73	-0.40	-7.00	-1.00	1.732	2.096	99.78	181.55
74	-0.40	-7.00	-0.60	1.714	1.816	99.75	181.99
75	-0.40	-7.00	-0.20	1.708	1.720	99.71	181.87
76	-0.40	-7.00	0.20	1.692	1.669	99.65	181.51
77	-0.40	-7.00	0.60	1.685	1.603	99.58	180.96

78	-0.40	-7.00	1.00	1.698	1.473	99.49	180.29
79	-0.40	-5.20	-1.00	1.730	2.110	99.75	180.99
80	-0.40	-5.20	-0.60	1.714	1.820	99.73	181.43
81	-0.40	-5.20	-0.20	1.708	1.724	99.69	181.33
82	-0.40	-5.20	0.20	1.693	1.675	99.63	180.98
83	-0.40	-5.20	0.60	1.685	1.607	99.56	180.47
84	-0.40	-5.20	1.00	1.697	1.476	99.47	179.80
85	-0.40	-3.40	-1.00	1.725	2.115	99.72	180.21
86	-0.40	-3.40	-0.60	1.707	1.812	99.69	180.71
87	-0.40	-3.40	-0.20	1.700	1.717	99.66	180.66
88	-0.40	-3.40	0.20	1.686	1.666	99.60	180.35
89	-0.40	-3.40	0.60	1.679	1.600	99.53	179.87
90	-0.40	-3.40	1.00	1.691	1.470	99.44	179.24
91	-0.40	-1.60	-1.00	1.723	2.113	99.65	178.58
92	-0.40	-1.60	-0.60	1.705	1.814	99.63	179.21
93	-0.40	-1.60	-0.20	1.698	1.718	99.61	179.25
94	-0.40	-1.60	0.20	1.683	1.668	99.57	179.02
95	-0.40	-1.60	0.60	1.677	1.603	99.49	178.60
96	-0.40	-1.60	1.00	1.689	1.472	99.41	178.04
97	-0.40	0.20	-1.00	1.719	2.087	99.57	175.06
98	-0.40	0.20	-0.60	1.698	1.816	99.58	175.88
99	-0.40	0.20	-0.20	1.691	1.719	99.56	176.05
100	-0.40	0.20	0.20	1.676	1.670	99.52	175.94
101	-0.40	0.20	0.60	1.671	1.605	99.45	175.64
102	-0.40	0.20	1.00	1.683	1.474	99.37	175.20
103	-0.40	2.00	-1.00	1.713	2.083	99.59	168.27
104	-0.40	2.00	-0.60	1.693	1.829	99.59	169.27
105	-0.40	2.00	-0.20	1.686	1.722	99.58	169.57
106	-0.40	2.00	0.20	1.671	1.673	99.53	169.59
107	-0.40	2.00	0.60	1.666	1.608	99.46	169.43
108	-0.40	2.00	1.00	1.678	1.477	99.38	169.14
109	-0.10	-7.00	-1.00	1.732	2.096	99.78	181.55
110	-0.10	-7.00	-0.60	1.714	1.816	99.75	181.99
111	-0.10	-7.00	-0.20	1.708	1.720	99.71	181.87
112	-0.10	-7.00	0.20	1.692	1.669	99.65	181.51
113	-0.10	-7.00	0.60	1.685	1.603	99.58	180.96
114	-0.10	-7.00	1.00	1.698	1.473	99.49	180.29
115	-0.10	-5.20	-1.00	1.730	2.110	99.75	180.99
116	-0.10	-5.20	-0.60	1.714	1.820	99.73	181.43
117	-0.10	-5.20	-0.20	1.708	1.724	99.69	181.33
118	-0.10	-5.20	0.20	1.693	1.675	99.63	180.98
119	-0.10	-5.20	0.60	1.685	1.607	99.56	180.47
120	-0.10	-5.20	1.00	1.697	1.476	99.47	179.80
121	-0.10	-3.40	-1.00	1.725	2.115	99.72	180.21

122	-0.10	-3.40	-0.60	1.707	1.812	99.69	180.71
123	-0.10	-3.40	-0.20	1.700	1.717	99.66	180.66
124	-0.10	-3.40	0.20	1.686	1.666	99.60	180.35
125	-0.10	-3.40	0.60	1.679	1.600	99.53	179.87
126	-0.10	-3.40	1.00	1.691	1.470	99.44	179.24
127	-0.10	-1.60	-1.00	1.723	2.113	99.65	178.58
128	-0.10	-1.60	-0.60	1.705	1.814	99.63	179.21
129	-0.10	-1.60	-0.20	1.698	1.718	99.61	179.25
130	-0.10	-1.60	0.20	1.683	1.668	99.57	179.02
131	-0.10	-1.60	0.60	1.677	1.603	99.49	178.60
132	-0.10	-1.60	1.00	1.689	1.472	99.41	178.04
133	-0.10	0.20	-1.00	1.719	2.087	99.57	175.06
134	-0.10	0.20	-0.60	1.698	1.816	99.58	175.88
135	-0.10	0.20	-0.20	1.691	1.719	99.56	176.05
136	-0.10	0.20	0.20	1.676	1.670	99.52	175.94
137	-0.10	0.20	0.60	1.671	1.605	99.45	175.64
138	-0.10	0.20	1.00	1.683	1.474	99.37	175.20
139	-0.10	2.00	-1.00	1.713	2.083	99.59	168.27
140	-0.10	2.00	-0.60	1.693	1.829	99.59	169.27
141	-0.10	2.00	-0.20	1.686	1.722	99.58	169.57
142	-0.10	2.00	0.20	1.671	1.673	99.53	169.59
143	-0.10	2.00	0.60	1.666	1.608	99.46	169.43
144	-0.10	2.00	1.00	1.678	1.477	99.38	169.14
145	0.20	-7.00	-1.00	1.682	1.983	99.76	181.92
146	0.20	-7.00	-0.60	1.633	1.721	99.72	182.61
147	0.20	-7.00	-0.20	1.630	1.715	99.67	182.48
148	0.20	-7.00	0.20	1.628	1.604	99.60	182.06
149	0.20	-7.00	0.60	1.656	1.520	99.52	181.34
150	0.20	-7.00	1.00	1.672	1.413	99.43	180.59
151	0.20	-5.20	-1.00	1.680	1.983	99.74	181.31
152	0.20	-5.20	-0.60	1.630	1.726	99.69	182.05
153	0.20	-5.20	-0.20	1.627	1.725	99.64	181.94
154	0.20	-5.20	0.20	1.625	1.619	99.58	181.54
155	0.20	-5.20	0.60	1.655	1.525	99.50	180.82
156	0.20	-5.20	1.00	1.671	1.418	99.41	180.09
157	0.20	-3.40	-1.00	1.675	1.984	99.70	180.38
158	0.20	-3.40	-0.60	1.629	1.723	99.65	181.18
159	0.20	-3.40	-0.20	1.626	1.721	99.61	181.14
160	0.20	-3.40	0.20	1.623	1.613	99.55	180.80
161	0.20	-3.40	0.60	1.650	1.519	99.47	180.14
162	0.20	-3.40	1.00	1.666	1.413	99.38	179.46
163	0.20	-1.60	-1.00	1.673	1.984	99.61	178.50
164	0.20	-1.60	-0.60	1.627	1.727	99.59	179.46
165	0.20	-1.60	-0.20	1.624	1.723	99.56	179.52

166	0.20	-1.60	0.20	1.621	1.614	99.50	179.27
167	0.20	-1.60	0.60	1.648	1.522	99.43	178.72
168	0.20	-1.60	1.00	1.664	1.415	99.34	178.11
169	0.20	0.20	-1.00	1.669	1.982	99.53	174.51
170	0.20	0.20	-0.60	1.623	1.733	99.54	175.69
171	0.20	0.20	-0.20	1.620	1.727	99.51	175.90
172	0.20	0.20	0.20	1.618	1.616	99.46	175.80
173	0.20	0.20	0.60	1.642	1.525	99.39	175.39
174	0.20	0.20	1.00	1.658	1.418	99.30	174.92
175	0.20	2.00	-1.00	1.662	1.957	99.57	167.14
176	0.20	2.00	-0.60	1.617	1.740	99.57	168.47
177	0.20	2.00	-0.20	1.613	1.734	99.55	168.84
178	0.20	2.00	0.20	1.611	1.622	99.50	168.88
179	0.20	2.00	0.60	1.636	1.528	99.43	168.64
180	0.20	2.00	1.00	1.653	1.420	99.34	168.33
181	0.50	-7.00	-1.00	1.609	1.826	99.74	182.42
182	0.50	-7.00	-0.60	1.618	1.880	99.66	183.00
183	0.50	-7.00	-0.20	1.617	1.713	99.60	182.88
184	0.50	-7.00	0.20	1.598	1.609	99.52	182.55
185	0.50	-7.00	0.60	1.629	1.507	99.44	181.78
186	0.50	-7.00	1.00	1.675	1.398	99.34	180.95
187	0.50	-5.20	-1.00	1.606	1.826	99.71	181.74
188	0.50	-5.20	-0.60	1.618	1.878	99.63	182.38
189	0.50	-5.20	-0.20	1.617	1.711	99.57	182.30
190	0.50	-5.20	0.20	1.595	1.607	99.50	181.99
191	0.50	-5.20	0.60	1.627	1.506	99.41	181.25
192	0.50	-5.20	1.00	1.674	1.398	99.32	180.44
193	0.50	-3.40	-1.00	1.604	1.826	99.65	180.55
194	0.50	-3.40	-0.60	1.613	1.873	99.59	181.36
195	0.50	-3.40	-0.20	1.612	1.706	99.53	181.36
196	0.50	-3.40	0.20	1.594	1.603	99.46	181.11
197	0.50	-3.40	0.60	1.626	1.502	99.38	180.45
198	0.50	-3.40	1.00	1.672	1.394	99.29	179.70
199	0.50	-1.60	-1.00	1.601	1.824	99.54	178.27
200	0.50	-1.60	-0.60	1.608	1.868	99.51	179.30
201	0.50	-1.60	-0.20	1.607	1.701	99.47	179.43
202	0.50	-1.60	0.20	1.591	1.599	99.41	179.29
203	0.50	-1.60	0.60	1.623	1.499	99.33	178.74
204	0.50	-1.60	1.00	1.669	1.392	99.25	178.09
205	0.50	0.20	-1.00	1.596	1.823	99.47	173.56
206	0.50	0.20	-0.60	1.607	1.865	99.46	174.88
207	0.50	0.20	-0.20	1.606	1.698	99.44	175.19
208	0.50	0.20	0.20	1.586	1.597	99.39	175.20
209	0.50	0.20	0.60	1.620	1.496	99.32	174.82

210	0.50	0.20	1.00	1.666	1.389	99.23	174.33
211	0.50	2.00	-1.00	1.584	1.825	99.54	165.26
212	0.50	2.00	-0.60	1.598	1.857	99.53	166.78
213	0.50	2.00	-0.20	1.597	1.691	99.52	167.25
214	0.50	2.00	0.20	1.577	1.591	99.48	167.40
215	0.50	2.00	0.60	1.614	1.493	99.40	167.21
216	0.50	2.00	1.00	1.659	1.387	99.30	166.89

Rotor parameter interactions evaluation table with conditional formatting:

Version #	x9 [mm]	x12 [mm]	x13 [mm]	Br_{max} [T]	Bt_{max} [T]	Efficiency [%]	Torque [Nm]
1	-0.50	-5.00	-2.50	1.580	1.838	99.53	151.86
2	-0.50	-5.00	-2.00	1.594	1.853	99.15	154.64
3	-0.50	-5.00	-1.50	1.608	1.886	99.24	157.42
4	-0.50	-5.00	-1.00	1.610	1.932	99.80	160.27
5	-0.50	-5.00	-0.50	1.601	1.986	99.92	161.83
6	-0.50	-5.00	0.00	1.585	2.050	99.88	161.82
7	-0.50	-3.90	-2.50	1.579	1.857	99.56	153.00
8	-0.50	-3.90	-2.00	1.600	1.868	99.18	155.74
9	-0.50	-3.90	-1.50	1.613	1.899	99.31	158.53
10	-0.50	-3.90	-1.00	1.615	1.941	99.85	161.26
11	-0.50	-3.90	-0.50	1.611	1.987	99.87	162.75
12	-0.50	-3.90	0.00	1.600	2.044	99.88	162.79
13	-0.50	-2.80	-2.50	1.590	1.867	99.57	154.16
14	-0.50	-2.80	-2.00	1.610	1.877	99.19	156.78
15	-0.50	-2.80	-1.50	1.622	1.904	99.39	159.60
16	-0.50	-2.80	-1.00	1.626	1.941	99.90	162.33
17	-0.50	-2.80	-0.50	1.625	1.981	99.84	163.63
18	-0.50	-2.80	0.00	1.624	2.026	99.88	163.81
19	-0.50	-1.70	-2.50	1.605	1.871	99.58	155.22
20	-0.50	-1.70	-2.00	1.624	1.879	99.22	157.85
21	-0.50	-1.70	-1.50	1.637	1.901	99.48	160.75
22	-0.50	-1.70	-1.00	1.642	1.931	99.93	163.32
23	-0.50	-1.70	-0.50	1.646	1.964	99.77	164.35
24	-0.50	-1.70	0.00	1.653	1.999	99.89	164.78
25	-0.50	-0.60	-2.50	1.622	1.867	99.57	156.29
26	-0.50	-0.60	-2.00	1.641	1.872	99.25	158.92
27	-0.50	-0.60	-1.50	1.653	1.890	99.59	161.86
28	-0.50	-0.60	-1.00	1.656	1.915	99.95	164.17
29	-0.50	-0.60	-0.50	1.668	1.937	99.72	165.22
30	-0.50	-0.60	0.00	1.677	1.970	99.99	165.90
31	-0.50	0.50	-2.50	1.638	1.857	99.58	157.33
32	-0.50	0.50	-2.00	1.657	1.859	99.28	159.90
33	-0.50	0.50	-1.50	1.667	1.874	99.70	162.89
34	-0.50	0.50	-1.00	1.673	1.895	99.92	164.97
35	-0.50	0.50	-0.50	1.681	1.920	99.73	166.22
36	-0.50	0.50	0.00	1.692	1.944	99.97	166.88
37	-0.30	-5.00	-2.50	1.615	1.802	99.35	155.64
38	-0.30	-5.00	-2.00	1.625	1.819	99.01	158.32

39	-0.30	-5.00	-1.50	1.637	1.852	99.15	161.00
40	-0.30	-5.00	-1.00	1.638	1.899	99.65	163.63
41	-0.30	-5.00	-0.50	1.633	1.951	99.69	164.91
42	-0.30	-5.00	0.00	1.619	2.014	99.55	165.37
43	-0.30	-3.90	-2.50	1.612	1.822	99.36	156.76
44	-0.30	-3.90	-2.00	1.631	1.834	99.04	159.40
45	-0.30	-3.90	-1.50	1.642	1.865	99.22	162.08
46	-0.30	-3.90	-1.00	1.644	1.907	99.70	164.58
47	-0.30	-3.90	-0.50	1.641	1.955	99.69	165.83
48	-0.30	-3.90	0.00	1.635	2.008	99.55	166.32
49	-0.30	-2.80	-2.50	1.623	1.832	99.39	157.89
50	-0.30	-2.80	-2.00	1.640	1.843	99.07	160.42
51	-0.30	-2.80	-1.50	1.651	1.870	99.30	163.11
52	-0.30	-2.80	-1.00	1.655	1.907	99.75	165.59
53	-0.30	-2.80	-0.50	1.655	1.949	99.68	166.68
54	-0.30	-2.80	0.00	1.658	1.990	99.58	167.32
55	-0.30	-1.70	-2.50	1.636	1.836	99.40	158.93
56	-0.30	-1.70	-2.00	1.653	1.844	99.11	161.46
57	-0.30	-1.70	-1.50	1.665	1.867	99.39	164.20
58	-0.30	-1.70	-1.00	1.671	1.898	99.79	166.52
59	-0.30	-1.70	-0.50	1.676	1.932	99.63	167.36
60	-0.30	-1.70	0.00	1.688	1.962	99.61	168.26
61	-0.30	-0.60	-2.50	1.652	1.833	99.41	159.97
62	-0.30	-0.60	-2.00	1.669	1.838	99.15	162.49
63	-0.30	-0.60	-1.50	1.681	1.856	99.49	165.22
64	-0.30	-0.60	-1.00	1.690	1.880	99.81	167.37
65	-0.30	-0.60	-0.50	1.701	1.905	99.58	168.14
66	-0.30	-0.60	0.00	1.712	1.932	99.69	169.46
67	-0.30	0.50	-2.50	1.667	1.822	99.43	160.96
68	-0.30	0.50	-2.00	1.685	1.825	99.20	163.42
69	-0.30	0.50	-1.50	1.693	1.841	99.60	166.19
70	-0.30	0.50	-1.00	1.709	1.859	99.76	168.02
71	-0.30	0.50	-0.50	1.712	1.884	99.56	169.05
72	-0.30	0.50	0.00	1.726	1.906	99.70	170.43
73	-0.10	-5.00	-2.50	1.637	1.774	99.10	159.23
74	-0.10	-5.00	-2.00	1.644	1.793	98.85	161.88
75	-0.10	-5.00	-1.50	1.655	1.827	99.05	164.48
76	-0.10	-5.00	-1.00	1.657	1.875	99.52	166.89
77	-0.10	-5.00	-0.50	1.653	1.928	99.50	167.72
78	-0.10	-5.00	0.00	1.644	1.987	99.36	168.19
79	-0.10	-3.90	-2.50	1.632	1.795	99.10	160.34
80	-0.10	-3.90	-2.00	1.649	1.808	98.89	162.96
81	-0.10	-3.90	-1.50	1.660	1.840	99.12	165.52
82	-0.10	-3.90	-1.00	1.663	1.883	99.57	167.79

83	-0.10	-3.90	-0.50	1.662	1.930	99.52	168.77
84	-0.10	-3.90	0.00	1.658	1.985	99.44	169.18
85	-0.10	-2.80	-2.50	1.642	1.806	99.14	161.46
86	-0.10	-2.80	-2.00	1.658	1.817	98.93	163.96
87	-0.10	-2.80	-1.50	1.669	1.845	99.21	166.51
88	-0.10	-2.80	-1.00	1.674	1.883	99.62	168.73
89	-0.10	-2.80	-0.50	1.677	1.924	99.51	169.59
90	-0.10	-2.80	0.00	1.683	1.966	99.48	170.14
91	-0.10	-1.70	-2.50	1.656	1.810	99.17	162.48
92	-0.10	-1.70	-2.00	1.671	1.818	98.98	164.96
93	-0.10	-1.70	-1.50	1.683	1.841	99.30	167.54
94	-0.10	-1.70	-1.00	1.690	1.873	99.65	169.60
95	-0.10	-1.70	-0.50	1.699	1.905	99.49	170.23
96	-0.10	-1.70	0.00	1.713	1.937	99.54	171.21
97	-0.10	-0.60	-2.50	1.670	1.803	99.18	163.50
98	-0.10	-0.60	-2.00	1.686	1.811	99.04	165.95
99	-0.10	-0.60	-1.50	1.699	1.830	99.40	168.49
100	-0.10	-0.60	-1.00	1.710	1.855	99.67	170.38
101	-0.10	-0.60	-0.50	1.724	1.878	99.47	171.09
102	-0.10	-0.60	0.00	1.737	1.906	99.61	172.23
103	-0.10	0.50	-2.50	1.686	1.792	99.24	164.45
104	-0.10	0.50	-2.00	1.702	1.798	99.10	166.83
105	-0.10	0.50	-1.50	1.711	1.815	99.50	169.40
106	-0.10	0.50	-1.00	1.730	1.832	99.65	171.09
107	-0.10	0.50	-0.50	1.735	1.858	99.43	171.84
108	-0.10	0.50	0.00	1.751	1.881	99.66	173.19
109	0.10	-5.00	-2.50	1.489	1.798	98.94	165.49
110	0.10	-5.00	-2.00	1.508	1.805	98.75	167.99
111	0.10	-5.00	-1.50	1.527	1.811	99.03	170.51
112	0.10	-5.00	-1.00	1.538	1.818	99.48	172.71
113	0.10	-5.00	-0.50	1.539	1.819	99.42	173.31
114	0.10	-5.00	0.00	1.543	1.824	99.30	173.63
115	0.10	-3.90	-2.50	1.486	1.811	98.90	166.54
116	0.10	-3.90	-2.00	1.511	1.812	98.80	169.04
117	0.10	-3.90	-1.50	1.528	1.814	99.11	171.51
118	0.10	-3.90	-1.00	1.537	1.817	99.52	173.40
119	0.10	-3.90	-0.50	1.537	1.814	99.43	174.09
120	0.10	-3.90	0.00	1.568	1.811	99.33	174.59
121	0.10	-2.80	-2.50	1.492	1.814	98.95	167.64
122	0.10	-2.80	-2.00	1.514	1.812	98.85	169.98
123	0.10	-2.80	-1.50	1.529	1.810	99.18	172.42
124	0.10	-2.80	-1.00	1.538	1.807	99.55	174.36
125	0.10	-2.80	-0.50	1.555	1.798	99.43	175.00
126	0.10	-2.80	0.00	1.604	1.789	99.43	175.41

127	0.10	-1.70	-2.50	1.498	1.810	98.99	168.60
128	0.10	-1.70	-2.00	1.518	1.804	98.91	170.92
129	0.10	-1.70	-1.50	1.533	1.797	99.27	173.36
130	0.10	-1.70	-1.00	1.545	1.788	99.58	175.14
131	0.10	-1.70	-0.50	1.590	1.774	99.42	175.69
132	0.10	-1.70	0.00	1.642	1.760	99.47	176.35
133	0.10	-0.60	-2.50	1.507	1.799	99.04	169.53
134	0.10	-0.60	-2.00	1.526	1.789	98.97	171.82
135	0.10	-0.60	-1.50	1.543	1.777	99.36	174.20
136	0.10	-0.60	-1.00	1.571	1.762	99.58	175.82
137	0.10	-0.60	-0.50	1.624	1.744	99.38	176.31
138	0.10	-0.60	0.00	1.661	1.737	99.53	177.28
139	0.10	0.50	-2.50	1.525	1.778	99.08	170.36
140	0.10	0.50	-2.00	1.540	1.768	99.03	172.61
141	0.10	0.50	-1.50	1.561	1.752	99.43	174.98
142	0.10	0.50	-1.00	1.602	1.734	99.56	176.42
143	0.10	0.50	-0.50	1.627	1.728	99.36	177.01
144	0.10	0.50	0.00	1.665	1.719	99.60	178.20
145	0.30	-5.00	-2.50	1.525	1.756	98.75	168.37
146	0.30	-5.00	-2.00	1.561	1.760	98.62	170.86
147	0.30	-5.00	-1.50	1.577	1.765	98.96	173.39
148	0.30	-5.00	-1.00	1.599	1.771	99.37	175.45
149	0.30	-5.00	-0.50	1.597	1.774	99.25	175.91
150	0.30	-5.00	0.00	1.587	1.779	99.14	176.22
151	0.30	-3.90	-2.50	1.522	1.771	98.72	169.40
152	0.30	-3.90	-2.00	1.553	1.768	98.69	171.89
153	0.30	-3.90	-1.50	1.581	1.768	99.04	174.34
154	0.30	-3.90	-1.00	1.601	1.770	99.42	176.11
155	0.30	-3.90	-0.50	1.597	1.768	99.27	176.62
156	0.30	-3.90	0.00	1.585	1.766	99.19	177.06
157	0.30	-2.80	-2.50	1.529	1.773	98.78	170.47
158	0.30	-2.80	-2.00	1.558	1.767	98.75	172.86
159	0.30	-2.80	-1.50	1.585	1.763	99.11	175.17
160	0.30	-2.80	-1.00	1.602	1.759	99.45	176.89
161	0.30	-2.80	-0.50	1.597	1.751	99.26	177.43
162	0.30	-2.80	0.00	1.596	1.742	99.25	177.90
163	0.30	-1.70	-2.50	1.536	1.767	98.82	171.40
164	0.30	-1.70	-2.00	1.564	1.757	98.81	173.73
165	0.30	-1.70	-1.50	1.589	1.749	99.19	176.09
166	0.30	-1.70	-1.00	1.607	1.739	99.45	177.71
167	0.30	-1.70	-0.50	1.605	1.726	99.26	178.11
168	0.30	-1.70	0.00	1.634	1.712	99.38	178.81
169	0.30	-0.60	-2.50	1.546	1.753	98.87	172.31
170	0.30	-0.60	-2.00	1.574	1.740	98.88	174.59

171	0.30	-0.60	-1.50	1.600	1.727	99.27	176.90
172	0.30	-0.60	-1.00	1.621	1.713	99.44	178.34
173	0.30	-0.60	-0.50	1.626	1.696	99.23	178.71
174	0.30	-0.60	0.00	1.650	1.690	99.45	179.71
175	0.30	0.50	-2.50	1.561	1.733	98.92	173.13
176	0.30	0.50	-2.00	1.590	1.717	98.94	175.36
177	0.30	0.50	-1.50	1.619	1.701	99.33	177.62
178	0.30	0.50	-1.00	1.644	1.684	99.40	178.87
179	0.30	0.50	-0.50	1.649	1.681	99.22	179.39
180	0.30	0.50	0.00	1.680	1.673	99.55	180.65
181	0.50	-5.00	-2.50	1.572	1.730	98.61	170.81
182	0.50	-5.00	-2.00	1.611	1.736	98.50	173.26
183	0.50	-5.00	-1.50	1.622	1.742	98.83	175.76
184	0.50	-5.00	-1.00	1.644	1.750	99.17	177.68
185	0.50	-5.00	-0.50	1.631	1.753	99.03	178.16
186	0.50	-5.00	0.00	1.621	1.759	99.02	178.50
187	0.50	-3.90	-2.50	1.568	1.749	98.59	171.80
188	0.50	-3.90	-2.00	1.599	1.746	98.57	174.28
189	0.50	-3.90	-1.50	1.628	1.747	98.91	176.69
190	0.50	-3.90	-1.00	1.646	1.750	99.21	178.38
191	0.50	-3.90	-0.50	1.632	1.748	99.05	178.86
192	0.50	-3.90	0.00	1.619	1.746	99.08	179.29
193	0.50	-2.80	-2.50	1.576	1.751	98.64	172.85
194	0.50	-2.80	-2.00	1.605	1.746	98.64	175.23
195	0.50	-2.80	-1.50	1.631	1.742	98.98	177.49
196	0.50	-2.80	-1.00	1.647	1.739	99.23	179.12
197	0.50	-2.80	-0.50	1.633	1.731	99.08	179.57
198	0.50	-2.80	0.00	1.619	1.722	99.15	180.13
199	0.50	-1.70	-2.50	1.584	1.745	98.70	173.76
200	0.50	-1.70	-2.00	1.610	1.736	98.70	176.07
201	0.50	-1.70	-1.50	1.634	1.728	99.05	178.36
202	0.50	-1.70	-1.00	1.649	1.719	99.24	179.84
203	0.50	-1.70	-0.50	1.638	1.705	99.09	180.24
204	0.50	-1.70	0.00	1.646	1.689	99.22	180.89
205	0.50	-0.60	-2.50	1.592	1.731	98.74	174.64
206	0.50	-0.60	-2.00	1.618	1.718	98.77	176.91
207	0.50	-0.60	-1.50	1.642	1.705	99.12	179.12
208	0.50	-0.60	-1.00	1.659	1.691	99.23	180.42
209	0.50	-0.60	-0.50	1.655	1.673	99.08	180.83
210	0.50	-0.60	0.00	1.668	1.667	99.37	181.87
211	0.50	0.50	-2.50	1.605	1.710	98.78	175.44
212	0.50	0.50	-2.00	1.631	1.694	98.83	177.65
213	0.50	0.50	-1.50	1.657	1.678	99.17	179.79
214	0.50	0.50	-1.00	1.678	1.660	99.20	180.92

215	0.50	0.50	-0.50	1.667	1.656	99.10	181.52
216	0.50	0.50	0.00	1.702	1.648	99.50	182.81

Appendix B – Design space

In the second appendix, the whole design space is presented:

DP number	x2 [mm]	x5 [mm]	x6 [mm]	x12 [mm]	x13 [mm]	n [rpm]
1	-0.54	-0.26	-2.73	-0.16	-2.33	4465
2	0.52	0.1	-0.47	-2.95	-2.08	2425
3	-0.11	-0.94	0.31	-4.55	-1.18	5315
4	-0.33	-0.1	-0.70	-0.26	-0.18	3955
5	0.11	-0.86	-2.11	-4.15	-0.73	8375
6	-0.01	0.86	-1.79	-1.96	-2.38	9395
7	0.33	-0.14	-0.16	-0.46	-1.53	7695
8	0.98	0.82	-0.63	-4.95	-1.33	3445
9	0.27	-0.62	-1.56	-3.45	-0.83	5485
10	0.80	-0.74	0.85	-4.45	-1.08	8545
11	0.92	-0.46	-2.96	-4.25	-1.73	4975
12	-0.14	-0.78	-1.09	-2.75	-2.23	9225
13	0.24	-0.3	-1.25	-3.65	-1.78	8885
14	0.42	0.22	0.62	-3.15	-0.93	6335
15	0.58	-0.5	-2.26	-0.06	-0.38	2595
16	0.49	0.58	0.07	-0.86	-1.83	3615
17	0.67	0.5	-1.02	-4.05	-2.28	6845
18	0.36	0.06	0.70	-1.06	-0.68	9905
19	-0.42	-0.82	-1.41	-2.16	-1.98	3275
20	0.77	-0.9	0.77	-1.76	-0.63	3105
21	0.61	-0.34	-0.55	-2.55	-0.43	4805
22	-0.36	0.26	-2.57	-3.85	-1.38	2935
23	0.08	0.9	0.38	-1.46	-0.88	2255
24	0.89	-0.7	-2.49	-3.05	-1.88	2765
25	0.30	0.34	-0.94	-4.35	-0.03	6675
26	0.95	0.02	-1.48	-2.26	-1.43	7865
27	0.73	0.46	-1.64	-1.36	-1.68	7525
28	-0.23	0.18	-2.42	-3.55	-0.78	10415
29	-0.08	0.94	-1.72	-4.65	-0.48	5995
30	-0.51	-0.42	0.00	-2.36	-1.93	5145
31	-0.45	0.38	0.23	-3.75	-0.53	10075
32	-0.26	0.54	-0.08	-4.75	-2.48	4635
33	-0.17	-0.22	-1.33	-1.86	-1.63	7185
34	0.39	0.66	-0.24	-1.16	-2.43	8205
35	-0.48	-0.38	0.15	-2.06	-0.28	7355
36	0.02	-0.58	-2.65	-3.95	-1.23	8035
37	-0.20	0.78	-0.86	-2.46	-2.03	9055
38	0.55	0.74	-2.03	-1.26	-0.58	9565
39	0.05	0.62	-2.81	-2.85	-1.28	3785

40	-0.05	0.98	0.54	-1.66	-1.13	2085
41	0.86	-0.06	-1.95	-3.25	-1.48	4295
42	0.64	-0.18	0.46	-3.35	-2.18	8715
43	0.70	0.7	-2.89	-2.65	-0.33	4125
44	0.45	-0.66	-1.87	-0.76	-1.58	6505
45	0.83	0.42	-2.18	-0.36	-1.03	10245
46	0.14	0.3	-0.39	-0.56	-0.23	9735
47	-0.30	-0.02	-2.35	-0.96	-0.13	6165
48	-0.39	0.14	-1.17	-4.85	-0.08	5655
49	0.17	-0.54	-0.32	-0.66	-2.13	5825
50	0.20	-0.98	-0.78	-1.56	-0.98	7015

Appendix C – RSM results

In this third appendix, additional results from the RSM are presented. In the left side of the page, the maximum oscillation amplitude [mm] response to the variation of the remaining combination of design parameters is presented, for the base speed. On the right side, there are the same graphs for the maximum peak acceleration [m/s^2].

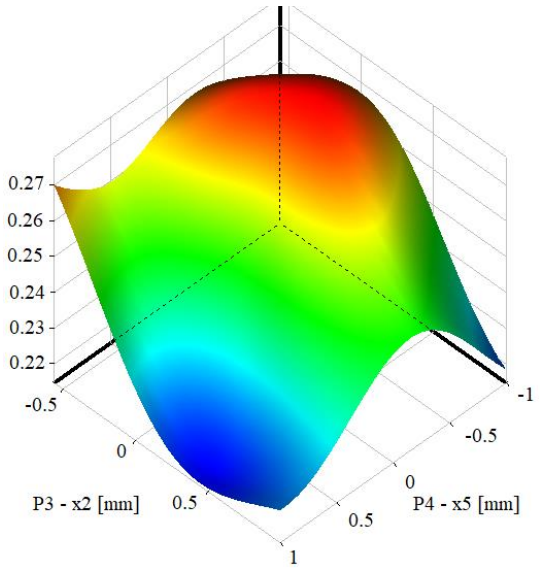

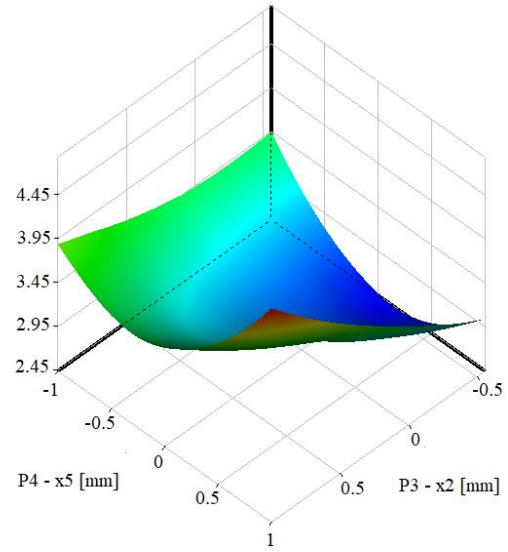

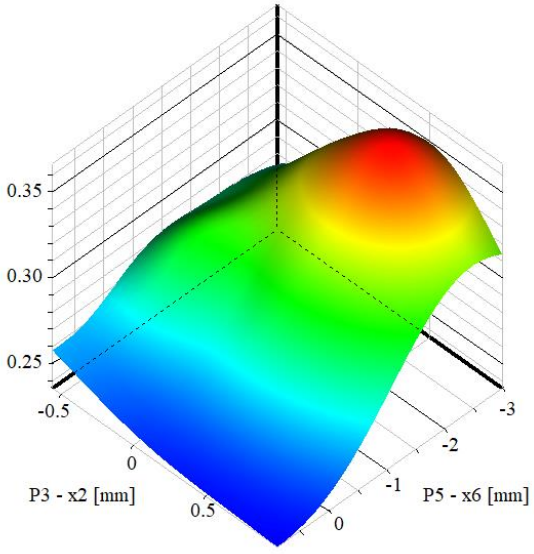

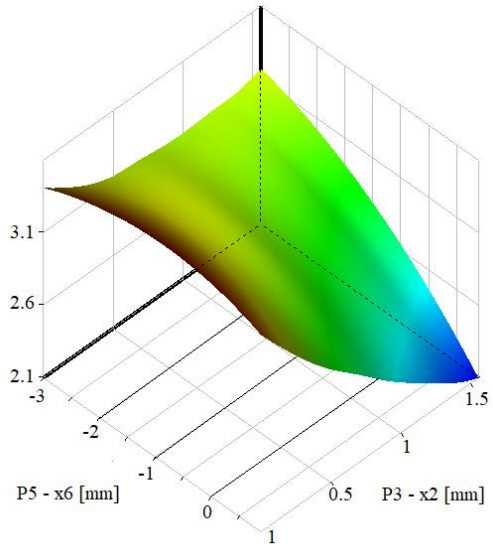

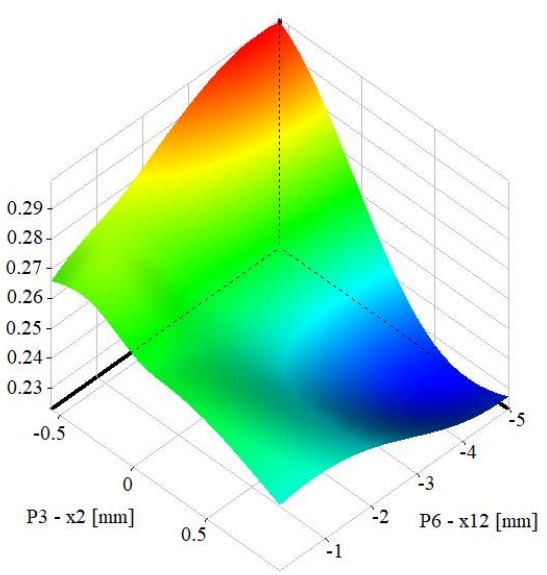
0.29
0.28
0.27
0.26
0.25
0.24
0.23
-0.5
0
0.5
P3 - x2 [mm]
-5
-4
-3
-2
-1
P6 - x12 [mm]

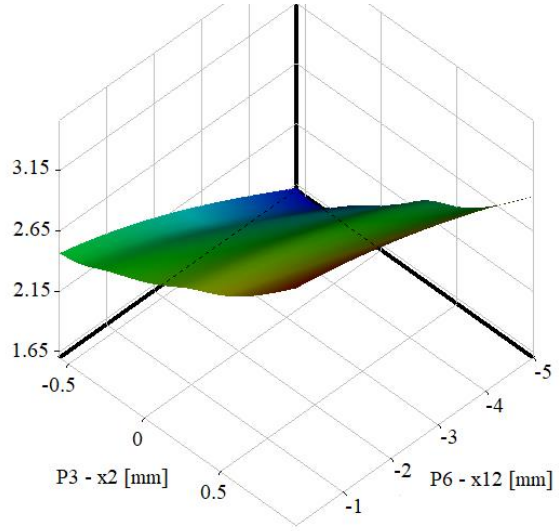
3.15
2.65
2.15
1.65
-0.5
0
0.5
P3 - x2 [mm]
-5
-4
-3
-2
-1
P6 - x12 [mm]

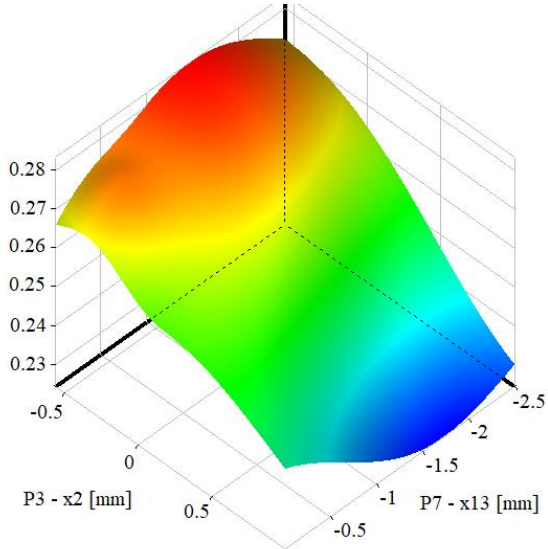
0.28
0.27
0.26
0.25
0.24
0.23
-0.5
0
0.5
P3 - x2 [mm]
-2.5
-2
-1.5
-1
-0.5
P7 - x13 [mm]

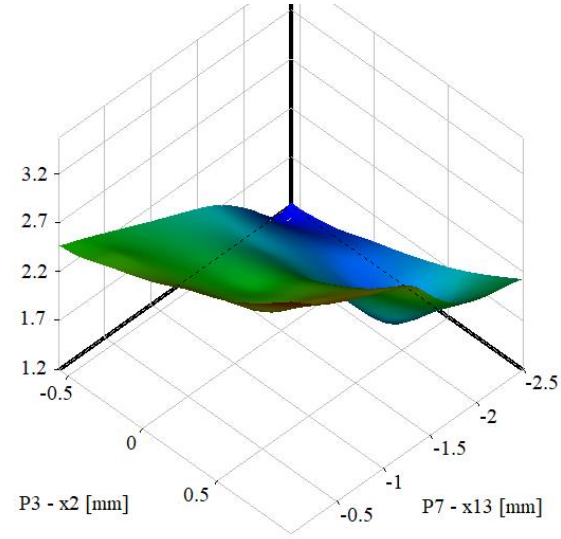
3.2
2.7
2.2
1.7
1.2
-0.5
0
0.5
P3 - x2 [mm]
-2.5
-2
-1.5
-1
-0.5
P7 - x13 [mm]

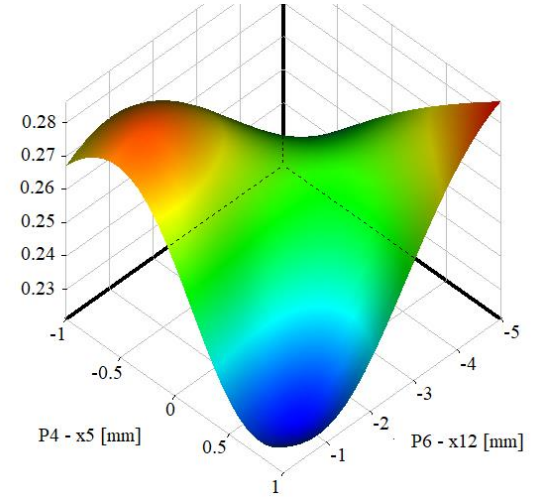
0.28
0.27
0.26
0.25
0.24
0.23
-1
-0.5
0
0.5
1
P4 - x5 [mm]
-5
-4
-3
-2
-1
P6 - x12 [mm]

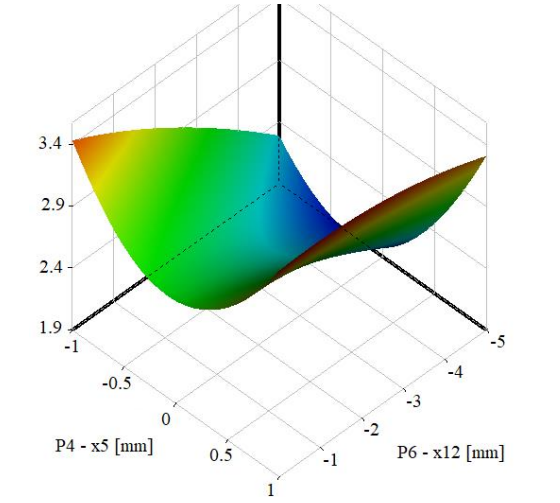
3.4
2.9
2.4
1.9
-1
-0.5
0
0.5
1
P4 - x5 [mm]
-5
-4
-3
-2
-1
P6 - x12 [mm]

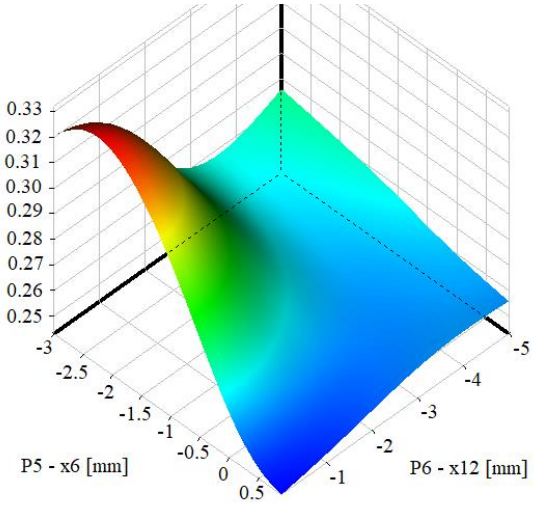
0.33
0.32
0.31
0.30
0.29
0.28
0.27
0.26
0.25
-3
-2.5
-2
-1.5
-1
-0.5
0
0.5
P5 - x6 [mm]
-5
-4
-3
-2
-1
P6 - x12 [mm]

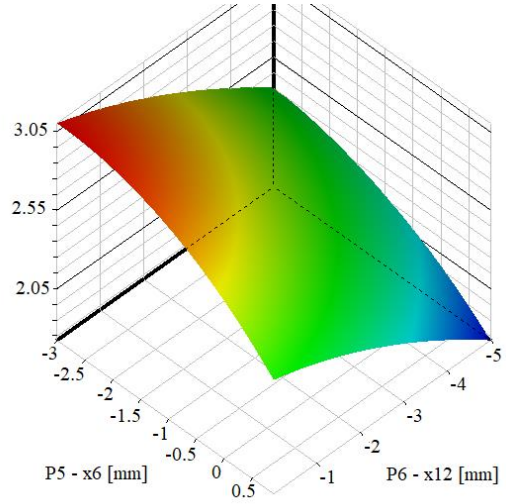
3.05
2.55
2.05
-3
-2.5
-2
-1.5
-1
-0.5
0
0.5
P5 - x6 [mm]
-5
-4
-3
-2
-1
P6 - x12 [mm]

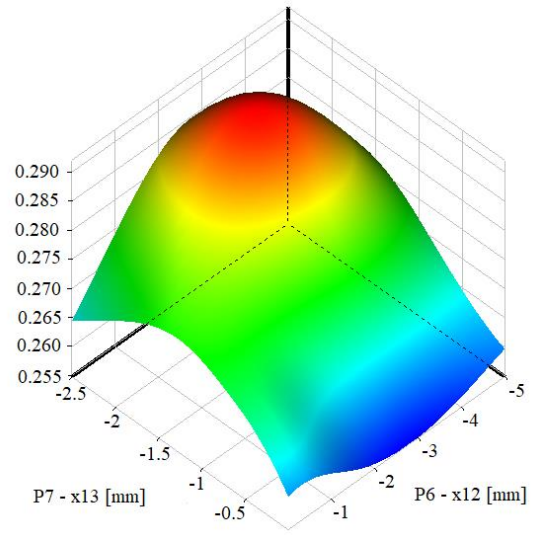
0.290
0.285
0.280
0.275
0.270
0.265
0.260
0.255
-2.5
-2
-1.5
-1
-0.5
P7 - x13 [mm]
-5
-4
-3
-2
-1
P6 - x12 [mm]

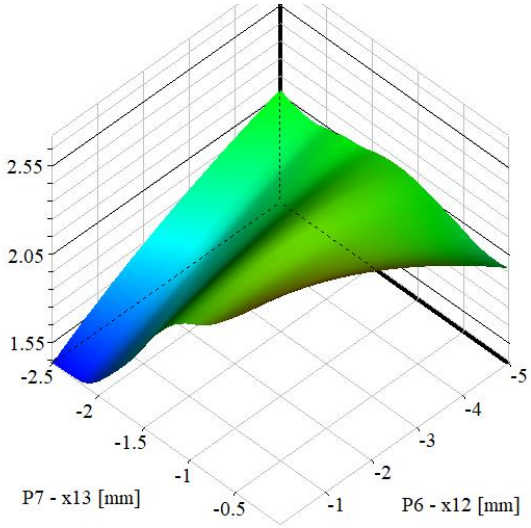
2.55
2.05
1.55
-2.5
-2
-1.5
-1
-0.5
P7 - x13 [mm]
-5
-4
-3
-2
-1
P6 - x12 [mm]

I have obtained permission to use, but do not own any of the figures taken from the cited sources.

VITA AUCTORIS

NAME:	Niccolò Remus
PLACE OF BIRTH:	Vercelli, VC, Italy
YEAR OF BIRTH:	1996
EDUCATION:	Liceo Scientifico A.Gramsci, Ivrea, TO, Italy, 2015
	Politecnico di Torino, B.Sc., Torino, TO, Italy, 2018